# JANUS PARTICLES IN A GAUSSIAN OPTICAL POTENTIAL: A COMPARATIVE EXPERIMENTAL STUDY

A THESIS SUBMITTED TO
THE GRADUATE SCHOOL OF ENGINEERING AND SCIENCE
OF BILKENT UNIVERSITY
IN PARTIAL FULFILLMENT OF THE REQUIREMENTS FOR
THE DEGREE OF
MASTER OF SCIENCE
IN
PHYSICS

By
Muhammed Bilgin
16 July 2020

Janus Particles in a Gaussian
Optical Potential: A Comparative
Experimental Study
By Muhammed Bilgin
16 July 2020

We certify that we have read this thesis and that in our opinion it is fully adequate, in scope and in quality, as a thesis for the degree of Master of Science.

Oğuz Gülseren(Advisor)

Agnese Callegari(Co-Advisor)

Ceyhun Bulutay

Alpan Bek

Approved for the Graduate School of Engineering and Science:

Ezhan Karaşan
Director of the Graduate School

# ABSTRACT

# JANUS PARTICLES IN A GAUSSIAN OPTICAL POTENTIAL: A COMPARATIVE EXPERIMENTAL STUDY

Muhammed Bilgin
M.S. in Physics
Advisor: Oğuz Gülseren
Co-Advisor: Agnese Callegari
16 July 2020

It has been shown recently that gold coated silica Janus particles can cluster when subject to a smooth optical field due to the presence of an attractive interaction of hydrodynamic nature (1). Such an interaction comes from the simultaneous presence of various factors: the thermophoretic flow around the Janus particle itself by the temperature gradient due to the partial absorption of the optical intensity on the gold cap of the particle, the presence of a boundary near the particle, the particular orientation (cap down) due to the gravity and the distinctive property of silica particles in water to move from colder to hotter regions. The model presented in the article suggests that there are various possibilities for driving the behaviour of the system: if the material constituting the particle had opposite thermophoretic features (particle moving from hotter to colder regions) then the sign of the hydrodynamic interaction would be reversed and we wouldn't observe any tendence to form clusters.

In this study we investigate the two cases stated above: we compared the behaviour of gold coated silica Janus particles with the behaviour of gold coated polystyrene Janus particles under the effect of a Gaussian optical potential, for two different kind of boundaries (glass slide, polymer slide). We find that in the case of polymer slide there is evidence of a repulsive hydrodynamic interaction among gold coated polystyrene Janus particles, which is less pronounced for gold coated silica Janus particles. Moreover, the interplay of optical forces and repulsive hydrodynamic interaction is such that, in case of a mixed solution with Janus colloids and normal colloids, we obtain a relatively fast separation

of the two species, that might find applications for particles sorting. Though relatively simple in the experimental realisation, this study shows how varied can be the interplay of different effects of different nature, i.e., due to external fields (optical, thermophoretic, hydrodynamic forces related to the beam itself) and due to the self-generated field (thermophoretic, hydrodynamic interaction due to the absorption by the gold cap). Understanding and engineering the experimental conditions might lead to realise systems where one can switch from clustering to sorting, opening possibilities for the realisation of reconfigurable colloidal structures, that might be interesting for cargo deliveries, or the realisation of micro-rotors.

Keywords: Janus Particles, Active Brownian Motiona.

# ÖZET

# GAUSSIAN POTANSİYEL İÇERİSİNDEKİ JANUS PARÇACIKLARI: KARŞILAŞTIRMALI DENEYSEL ÇALIŞMA

Muhammed Bilgin
Fizik, Yüksek Lisans
Tez Danışmanı: Oğuz Gülseren
İkinci Tez Danışmanı: Agnese Callegari
16 Temmuz 2020

Yakın zamanlarda gösterilmiştir ki, silika/altın Janus parçacıkları, homojen optik potansiyele maruz kaldıkları zaman, hidrodinamik doğalarından kaynaklanarak aralarında oluşan çekici kuvvet etkileşimlerinden dolayı kümeleşebilimektedirler. Bu etkileşimler aynı anda birkaç farklı faktörün bir araya gelmesinden doğmaktadırlar: altın kaplamadan dolayı optik yoğunluğun kısmi olarak soğurulması sonucu oluşan sıcaklık farkı neticesiyle Janus parçacığın kendi etrafında oluşturduğu termoforetik akış, parçacığın alt kısmında bulunan tabansal sınır koşulu, yerçekiminden dolayı parçacığın spesifik oryantasyonu (kaplı kısmın alt tarafa gelmesi) ve silica parçacıklarının su içerisindeyken kendilerine has özellikleri olan soğuk alanlardan sıcak alanlara doğru hareket etmeleri. Makale içerisinde sunulan modele göre, sistemin davranışını açıklayan birkaç mümkün olasılık var: eğer paçacığı oluşturan materyal, zıt kökenli termoforetik özelliklere sahip ise (paracık sıcak bölgeden soğuk bölgeye hareket ediyorsa), bu durumda hidrodinamik etkileşimler ters yöne döner ve kümeleşme gözlemlenmemiş olur. Diğer bir soru da, yüzey sınır koşulunun da bu kümeleşmede rol oynayıp oynamadığıyla alakalıdır. Bu çalışmada, yukarıda verilen iki durumu da incledik; silika-altın Janus parçacıkları ile poylstryene-altın Janus parçacıklarının Gausian potansiyel altındaki davranışsal farklarını iki farklı yüzeysel sınır koşuluyla beraber (cam lam ve polymer lam içinde) karşılaştırmak suretiyle incelemelerde bulunduk. Bulgularımıza göre, polymer lam kullanıldığı durumda, polymer-altın Janus parçacıkları için ortaya itici hidrodinamik etkileşimleri çıkmakta ve az miktarda da olsa aynı etkileşimler silika-altın Janus parçacıkları için de bulunmaktadır. Bunun yanı sıra, polymer-altın kaplamalı ve kaplamasız olmak üzere iki farklı türü içeren solüsyonlarda, optik kuvvetler ile hidrodinamik kuvvetlerin bir

arada bulunması dolayısıyla, iki türün nisbeten hızla ayrışmasını gözlemledik. Bu gözlemimizi parçacık sınıflandırmasında uygulamalı alanlarda işe yarayabilecek bir sonuç olarak görüyoruz. Deneysel anlamdaki basit sayılabilecek bu sonucun yanı sıra, bu çalışma ile ne kadar değişik çeşitlerde sistemin doğasında birarada bulunan kuvvetleri ayarlayarak değişik sonuçlar elde edebileceğimizi gösterdi.

Anahtar sözcükler: Janus Parçacıkları, Aktif Brownian Hareketi.

# Acknowledgement

This study is a product of numerous experimentations in the Soft Matter Lab. I spend day and night to find out something interesting, a novel behaviour. In a sense, I tasted both the desperation of inconclusive experiments and the joy of finding out something interesting.

Here, I would like to thank to people who are valuable for me along with my Master journey.

I would like to impress my gratitudes towards Denys and Iryna, post-docs in our lab, for their enjoyful discussions, all the support and wonderful times that we spend together in the lab. Without them, I don't know how would I pass through the most exhausted moments during all the experimentations in the lab.

I am very thankful to work with Agnese Callegari, who teached me Matlab for analysis of my experiments, for the support and guidance in experiments, for flexible but encouraging way of supervision during my Master studies. I am thankful for the head of our department, Prof Oğuz Gülseren, for patiently listening my struggles, and encouraging talks for me to find out my inner wishes and directions.

I am very grateful for my intern supervisor Prof Giorgio Volpe for the wonderful times that I spend in his lab and for teaching me how to prepare Janus particles and introducing me the methodology of science and the field of microworld. I am thankful for Prof Giovanni Volpe for the interesting ideas and guidance when he visited his Soft Matter Lab in Turkey.

I am thankful to have many nice memories with my precious friends, Onur, Koray, Tugba, Yağmur, Enes, Ferid, Abboud and all other precious ones, closes and distance ones, for making my life easier and enjoyful during my Master journey.

I am very greatful for my instructors, Prof Cemal Yalabık and Prof Ceyhun Bulutay. They teached me very elegant theories with a great patience against my ignorance in concepts and uneducated mind for scientific thinking. I am thankful for Prof Özgür Oktel and Prof Seymur Jahangirov, for being a perfect example scientists, and for having friendly conversations whenever I saw them.

I am thankful for my family, my brothers and my cousins for their supports and incentives.

With the completion of this thesis, I acknowledge that I enjoyed the adventure of careful investigations of an unknown, being an uncertain against unclear, and chasing the realities in different degrees of line of sights.

# Contents

# List of Figures

# Chapter 1

# Active Matter Systems: The Micrometric Objects

Over the last 50 years, scientists devoted a significant effort to study the world of microorganisms. The features of the motion of a microscopic organism immersed in a liquid is very different from the ones of a macroscopic object. In fact, the liquid is constituted by a huge number of very small molecules in constant motion, colliding with each other with a characteristic time usually below the microsecond, and therefore changing directions millions of times each second. This thermal agitation determines a sort of erratic motion of the microscopic particles or organisms, while the macroscopic ones are less affected by the collisions with the solvent molecules.

The molecular vibrations continually disturbs every micro-size object, thus yielding a perpetual stochastic motion where the position undergoes random fluctuations. Differently from "passively" jittering micro-objects, living organisms usually are motile, i.e., able to propel themselves to reach the nutrients or to get away from toxic substances or other microorganisms. They use varying different strategies to swim and stay alive under such stochastic environment. These peculiar features engender many intriguing questions about how the microorganisms handle with such stochasticity and propel themselves in a directed

way.

Needless to say, the understanding of the motion of eukaryotic and prokaryotic microswimmers is a fundamental issue in biology, biophysics as well as in medical science. The development of microscopy techniques showed that microorganisms like bacteria and cells have to employ clever strategies in order to propel themselves upon such conditions. In the last decade, physicists put a lot of effort to mimic the propulsion strategies of biological microorganisms using artificial micro-robots or self-propelled particles. Manmade micro-engines could, in fact, yield thriving opportunities for drug delivery applications. (2)

Before getting into the examples of living micro-organisms and how they are mimicked by the artificial microswimmers, it is important to understand the dynamics of the motion of the microparticles in their natural environment (in a viscous medium e.g. water, oil etc).

## 1.1 Stochasticity

As the scale is going down to the micro-world, the inertia phenomena is getting ineffective and thus the Brownian fluctuations plays an important role for particle's motion. The fact that everything at the molecular level is jittering results in increasing stochasticity and decreasing deterministic identifications in kinematics of matters.

To make a scale from a deterministic description to the point where the stochasticity overcomes, a well-known parameter is the Reynolds number for objects. Basically, it is the ratio of inertial forces to the viscous forces on a particle in a fluid, named after Irish scientist Osbourne Reynolds as a result of his investigations. For an approximated approach to explain the Reynolds number, we can consider an object which has size $a$ (average), density $\rho$ and velocity $v$ in a fluid. The inertial force can be thought as a necessary force to bring the object to rest over a distance of the order of its size, on the order of ($F_{inertial} \sim mv(v/a) \sim \rho a^2 v^2$).

The frictional force due to the fluid viscosity is on the order of ($F_{viscous} \sim \eta a v$). The ratio of these two forces is giving the Reynolds number;

$$Re = \frac{F_{inertial}}{F_{viscous}} = \frac{\rho a v}{\eta} \tag{1.1}$$

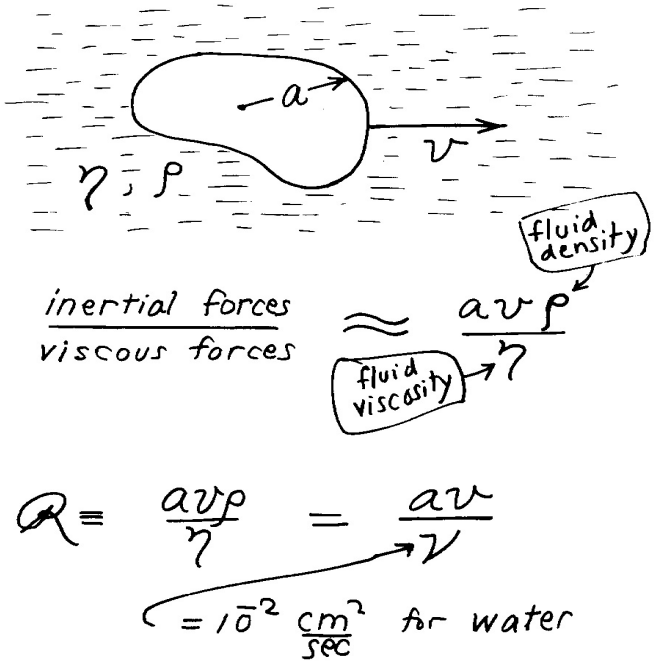


Figure 1.1: A sketch from the article of E.M. Purcell "Life at low Reynolds number" (3).

Our physical experiences of motion in fluids relate to the realm of large Reynolds number: We are mostly interested in water and room temperature, which has a kinematic viscosity of $\eta/\rho \approx 10^{-2} cm^2 s^{-1}$ ; and for an animal swimming in water $Re \approx 1(m) \times 1(ms^{-1})/10^6(m^2 s^{-1}) = 10^6 \gg 1$. Even if the motive force is stopped, the animal will continue to move in the fluid due to its inertia (Fig 1.1). (4)

Succinctly, as the spatial scale is going down to the micro- and nano-order, the randomness is becoming an important concept which has to be concerned while determining the nature of the motion of such smaller objects. One of the first

observations of such randomness in the form of jittering is reported by Robert Brown, declaring that the pollens dispersed in water are constantly jittering and after his observations, this motion is named as Brownian Motion. And back to the beginnings of 20th century, there is a well-known approach to model such bizzarre Brownian motions firstly developed by A. Einstein (5).

Before explaining the Einstein's model, I would like to give the examples of living organisms at the microscale to prepare the reader to the Brownian kinematics phenomena.

## 1.2 Microorganisms

One of the model organism for a living active Brownian particle is *E. Coli (Escherichia coli)*. ( Fig 1.2 ) *E. Coli* is a very small, 2.5 micrometer ($\mu m$) long, about 1 ($\mu m$) diameter width, rod shape bacterium that lives in our gut. (7) It has long flexible tail, called flagellum that can be driven by bacterium itself, triggered by a proton flux so that it rotates as rotary motor. In this way, the cell is adapted itself to be able to swim in a particular direction.

Figure 1.2: Escherichia coli. (6)

Swimming in micro-scale has different characteristics than we used to see at the macro-scale. Probably, one of the simplest biological entities in nature on an aspect of swimming in a viscous environment is a scallop. (Fig 1.4a) A scallop has an ability to open up its shell slowly and closes it off fast, resulting flushing out the water. In this way, this animal can swim in a directed way but it is an intriguing question that what if this animal wouldn't have any inertial properties.

This actually be the case when the low Reynolds number regime is of importance. To understand it better, we can look at the Navier-Stokes equation which

determines the equation of motion in a viscous medium in general. The hydrodynamic properties of the motion of an object swimming in a liquid of viscosity is described by the classical Navier-Stokes equation is given as (1.2) [1]:

$$-\nabla p + \eta\nabla^2\mathbf{v} = \rho\cancelto{0}{\frac{\partial \mathbf{v}}{\partial t}} + \cancelto{0}{\rho(\mathbf{v}\cdot\nabla)\mathbf{v}} \tag{1.2}$$

The right hand-side of the equation are the inertial terms and they are neglected at the low Reynolds number regimes. One can easily see that, when the right-hand side of the equation is neglected, there is no time dependency on the left hand-side. This implies that, for particles at low Reynolds number, the time has reversal symmetry.
To understand it better, besides of mathematical expressions, we can simply go back to the scallop example and imagine that the scallop stops after flushing the water. When it is again opening up the shell, the water fill it back and it will turn back to the previous position again. So, one-degree of freedom is not enough to break this symmetry for scallops.

According to the Scallop theorem, there has to be at least two hinges so that an object can move forward in space (1.3). It is quite joyful to figure out how an object which has two hinges as in (Fig 1.4b) can have a directed motion. I will give the logical directions and leave the reader to imagine and figure out to find the directed motion.
Firstly, one has to think of the following sequence of motion; ($\theta_1 : +90 \rightarrow -90$ $\theta_2 : +90$) ($\theta_1 : -90$ $\theta_2 : +90 \rightarrow -90$) ($\theta_1 : -90 \rightarrow +90$ $\theta_2 : -90$) ($\theta_1 : +90$ $\theta_2 : -90 \rightarrow +90$)
Secondly, do not forget, the object can *rotate* and it can have 3-D movement.

[1] The first term in the equation "$-\nabla p$" is the gradient of the pressure. The second term "$\eta\nabla^2\mathbf{v}$" is the diffusion of the momentum of the fluid caused by the viscousity of the fluid. The right hand side is basically the inertial term comprised of the derivative of the velocity " $\rho\frac{\partial \mathbf{v}}{\partial t}$" and the convective flow "$\rho(\mathbf{v}\cdot\nabla)\mathbf{v}$ ".

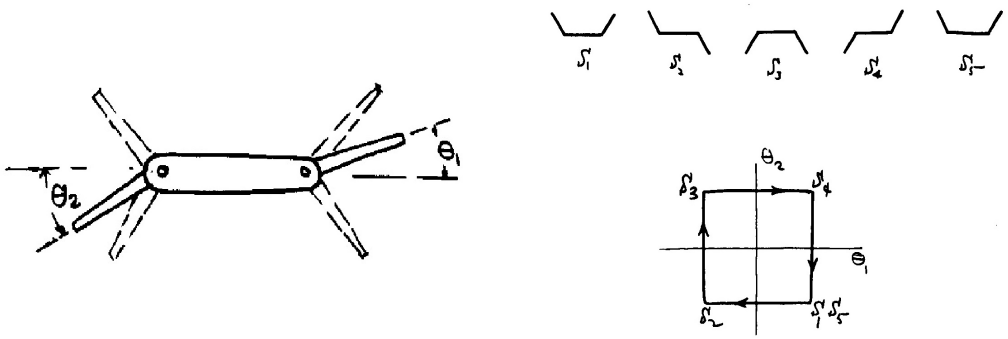


Figure 1.3: Sketches from Purcell's paper "Life at low Reynolds number" (3) for the description of an animal which has two hinges can swim. After a full cycle, the non-reciprocal series of angle configurations creates a net displacement. (8)

Here, as a reminder, all the particles at micron-size are having random motion with zero mean, which will be explained in theory part, meaning that they will be randomly swimming but will not be leading through a particular direction.

However, living animates (e.g. bacteria) can go through a particular direction thanks to their ability to break the time reversal symmetry (e.g. by flagella) Their motion is called as "active" Brownian motion in literature.

A paradigmatic example is the swimming behaviour of bacteria such as *Escherichia Coli*. *E. Coli* has long helical filaments, called flagella, that enable them to swim (9). Actually, this property of bacteria has very well studied, and it has been showed that it can propel itself by rotating its flagella (10) .

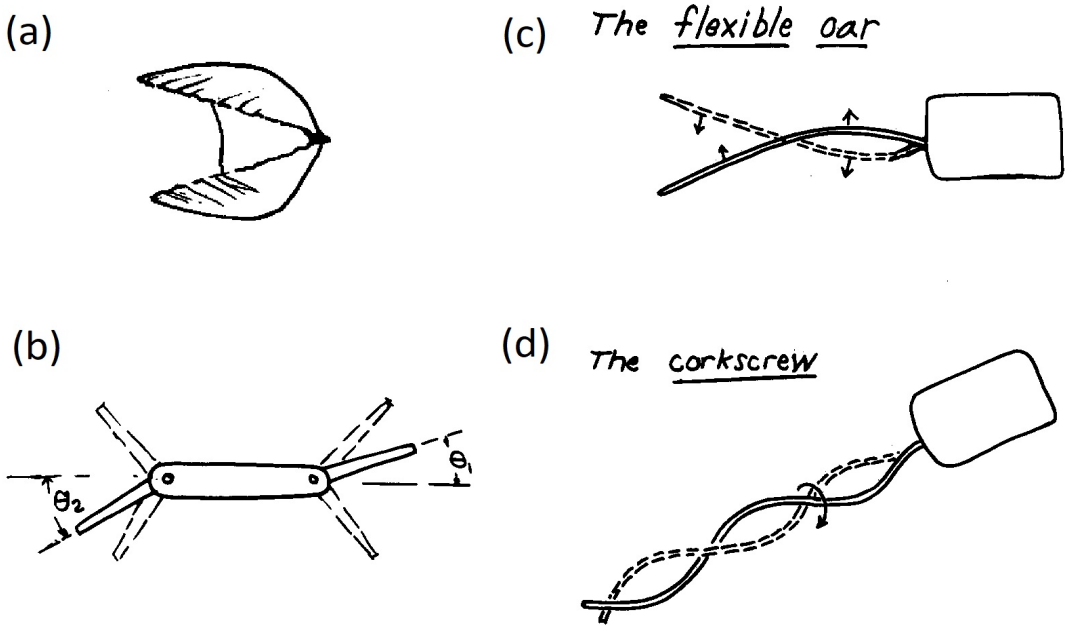


Figure 1.4: Sketches from the article of E.M. Purcell "Life at low Reynolds number". (3) At low Reynold number regime, (a) a scallop can not perform controllable directed motion. But organisms such that having more than two hinges (b), or having more than one degree of freedom {e.g. a flexible oar (c) or a corkscrew (d)} can propel themselves towards a particular direction.

## 1.3 Artificial Micro-Swimmers

These observations of microorganisms' ability of swimming with their flagella like apparatus led scientists to try to mimic biological entities to intervene the micro-world.

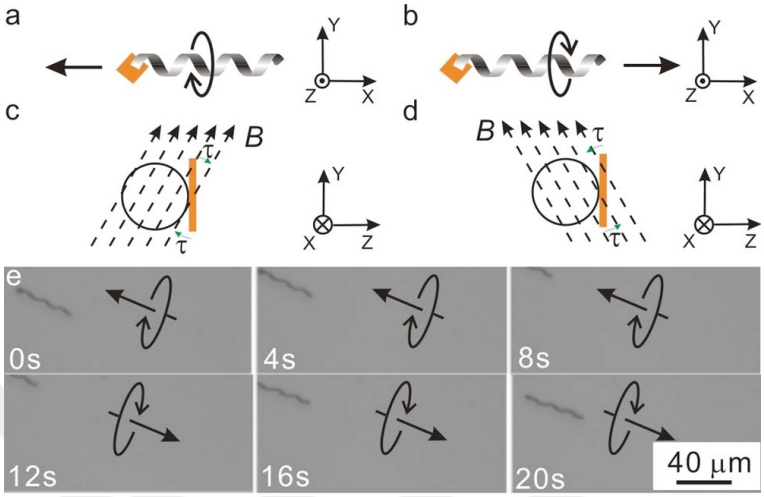


Figure 1.5: Artificial rod like helical flagella

In 2010, it has been reported that the flagella like rod can actually be activated and have directed motion under proper conditions (11). It was depending on magnetic property of the swimmer as it is easier to control it remotely. They used special lithography and etching methods (e.g. photo-lithography and wet etching) to synthesize the flagella like helical rods. Remarkably, by modifying the magnetic field on the sample, the motion of these small rods (1 $\mu$m) can be tuned and controlled. This example is totally mechanical way of swimming of a body controlled by the interaction of the external fields with the material of essence of the swimmer. Nevertheless, this method doesn't provide a control over individual agents in the sample because of the difficulty in applying magnetic field with a precision of 1 $\mu$m. Moreover, the forces acting on the particle is considered as external here, thus, the active swimming is not an intrinsic property of these metal rods.

The latest trend in scientific community is to investigate the Janus particles (JPs) as an artificial active swimmer. Janus particles are the ones which have two different materials on one body. There are several driving mechanisms for Janus particles. Mainly, thermophoretic forces (12), diffusiophoretic forces (13), (14), (15) are the ones actuated by particle itself, because of asymmetric material distribution on itself. (Fig 1.6)

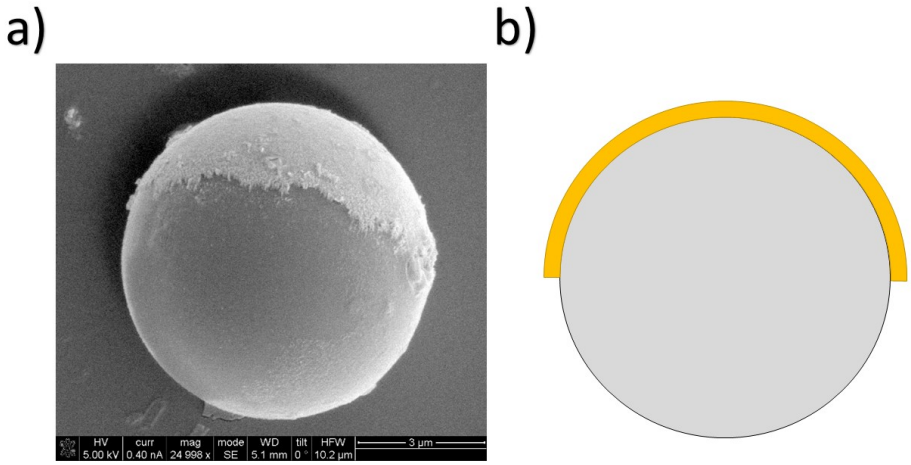


Figure 1.6: a) SEM image of Gold coated ($50nm$) Silica sphere ($6,24\mu m$). b) Sketch of side view of a typical Janus particle.

## 1.4 Promising Applications

On 29 December 1959, Richard Feynman (Fig 1.7) gave a public lecture named "There's Plenty of Room at the Bottom" which is then published as an article by Caltech (17) . That speech includes many promising ideas that can be delivered by the scientific developments such as storing information into bits in an atomic size, designing a better electron microscopes and *manufacturing a small bio-inspired agents that can perform a task at a micro-scale.*

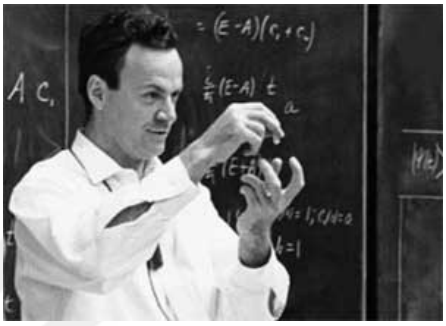

Figure 1.7: Richard Feynman lecturing (16)

After a decade, in 1986, Arthur Ashkin showed that a spherical particle under a tightly focused Gaussian beam can be trapped and manipulated by using advanced optical techniques which he has got the Nobel prize for this discovery in 2018. (18) (19)

Richard Feynman envisioned tiny machines able to perform by mechanical manipulation of atoms (20) and Arthur Ashkin opened up a possibility of micro-manipulation by using principles of optics.

The vision of Feynman, creation of tiny machines, hasn't been realized yet, but the studies showed us that it is not far from reality anymore because it is well-known that only by adjusting particle property, it can behave like an engine with a reversible controlling property based on external fields. (21; 22; 23; 24; 25; 26)

Also Volpe and et al mentioned about broad spectrum that the artificial micro-swimmers are promising to bring solutions, in particular, personalized healthcare, environmental sustainability, and security. (9) In Fig 1.8, the potential applications that can be addressed as a solution of former is represented around the core three functionalities; transport, sensing, and manipulation.

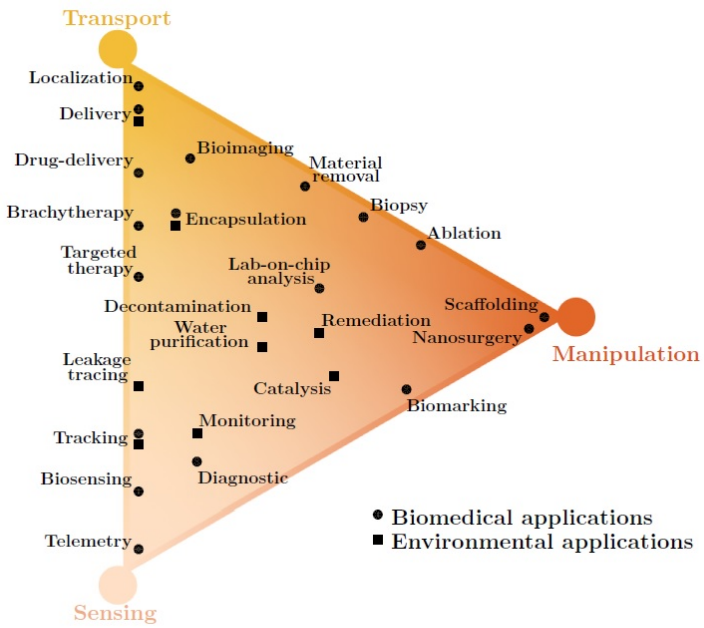


Figure 1.8: Potential key applications for active Brownian particles built around their core functionalities, i.e. transport, sensing, manipulation. (9)

Even more exciting applications on the horizon will exploit the Janus particles to form useful structures via a bottom-up approach of spontaneous self-assembly. (27) In our daily life, we always observe with formation of complex structures in nature by self-assembly of its constituents. However, our micro-/nano- printing techniques are far from nature's way of doing it. For example, nowadays, lithography techniques requires prepared masks beforehand, and by applying intense light and lift-off processes, finally one can get desired structures which takes too much time and effort and expertise. Best recent developments in lithography is based on nonlinear optics and feedback mechanisms from the local interest of region, which is providing high-speed, low-cost printing on flexible surfaces for metal-oxide. (28)

Yet, there is a need to discover basic principles of self-assembly of living and inanimate active matter systems so that we can come close to mimic the nature much better. One of the important ingredient for self-assembly is to have an interaction between sub-agents and internal driving mechanism.

In this thesis, I will show an example of internal driving mechanisms of JPs triggered by external field and how this mechanism can lead to inter-particle attractive forces, resulting with self-assembled structures and moreover, under which conditions, these mechanisms that trigger the self-assembling can be removed from the system.

# Chapter 2

# Theoretical Background

At a very fundamental level, microparticles in viscous medium undergo Brownian motion. To give a clear pedagogical picture of the model that developed so far regarding such intrinsic 'restless' motion, the Langevin dynamics are giving enough insider information about the kinematics at the basic level such as position of the particle in temporal evolution.

While the motion of passive Brownian particles is driven by equilibrium thermal fluctuations due to random collisions with the surrounding fluid molecules (29), active Brownian particles are able to propel themselves, and therefore exhibit an interplay between random fluctuations and active swimming that drives them into a far-from-equilibrium state (Erdmann et al., 2000; Hanggi and Marchesoni, 2009; Hauser and Schimansky-Geier, 2015; Schweitzer, 2007). Thus, their behavior can only be explained and understood within the framework of nonequilibrium physics (30), for which they provide ideal model systems.

## 2.1 Brownian Motion & The Random Walk Trajectories

In 1828, the botanist Robert Brown described a motion that he observed during his investigations of the pollens of different plants under the microscope. He observed that pollen dispersed in water in a great number of particles which he perceived to be uninterrupted and irregular erratic motion. (31) 'These motions were arose neither from currents in the fluid, nor from its gradual evaporation, but belonged to the particle itself.' he said. (32)

For more than half a century following, several scientists studied this motion, common to organic and inorganic particles of microscopic size when suspended in a liquid, to determine the causes and the dynamics of the motion.(5)

Einstein's first paper is on this topic (1905). He discussed an osmotic pressure forces by liquid on particle and the frictional forces by viscosity of the liquid and he introduced his famous relation between the friction coefficient and the diffusion coefficient of particle (5). Meanwhile, the Polish physicist Marian von Smoluchowski was also working on the same topic with a different approach and he also gave an estimate of diffusivity (1906) and these two approaches was giving a very close estimate of diffusivity to each other. In 1908, French physicist Paul Langevin reports a more Newtonian approach to the problem with a very straightforward way (33) .

Before explaining the Langevin's pedagogical approach, I want to illustrate a simplified model where a microscopic particle is surrounded by a huge number of identical molecules which move in all directions, but at constant speed, and repeatedly hit the particle. The molecules are smaller in size and mass with respect to the particle. The resulting motion of the particle is has the characteristics of Brownian motion. This example, though simple, is meant to give a better understanding of the causes of Brownian motion.

Imagine that a thousand of small molecules are hitting a relatively bigger ball

with 10 times heavier mass without loosing any energy. The resulting motion of the big ball is exactly what Brownian motion is. In Fig 2.1 below, the described system (1000 molecules and a ball) is simulated in Matlab by only using conservation of momentum law and the resulting trajectory (represented by the red line) is far from deterministic description, indeed it is showing the stochastic motion of the big ball.

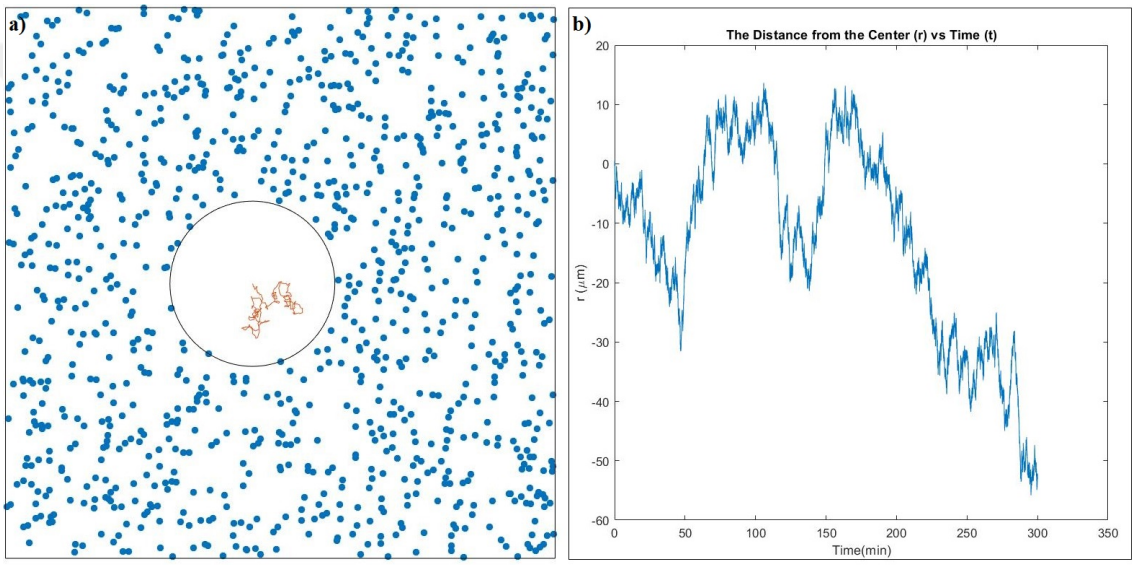


Figure 2.1: Simulation of a big ball with 1000 small molecules hitting it and each other with conservation of momentum law resulting with the big ball's *Brownian motion*. a) is showing the trajectory of the big ball (Brownian particle). b) is showing the radial distance of the geometric center of the Brownian particle from it's initial position in temporal evolution.

### 2.1.1 The Langevin Dynamics

If we consider a particle with mass m suspended in a liquid of viscosity $\eta$, the Langevin model for the motion of a Brownian particle suggests the following equation for 1 dimensional force balance;

$$m\frac{dv}{dt} = -\gamma v + \xi(t) \tag{2.1}$$

where m is its mass, $\gamma$ is the friction coefficient, $\xi(t)$ is the stochastic fluctuating force due to random impulses from the many neighboring fluid molecules.

If the particle is in some varying potential landscape (assuming that it is constant in time), then we need to impose the force coming from the gradient of the potential as well:

$$m\ddot{x} = -\gamma\dot{x}(t) - \frac{dU_{(x)}}{dr} + \xi(t)$$

Considering that the inertial effects are negligible at the microscale as explained before in section 1.1, the equation becomes;

$$\cancelto{0}{m\ddot{x}} = -\gamma\dot{x}(t) - \frac{dU_{(x)}}{dr} + \xi(t)$$

If there is smooth attractive Gaussian potential, then we can simply model it to the harmonic attractive potential with a spring constant "$k$";

$$\gamma\dot{x}(t) = -kx(t) + \xi(t) \tag{2.2}$$

Here, this equation is analytically unsolvable since there is an additional random impulse term $\xi(t)$ in the equation of motion. Yet, we have a minor statistical restrictions about this random term and it fits with the trajectory of a Brownian particle very well.

- Firstly, $\xi(t)$ is an isotropic in time over infinite time interval $\langle\xi(t)\rangle = 0$.
- Secondly, $\xi(t)$ force is neither correlated with any of the previous forces nor correlated with the position and the velocity of the particle.
  $\langle\xi_i(t)\xi_j(t')\rangle = \delta_{tt'}\delta_{ij}$
  $\langle\xi_i(t)x(t)\rangle = 0$
  $\langle\xi_i(t)v(t)\rangle = 0$

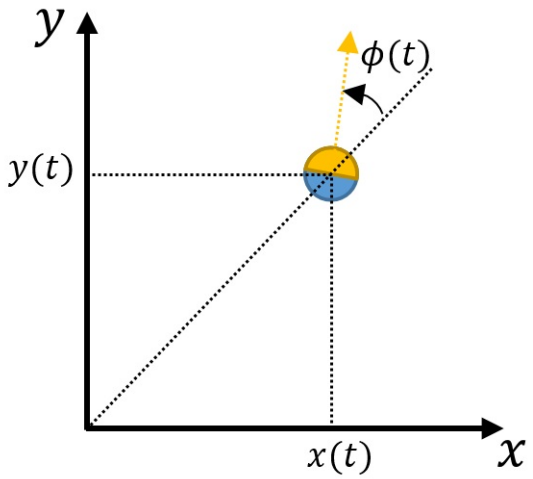


Figure 2.2: Orientation of the particle.

Under these assumptions, and by fluctuation-dissipation theorem ((34) pg 197), one can obtain following equations, with translational ($D_T$) and rotational ($D_R$) diffusion coefficients[1];

$$\begin{aligned} D_T &= \frac{k_B T}{6\pi\eta R} \\ D_R &= \frac{k_B T}{8\pi\eta R^3} \end{aligned} \tag{2.3}$$

$$\begin{aligned} \dot{x} &= -\frac{k_x x(t)}{\gamma} + \sqrt{2D_T}\xi(x) \\ \dot{y} &= -\frac{k_y y(t)}{\gamma} + \sqrt{2D_T}\xi(y) \\ \dot{\phi} &= \sqrt{2D_R}\xi(\phi) \end{aligned} \tag{2.4}$$

where $k_B$ is Boltzmann's constant and $T$ is the absolute temperature of the bath, $\eta$ the fluid viscosity, and $k_x$ and $k_y$ are trap stiffnesses. $\gamma = 6\pi\eta R$

[1] Assuming that the viscosity force, the harmonical attractive force and the random term in the equation 2.2 are orthogonal in x, y, z direction.

Although we can not exactly solve the equations above, we can derive the mean square displacement of a particle in 1D (2D is straightforward because of orthogonality) by applying the statistical assumptions we made before (also we know that mean position is zero);

$$\begin{aligned} \langle x(t) \rangle &= 0 \\ \langle x^2(t) \rangle &= 2D_T t \end{aligned} \tag{2.5}$$

where $t_0 = \gamma / k_x$ is the trap characteristic time. (35)

These are the usual equations for a free particle in viscous medium.

## 2.2 Active Brownian Motion

Until here, careful reader must have an idea on the basic nature of being in stochastic environment. This intrinsic restless environment, due to thermal fluctuations, when suspended in a liquid is well-explained by Brownian diffusion phenomena and it describes the agitation (both translational and rotational) of objects in equilibrium in a fluid at $T \neq 0$ K. When these thermal fluctuations are coupled with self-propulsion, we observe a novel type of motion that naively inherits the properties of both contributions. To underline this double nature people commonly address this behavior as active Brownian motion. (2)

Back to the microorganisms examples, we saw that there can be internal driving mechanisms depending on the shape of the microorganisms (e.g flexible tail). In such cases, the microorganisms are not only jittering but also having a directed motion (e.g. direct motion) to the nutrients or to get away from toxins. For living animates, for example, for E. coli, the flagella is flexible and it changes its shape, thus mechanical motion causes the burst of water.

However, the geometrical shape alterations of an agent is not the only way to break the time-reversal symmetry which characterizes directed motion. Another option is to modify the local environment via e.g. phoretic interactions. Some of the artificial microswimmers can propel themselves without any geometrical

change in their shape, simply by changing the thermal state of their surrounding medium. These kind of microswimmers are usually addressed as *self propelled phoretic particles* and they can modify their local environment by converting the heat to the mechanical motion by e.g. thermophoresis without having any flexibility in their shape.

In this sections, I will briefly give the kinematic properties of active Brownian motion and then I will explain some of the driving mechanisms of such active motion, in particular, phoretic propulsion mechanisms for Janus particles such as *thermophoresis*, *diffusiophoresis* and *electrophoresis*.

### 2.2.1 The persistent random walk & Ballistic Trajectories

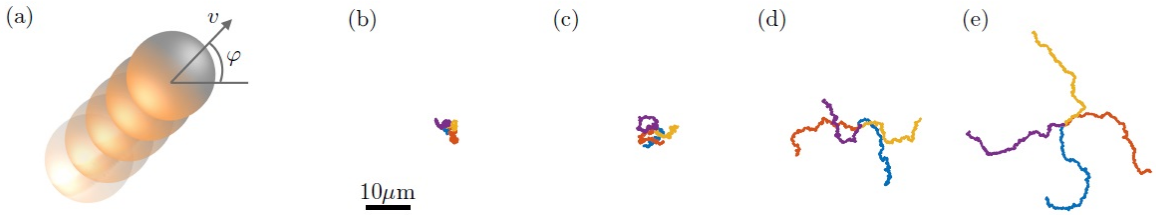


Figure 2.3: Active Brownian particle trajectory in 2D. For a particle which has radius 1 $\mu m$ and immersed in $\eta = 0.001 Pas$ viscous liquid, the trajectories for when the particle propel itself with constant velocity b) $v = 0$, c) $v = 1\mu m/s$, d) $v = 2\mu m/s$, e) $v = 3\mu m/s$. (9)

To model active Brownian motion, in the simplistic case, we can think of it is dragged by constant velocity under random angular orientations.

$$\begin{aligned} \dot{\phi} &= \sqrt{2D_R}\xi(\phi) \\ \dot{x} &= v_0 cos(\phi) + \sqrt{2D_T}\xi(x) \\ \dot{y} &= v_0 sin(\phi) + \sqrt{2D_T}\xi(y) \end{aligned} \tag{2.6}$$

Unlike the trajectory of non-active Brownian particle (see Fig 2.1), the mean displacement of the active Brownian particle is not zero, thus it has directed motion (Fig 2.4). (e.g. for initial condition that $x(0) = y(0) = t(0) = 0$) (36)

$$\begin{aligned} \langle x(t) \rangle &= \frac{v_0}{D_R}[1 - exp(-D_R t)] \\ \langle x^2(t) \rangle &= (4D_T + \frac{v_0^2}{D_R})t + \frac{v_0^2}{2}\frac{1}{D_R^2}[e^{-2tD_R} - 1] \end{aligned} \tag{2.7}$$

This implies that, on average, a swimmer will move along the direction of its initial orientation for a finite *persistence length*;

$$L = \frac{v}{D_R}$$

Meaning that, on average, every $1/D_R$ time, the particle reorient itself and then it goes straight along a new reoriented direction.

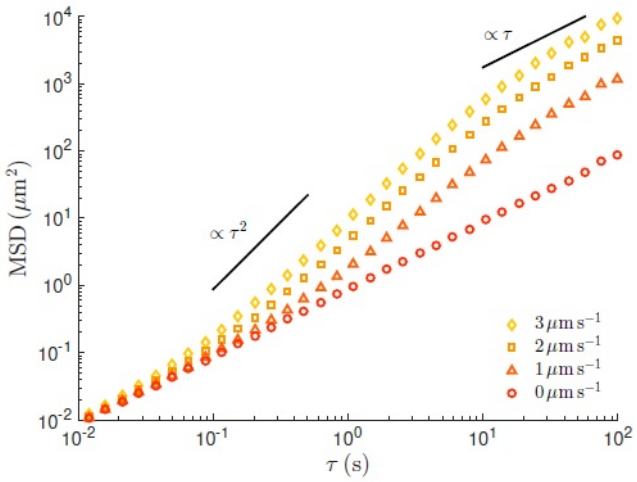


Figure 2.4: Mean Square Displacement (MSD "$\langle x(\tau)^2 \rangle$") of active Brownian particles with velocity $v = 0\mu m/s$ (circles), $v = 1\mu m/s$ (triangles), $v = 2\mu m/s$ (squares), and $v = 3\mu m/s$ (diamonds). For passive Brownian particles with velocity $v = 0\mu m/s$ (circles) the motion is always diffusive (MSD($\tau$) $\propto \tau$), while for active Brownian particles the motion is diffusive with diffusion constant $D_T$ at very short time scales (MSD($\tau$) $\propto \tau$ for $\tau << \tau_R$), ballistic at intermediate time scales (MSD($\tau$) $\propto \tau^2$ for $\tau = \tau_R$), and again diffusive but with an enhanced diffusion constant at long time scales (MSD($\tau$) $\propto \tau$ for $\tau >> \tau_R$). . (9)

### 2.2.2 Phoretic Forces

Phoretic motion arises due to the out of equilibrium state of the vicinity of the particle. Unlike other external forces, phoretic swimmers are not exposed to any external net force, yet they are able to swim as efficient as externally triggered microswimmers (e.g. in section 1.3, flagella like rod). Nevertheless, a clear explanatory theory for phoretic phenomena hasn't been totally constructed yet, but the experimental observations of it goes back to 19th century. Ferdinand Frederic Reuss found out that clay particles floating in common water respond to a constant electric field with a net motion. (37) Although the clay particles are not responsive to the electric field normally, due to the interaction inside the Debye length of the electrostatic charge distribution, the rearrangement of the water

ions around the clay particles results in a net slip velocity of clay particles.

The drift of a particle during such phoretic migration is caused by local change of the thermal state due to either the heterogeneity of the material property of the particle or the ionic/molecular response of the medium to the external field, thus it is purely a non-equilibrium effect. Even there is no net charge on the particle, if there are a gradient field and freely moving charges in the solution, then the freely moving charges in the vicinity of the particle is going to be following the induced gradient locally.

The general necessity to observe a phoretic effect is to have a gradient in the vicinity of the particle. Depending on the source of the gradient, the phenomena can be autonomous or not. If the gradient in the vicinity of the particle is exerted by the particle itself, then the name has the suffix "self-" (*self-phoresis*), if not, then it is *phoresis*. (Fig 2.5) The self-phoretic particles such as Janus particles plays a crucial importance for achieving the potential applications.

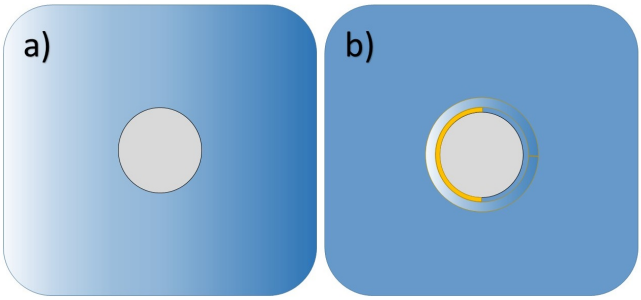


Figure 2.5: Sketch explaining the difference between *phoresis* (a) and *self-phoresis* (b). (The gradient is represented with different shades of blue color)

The phoretic motion in the example of clay particles is categorized as *electrophoresis*. There are also other subcategories of self-phoretic swimmers, such as *thermophoresis* and *diffusiophoresis*. Now, I will explain these mechanisms briefly.

#### 2.2.2.1 Self-Thermophoretic Forces

One type of the phoretic mechanism for JPs is called self-thermophoresis: i.e., absorption of a laser at the metal-coated side of the particle creates local temperature gradient which in turn drives the particle by thermophoresis. In an optical potential, the temperature distribution and a thermal slip flow field around the Janus particle is varying due to the inhomogeneity of JP. For this reason, the particle is moving along the "axis" of the JP in a "directed" way. Before going through the JP example, let's approach to the phenomena of thermophoresis from a broader perspective. When the liquid is homogeneous and in thermal equilibrium with a temperature gradient, it has been shown that the microparticles drift through the direction of temperature gradient. Back to 1856, Carl Ludwig discovered that in the presence of the temperature gradient, the salt in water is drifted to colder regions. (38) In 1879, Charles Soret gives a theoretical model for this observation (39). Since then, the relation between the temperature gradient and the drift velocity of the particle is given by the thermal diffusion coefficient, which is related to the diffusion coefficient of the particle via the *Soret* coefficient (Eq 2.10). Depending on the materials' medium properties, the Soret coefficient changes in magnitude but also in sign, thus the direction of the motion changes. This model is named as Ludwig-Soret model and it has been used to describe the thermophoretic effects since then (an example experimental study (12))

$$v_s = -nS_T \frac{dT}{dx} \tag{2.8}$$

Just to make it sense in terms of simple physical laws, it is much easier to think in terms of molecular momentum transfers. Imagine a particle made up of heterogeneous material property, e.g. half gold coated silica sphere (Janus particle). When one shine an infrared laser on this particle, the gold part will absorbs the laser light more than silica part because of it's absorption coefficient for IR is much greater than silica. (40) Thus, the gold part is going to be heated and there will be local temperature gradient around the particle (Fig 2.6). Now, considering the molecular vibrations at the hot part is going to be much higher

than the cold part, the molecular momentum transfer to the particle at the hot part is going to be higher than the cold part, resulting with the particle's net motion from hot to cold (thermophoresis).

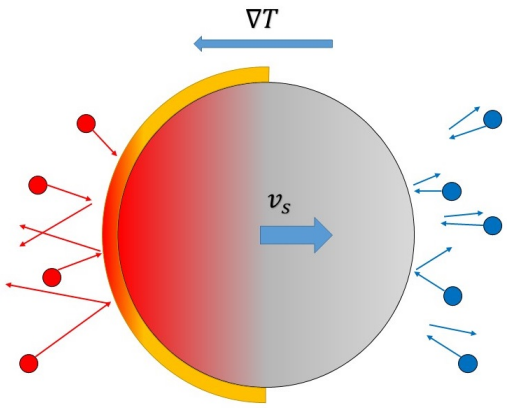


Figure 2.6: Representative sketch for explaining *thermophoresis* via an analogy with molecular momentum transfers to the particle. The gray sphere is representing a silica colloid. The yellow part is thin gold coating layer. The reddish part is representing the temperature increase due to light absorption of the gold. The small red and blue balls are representing the hot and the cold molecules. The arrows represent the velocity vectors. At the hot part, the molecules (the red balls) are much faster than the cold part (the blue balls). Thus, the momentum transfer differ each side, resulting with net impulsive force to the big ball (Janus particle).

Of course, the real physics behind the thermophoretic mechanism is much more sophisticated because it is explained under the scope of non-equilibrium thermodynamics. One of the ways to make a clear picture for this effect experimentally could be the observation of flow around the particle by using small tracers. In 2010, Jiang et. al. conducted such experiment. They put JPs with small fluorescent tracers and they recorded the flow of tracers. According to those observations, depending on the medium property, the Soret coefficient changes, thus the direction of the motion of the JP changes. (Fig 2.7c)

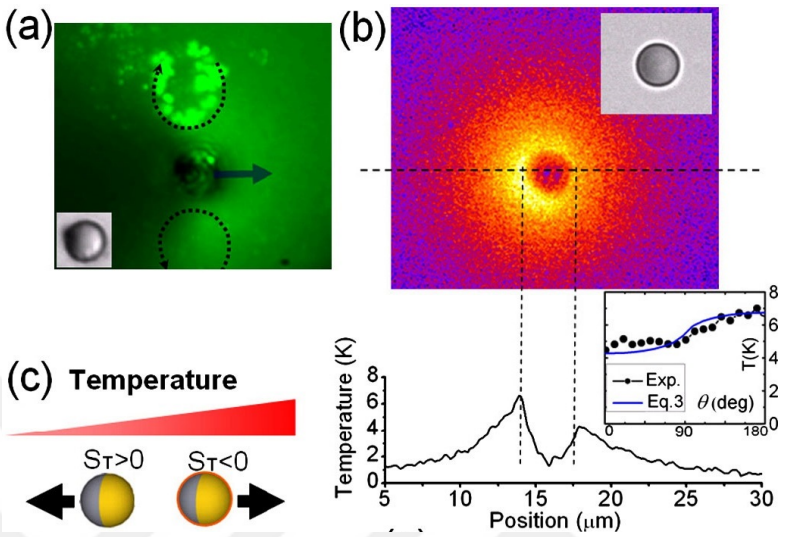


Figure 2.7: Experimental pictures taken from Jiang's paper are showing a $3\mu m$ Janus particle immersed in water with $40nm$ fluorescent tracers. Fig (a) shows the direction of motion of the JP and the tracers, thus the direction of the flow. (c) Depending on the Soret coefficient, the direction of motion changes. In Fig (b), the Janus particle is stuck to the surface, thus it is motionless and the picture shows the temperature profile around the particle thanks to the tracers. (12)

Nevertheless, in spite of all the additional theoretical efforts during the last century, the literature still lacks a self-standing predictive model for the thermophoretic drift of microparticles in a liquid. (2)

#### 2.2.2.2 Self-Diffusiophoretic Forces

The basic mechanism of the self-diffusiophoretic motion depended on the gradient of solute concentration around the particle.

When an infra-red light illuminated through the particles, active Brownian particles (e.g. Janus particle) absorb light and heat their local environment. For example, in the water-lutidine (2,6) critical mixture at the critical temperature, the lutidine will be dissolved from the water and the local intensity of the solution will change.

In this way, the particles can move the direction which have less intensity. This type of active motion is called self-diffusiophoretic motion. Illumination-born heating induces a local asymmetric demixing of the binary mixture, generating a spatial chemical concentration gradient which is responsible for the particles self-diffusiophoretic motion (14; 41). In the case where the thermophoretic forces are of importance, the gradient of the temperature is in concern primarily. Such like that, for the diffusiophoretic forces, the primary role for the motion can be characterized by the gradient of the solute. Thinking of a heat bath, obeying the ideal gas equation with a fixed temperature and varying concentration, the gradient of the pressure would be;

$$\nabla P = k_B T \nabla n \tag{2.9}$$

Remembering that the pressure is proportional with the forces acting on the particle, if we apply Eq 2.9, to the Langevin Eq 2.4, we can see that the slip velocity of the particle by the diffusiophoretic forces is directly proportional with the gradient of the solute with some constants. For more information for the derivation, see (42).

$$v_s = -\frac{k_B T}{\eta} K L^* \frac{dn}{dx} \tag{2.10}$$

To differentiate the effect of the diffusiophoretic force from the others, again let's make an analogy with the molecular momentum transfer example. (Fig 2.8) Imagining that the number of the molecular collisions at the half-part of the particle is considerably higher than the other half-part of the particle, assuming the temperature and the other conditions (e.g. ionic distributions) are fixed, then the direct consequence of this case is that the particle would be exposed to a net momentum transfer by the molecular collisions. As a result, the particle will move to a particular direction.

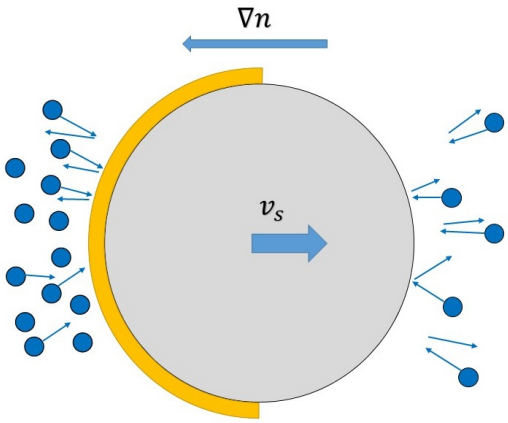


Figure 2.8: Representative sketch for explaining *diffusiophoresis* via an analogy with molecular momentum transfers to the particle. The gray sphere is representing a silica colloid. The yellow part is thin gold coating layer. Due to light absorption of the gold, there will be local temperature increase in left part. In the case where the JP is immersed in water-lutidine (2,6) critical mixture, the solvent density profile is locally changed by the temperature. The small blue balls are representing the molecules. The arrows represent the particles hitting the ball. At the left part, if the concentration of the molecules (the blue small balls) are much higher than the right part then the momentum transfer differ each side, resulting with net impulsive force to the big ball (Janus particle).

One of the experimental observations of self-diffusiophoresis is by Buttinoni et al. (14) Usually, when the Janus particles are exposed to IR light, their coated part absorbs the light and the temperature increases a bit locally. In the case where the JP is immersed in water-lutidine (2,6) critical mixture, the mixture has such a property that it decomposes it's components above the critical temperature $T_C = 307K$. If the environment is kept at nearby this critical temperature, then a local increase in temperature (e.g. at coated part of the JP) will alter the water and lutidine concentration locally. 2.9 Depending on the hydrophilicity of the material on the particle, the particle will move towards or away from the coated part. This observation is direct consequence of diffusiophoresis and a good example for self-diffusiphoretic motion.

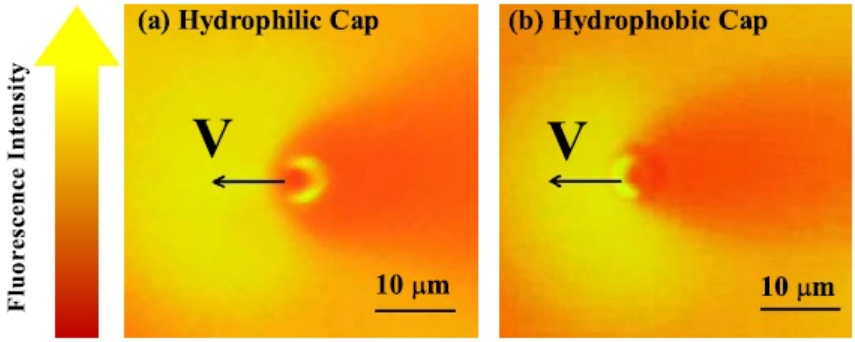


Figure 2.9: Experimental fluorescent images of JP in water-lutidine (2,6) critical mixture solution illuminated by Rhodamine 6G taken from Buttinoni's paper. The gold cap (bright half-moon shape) gets heated under illumination, thus shining. The direction of motion is from the cap to the non-cap when the cap is hydrophilic, and vice versa. (14)

#### 2.2.2.3 Electrophoretic Forces

The discovery of the migration of particles due to the electrophoretic effect is one of the first kind amongst the propulsion mechanisms exerted by phoretic effects. The generic propulsion in electrophoretic phenomena comes from the reaction of the ions inside the medium to the external electrical field. By taking advantage of the foundation of electrophoretic phenomena, there are many useful applications for biological systems e.g. sorting proteins (43; 44). As because almost all natural liquid medium contains ions, this phenomena always needs to be addressed when the analysis for migration has been conducting.

To make a more clear picture in mind, lets start with physical facts of the situation. First of all, the particles that are dragged by the electrophoretic forces are not directly affected by the external electrical field because they are neutral particles in principle. However, if we look at the outer shell of the particle, when it is immersed in ionised liquid, the chemistry of the outer shell is slightly altered and take a form such that it is surrounded by the free counter-ions inside the medium. Although the attracted counter-ions and the surface charges cancel each other,

there is still some diffusive region containing counter-ions in the medium. The electrostatic potential for this layered ionic charges can be derived by Poisson-Boltzman equation as;

$$\phi(r) = \phi(0)e^{-kr} \tag{2.11}$$

where r is the distance from the particle surface, and $\phi(0)$ is the surface potential of the particle. The inverse of the coefficient k is where the potential reduces down to it's one exponent. It is called the *Debye screening length* (see Fig 2.10) and is given by;

$$l^{-1} = k = \sqrt{\frac{e^2 \sum c_i z_i^2}{\epsilon k_B T}} \tag{2.12}$$

where $z_i$'s are the valence electrons of the particle, $\epsilon$ is the electrical permittivity of the medium and T is the temperature of the medium. The potential that corresponds to the Debye length is *Zeta Potential*.

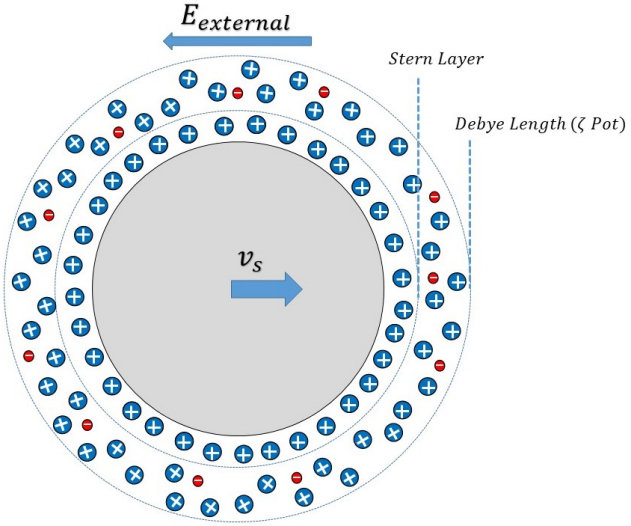


Figure 2.10: A sketch pointing the places of the $\zeta$ potential, screening length/Debye length and stern layer.

The sum of the particle's net electrical inner surface charge and the Stern layer's ionic charge is making particle as if it is an uncharged particle. Therefore, when an electrical field is applied, one expect particle wouldn't be affected. However, meanwhile the ionic cloud around the particle is affected by the electrical field and there will be flow of charges. Therefore, the particle is going to be propelled by the flow of the cloud charges around it's outer surface. Shortly, the Coulomb force is only acting on the ions, not the particle directly, and the ions are triggering the particle to move because of the finite interaction layer between particle and the ions. This force due to the finite screening length between particle and the ions is named *retardation force*.

To make a quantitative expression for this force, one has to consider the migration of the ions, hence the Stokes equation;

$$\eta \nabla^2 v + \rho_e E_{external} = 0 \tag{2.13}$$

Here, the charge distribution of the ions has to be taken from the Poisson equation;

$$\rho_e = -\frac{\epsilon}{4\pi} \nabla^2 \phi \tag{2.14}$$

By the approximation that the particle is much larger than the screening length, the slip velocity of the particle is proportional with the external electrical field;

$$v_s = -\frac{\epsilon \zeta}{4\pi\eta} E_{external} \tag{2.15}$$

## 2.3 Hydrodynamics in The Medium

This part is to explain the flow of the fluid due to the heat-absorption, either by the fluid itself or by the particle. When there is a local or global temperature gradient inside the medium, the fluid start flowing, locally or globally, thus the particles are affected by this flow. Mainly, examining the hydrodynamic flow in two categories makes it easier to understand in our case.

### 2.3.1 Marangoni Flow in Fluid

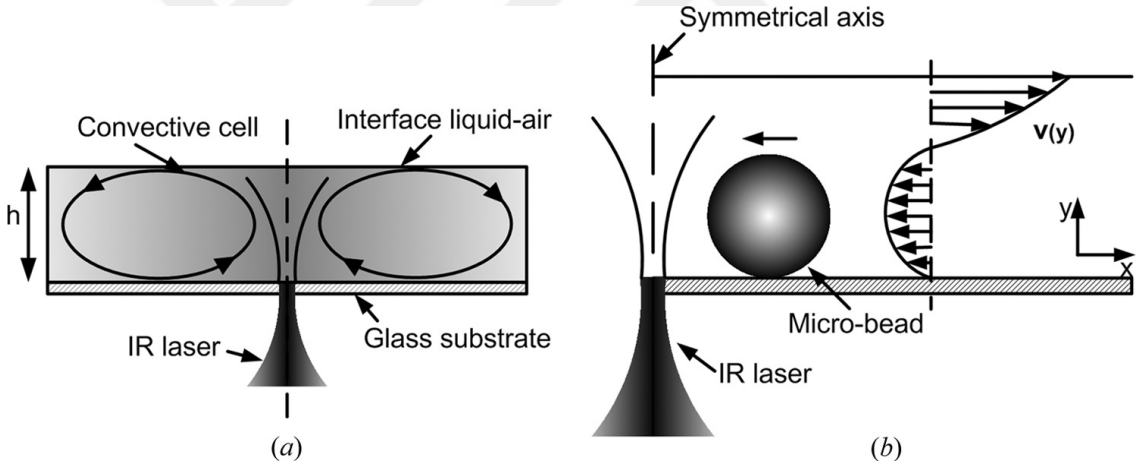


Figure 2.11: A representative sketch showing a Marangoni convection inside the sample chamber. (45) (a) Due to the light absorbtion of the water, the temperature increases locally, maximum at the center of the Gaussian beam. This temperature gradient inside the chamber causes a convective flow due to the Onsager's reciprocal symmetry relations. (46). (b) The microparticles and the tracers are dragged by this convective flow inside the chamber. The arrows shows the direction of the flow.

The first category is a huge convective flow inside the sample chamber which is due to the light absorption by water itself. When the infrared laser with Gaussian beam profile is focused on the bottom part of the sample, some part of the light is absorbed by the water. This generates a temperature gradient inside

the chamber, in which the maximum temperature is at the center of the Gaussian. This temperature gradient causes a convective flow up to a mm range radius. This effect is known as highly localized thermocapillary effect or Bénard–Marangoni convection.

As it is shown in Fig 2.11, when the IR laser is focused to the sample, there occurs a convective flow inside the chamber depending on the laser power, the size of the substrate and the liquid property. Thus, although the particles far away from the Gaussian beam center didn't feel the optical force, they are dragged by this Marangoni convection to the center of the Gaussian beam where the temperature is maximum.

### 2.3.2 Local Hydrodynamic Flow Due to Light Absorbtion of Gold Coated Part of Janus Particle

The second category of hydrodynamic flow is a discussion of the mechanism of the thermophoretic effect. The flow around the particle due to light absorbtion of gold layer is also called as "hydrodynamic". As it is discussed earlier in the thermophoretic forces chapter, the artificial active swimmers e.g. Janus patches, creates a local thermal gradient around their vicinity. This is due to the variance in the light absorption of the Janus particle on its surface. The temperature gradient is, in fact, the main key factor to create a local liquid flow around the particle. The theoretical framework for such hydrodynamic flow is the basis to explain the thermophoretic phenomena (47).

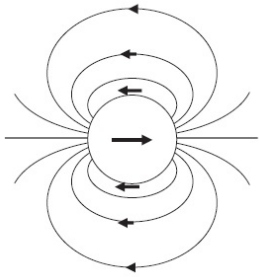

Figure 2.12: The local temperature difference around the particle creates local non-equilibrium conditions for the fluid around its vicinity. On the figure, using the tangential slip velocity boundary conditions, the resulting velocity profile is shown with arrows on the particle. (47)

With the boundary conditions as such; i) If we name the velocity of the particle as $u$ and the velocity of the liquid as $v(r)$ the normal velocity component is continuous at the boundary $r = a$ .

$$\mathbf{n} \cdot \mathbf{v} \mid_{r=a} = \mathbf{n} \cdot \mathbf{u} \tag{2.16}$$

ii) The net external force is zero. iii) The surface stress and the Marangoni forces counterbalances each other.

If one applies these boundary conditions, the resulting slip velocity of the particle comes as;

$$u = -\frac{a\gamma_T \kappa}{3\eta} T_x \tag{2.17}$$

where a is particle radius, $\kappa$ is the heat conductivity parameter, $\gamma_T$ is the derivative of the gradient of the surface energy with respect to temperature, $\eta$ is the viscosity of the water. (For more theoretical explanations see (47)).

Meanwhile, it is experimentally shown that slip flow of fluid due to temperature gradient in horizontal direction can cause an attractive potential among particles in lateral direction at the bottom of the substrate. (See Fig 2.13)

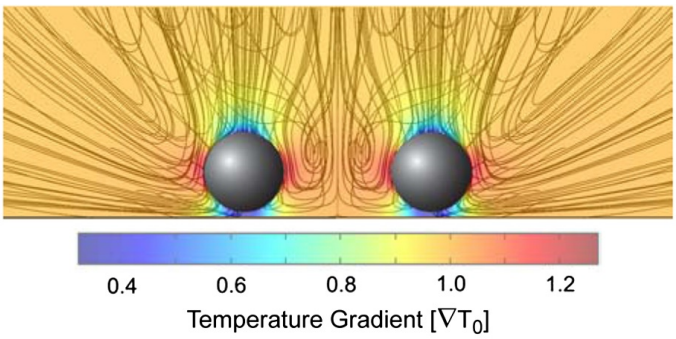


Figure 2.13: The numerical work is showing that the longitudinal temperature gradient can create transverse attractive potential among particles. The black lines are the flow directions. The temperature gradient is colour coded. (48)

Weinert shows that for particles which meet the condition of $\nabla T > 1/aS_T$, the local equilibrium model for thermophoresis doesn't work anymore. Thus, there occurs a slip flow of fluid around the particle. By depending on the sign of the *Soret coefficient*, the flow direction can vary. As in Fig 2.14, the polystyrene bead attract the tracers, indicating that the flow direction is from bottom to up. Meanwhile, the silica bead repels the tracers until a distance which the Brownian fluctuations can overcome, indicating that the flow direction is from up to bottom.

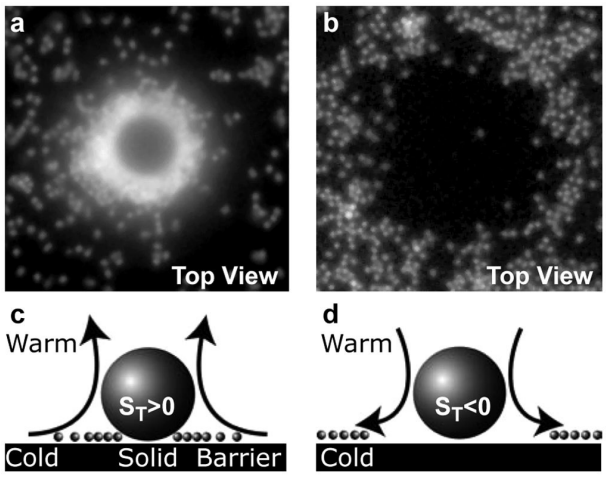


Figure 2.14: Thermophoresis theory. (48)

In the Weinert experiment, particles are homogeneous silica or polystyrene

beads. The temperature gradient is formed in between bottom and the top surfaces of the chamber. Yet, there is observed attraction among polystyrene beads and they form a reversible clusters triggered by the temperature gradient inside the sample chamber as in Fig 2.15. This shows a proof for the fact that non-equilibrium dynamics is on play for the thermophoresis mechanism. However, clear-cut explanation is still lack for this phenomenon and there is need to understand the physics behind it. In our experiments for example, we observed that a change in the substrate property can also affect the effective thermophoretic force fields, in a way that either suppressed by other forces or change in *Soret* coefficient. To examine this, one can see our results in Results section.

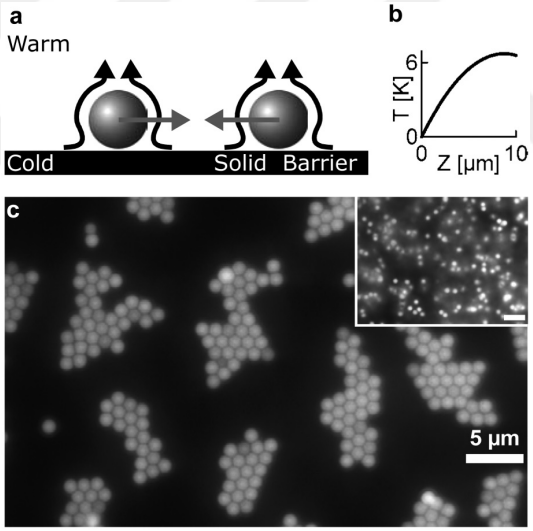


Figure 2.15: Polystyrene beads form clusters due to attractive forces arising from the hydrodynamic flow. (a) Curvy lines are the flow directions. (b) The temperature difference in z direction. (c) PS beads forms reversible clusters triggered by the temperature gradient inside the sample chamber. (48)

## 2.4 Optical Force

About a three decades ago, in 1986, it is shown that microparticles can be trapped by using a tightly focused laser beam by Arthur Ashkin which is rewarded with the Nobel prize in 2018 for this discovery. (18) (19) This famous technique is

nowadays known as optical trapping and the optical systems designed for this purpose are known as optical tweezers. Ranging from atoms to eukaryotic cells, the optical tweezers has been used for many scientific investigations and practical applications. (34)

The dual particle-wave nature of the light allows it to propagate softly from the medium and interact with the particles in an intriguing way so that we can manipulate the targeted particle by not touching anything else on the path. Depending on the optical design and sample properties, the physics of light beam should be treated with the proper approach.

Shortly explaining our experimental conditions here, we have an infrared light coming out of a fiber $\lambda_0 = 976$nm, focused with 35 mm Bi-convex lens to the sample, which gives $\omega_0 = 96$ $\mu$m beam waist on the focus. In the sample, we basically targeted the 6 $\mu$m polystyrene and silica particles, which has 1.59 and 1.45 refractive index respectively. (The refractive index of water is 1.33)

Under such conditions, the Ray optics (or "Geometrical" optics) is accurate enough to describe the physics and to determine the physical quantities on the particle such as optical forces. For the detailed information about an optical setup and the sample properties that we used, a reader can see the "The Experimental Conditions" chapter.

For particles of which the size are bigger than the wavelength of the incoming beam, the optical forces on the particles exerted by the laser beam can be accurately characterized by modeling the beam as a collectively propagating *light rays*.

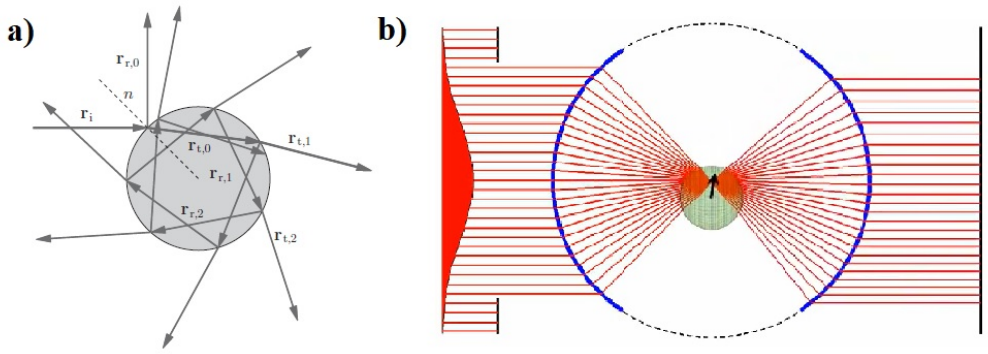


Figure 2.16: The momentum transfer from the light to the particle is exerting a net restoring force on the particle. (a) The light transmitting and reflecting multiple times inside the spherical particle. (b) At the end, when the Gaussian laser beam is tightly focused to a spherical particle, the force exerted on the particle by the momentum transfer from the light to the particle is restoring, thus the particle is trapped at the equilibrium position, e.g. center of the Gaussian beam. (49)

To reach out an expression for the optical forces, first, we can look for the momentum transfer by the light to the particle. When a monochromatic light is used to create an optical potential, the momentum carried by the "rays of beams" passing through an area "A" can be written by using energy-momentum relation of photons $pc = \varepsilon$. Here, the energy of the "rays of beams" can be obtained by multiplication of the area and the Poynting vector $\mathbf{S}$, which is, by definition, the density of the energy flux carried by the photons. The Poynting vector phenomena is defined by the electromagnetic wave nature of the light, given as $\vec{S} = \frac{1}{\mu}\vec{E} \times \vec{B} = \sqrt{\frac{\epsilon}{\mu}} \mid \vec{E}^2 \mid$.

Eventually, considering the fact that the laser power $W$ is the unit energy flux per time, than the momentum carried by the photons is going to be $\varepsilon/c$. As an example, in the case where the incoming beam totally reflected perpendicularly by e.g. a mirror, the net momentum transfer from the ray to the mirror would be;

$$\mathbf{F} = \frac{2W}{c}\hat{n} \tag{2.18}$$

However, when the light partially transmitted through the particle, then we need to know the amount of the portion that transmitted to the medium. It is basically given by the Fresnel equations. Depending on the polarization of the light, the Fresnel transmission and reflection coefficients are the recipe to know the percentage of the transmitted and the reflected light.

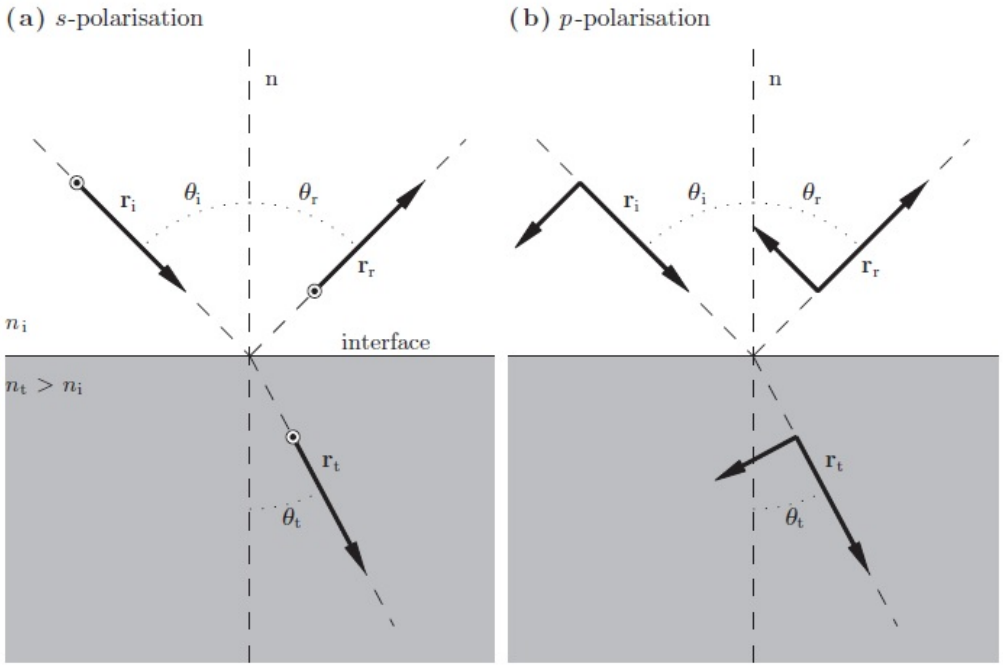


Figure 2.17: When the light is transmitting through a medium with a different refractive index, Fresnel equations give the transmission and reflection coefficients of the incident beam. It has two orthogonal forms as (a) an s-polarised or (b) a p-polarised ray of beam. $r_i$, $r_t$ and $r_r$ are the incident, the transmitted and the reflected beam directions. The arrows perpendicular to the rays represent the directions of the electric fields. (34)

Even though we know the transmission coefficient of the incident light, there is also ambiguous discussion about what happens to the momentum of the light when it is inside a medium. I will skip this part and leave it by saying that the

Hermann Minkowski (1908) suggested that the momentum p carried by a photon is inversely proportional to its wavelength $\lambda_0$; therefore, because in a medium of refractive index "n" the wavelength becomes $\lambda_0/n$, the photon momentum must increase by a factor n, (34) therefore, the force exerted by the transmitted light is;

$$\mathbf{F} = \frac{n_t W_t}{c}\hat{r} \tag{2.19}$$

Finally, the particle does not have a planar surface. When a ray of beam gets into a spherical particle, it has multiple reflection and transmission inside of it. Then, knowing the Fresnel coefficients, the optical force can be calculated by the vector sum of all the reflections and the transmissions, as;

$$\mathbf{F}_{ray} = \sum \frac{n_i W_i}{c}\hat{r_i} - \frac{n_i W_r}{c}\hat{r_r} - \frac{n_t W_t}{c}\hat{r_t} \tag{2.20}$$

This summation, is going to produce two orthogonal net forces, the *gradient force* $\mathbf{F}_{ray,g}$ and the *scattering force* $\mathbf{F}_{ray,s}$.

$$\mathbf{F}_{ray} = \mathbf{F}_{ray,s}\hat{r_i} + \mathbf{F}_{ray,g}\hat{r_\perp} \tag{2.21}$$

In our experiments, we have a very wide Gaussian width, so it is different from that of optical trapping figure 2.16. Our beam waist is around 90 micrometer, comparing with the particle size 6.24 micrometer, the beam covers a very large area. Yet the physics behind the attractive optical force is very similar with the explanations above. Once the particle gets exposed to the "optical rays", they feel the optical force and the area that the optical is of importance is marked with dashed red line in results section. One can question how the particles which are far away from the "beam rays" are dragged into the beam center. The answer can be given by the hydrodynamic convective flow inside the chamber because of the fact that the infrared light absorption of water is very large comparing with other wavelengths. (50)

# Chapter 3

# The Experiments with Janus Particles

The experiments are designed to test very particular feature of Janus particles; the attractive nature of Janus colloids under smooth Gaussian beam in water. The attractive behaviour emerges due to the combination of various effects; the particular orientation of Janus particle (cap down), the thermophoresis phenomena and the hydrodynamic flow of water triggered by the local thermal gradient around Janus colloids.

Shortly explaining, when the light beam is focused on floating microparticles in viscous medium, there occurs a varying potential energy landscape for transparent particles due to the light-matter interaction. The polystyrene colloids move into the local or global minima of the landscape to minimize their potential energy. However, the Janus particles behave differently than the polystyrene colloids. They create non-equilibrium conditions around their vicinity and this enables them to have more complicated dynamics than polystyrene particles.

To create an energy gradient in the environment, we shine a focused laser beam which has a wavelength in the infra-red (IR) regime ($\lambda = 976$ nm) and has a Gaussian beam profile. The RMS width of the Gaussian beam is chosen as 34

micrometer which is 5 times larger than particle diameter (D=6.24 micrometer). In this way, we are able to measure the drift velocity of particles due to Marangoni convective flow, the optical force and the thermophoretic mobility due to the coated part. Besides, these are the simplest conditions one can create to measure the additional effects coming from the Gold coating of the PS spheres.

To be able to characterize the motion of the Janus particles, we trace the particles until we get enough statistical data. We simply test the effect of the substrate to the thermophoretic driving mechanism of Janus particles. We also observed separation of mixture of particles, (symmetric microspheres & Janus microspheres), in the case of polymer based substrate.

Now, I will introduce our methodology to create such conditions given above, in particular, the methodology for preparing sample, fabrication of Janus particles and Optical setup.

## 3.1 Optical Setup

The optical setup consists of hand-made inverted microscope and smoothly wide-focused Gaussian laser beam. The optical components are Thorlabs holders and lenses. The camera is Basler ac A640-750 $\mu m$ camera. (51) The videos are taken by the camera and its own software. Later, the videos are analysed by digital video microscopy techniques by using Matlab. Both the determination of center of mass (by manual image processing) and circular haugh transform method ('imfindcircles' function embedded in Matlab) has been used to trace the particles.

The infra red laser is produced by diode laser as continuous wave (CW) laser, forwarded through a fiber and directed downwards by a collimator which makes the beam parallel after the fiber (a). Then, the IR beam is passing through the transparent glass slide, which effectively doesn't alter the beam (c). In the meanwhile, the illuminations is sent from the left side, and reflected to the sample

(b-c). Then, both the beam and the illumination is passing through the biconvex lens (with focal length 35 mm) and focused on the sample stage (d-e). After the sample, the objective collects the light and they are focused on the camera, whilst the IR light is filtered on the path (f-g-h-i).

We've chosen this orientation because it gives us convergent beam profile in a smooth and easy way. Single point trapping is far beyond our purposes because we would like to see the crowd behaviour of bunch of particles, not single particle property. This also enables us to balance every forces equally, such as optical forces, hydrodynamic forces and thermophoretic forces.

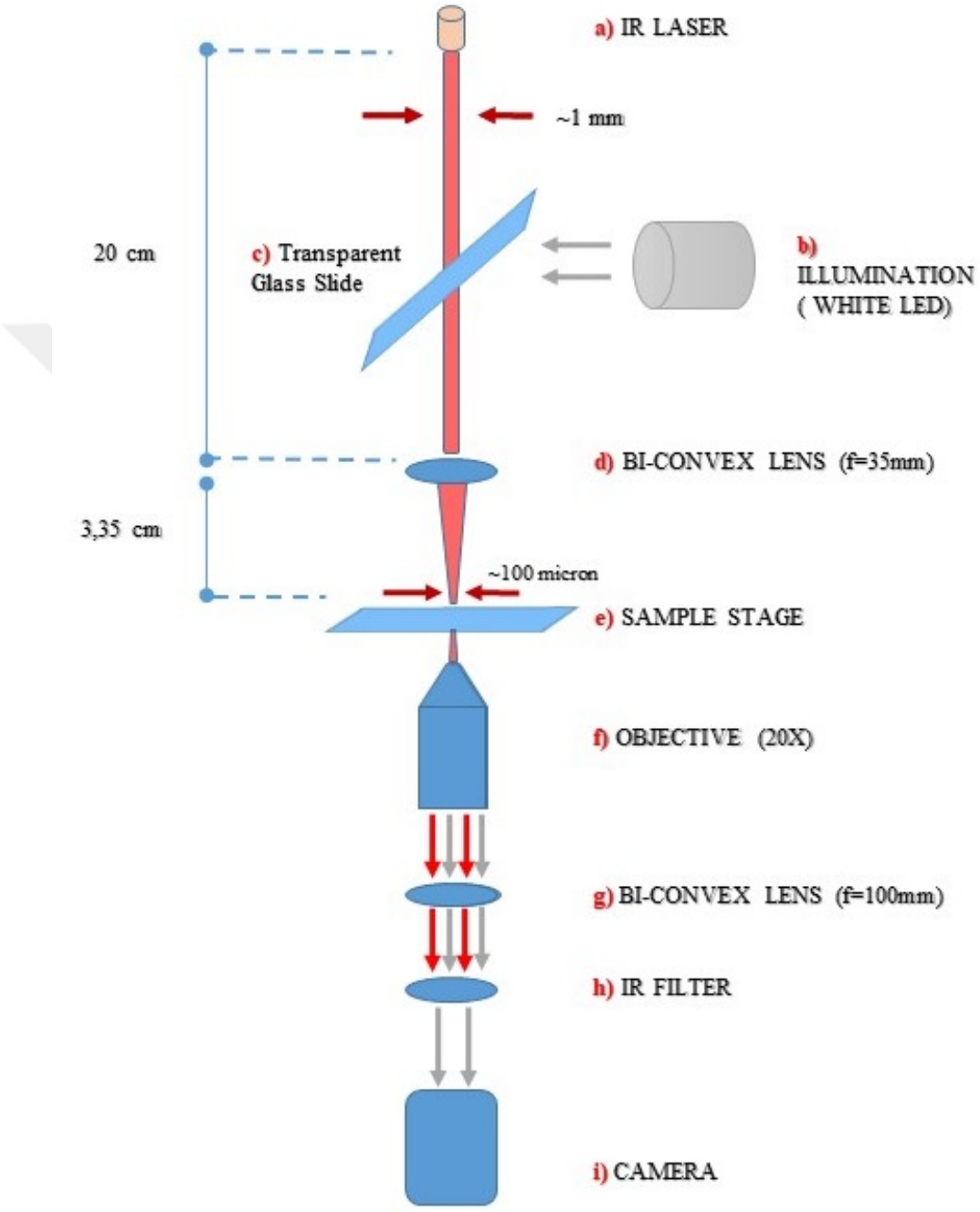


Figure 3.1: Illustration of optical setup.

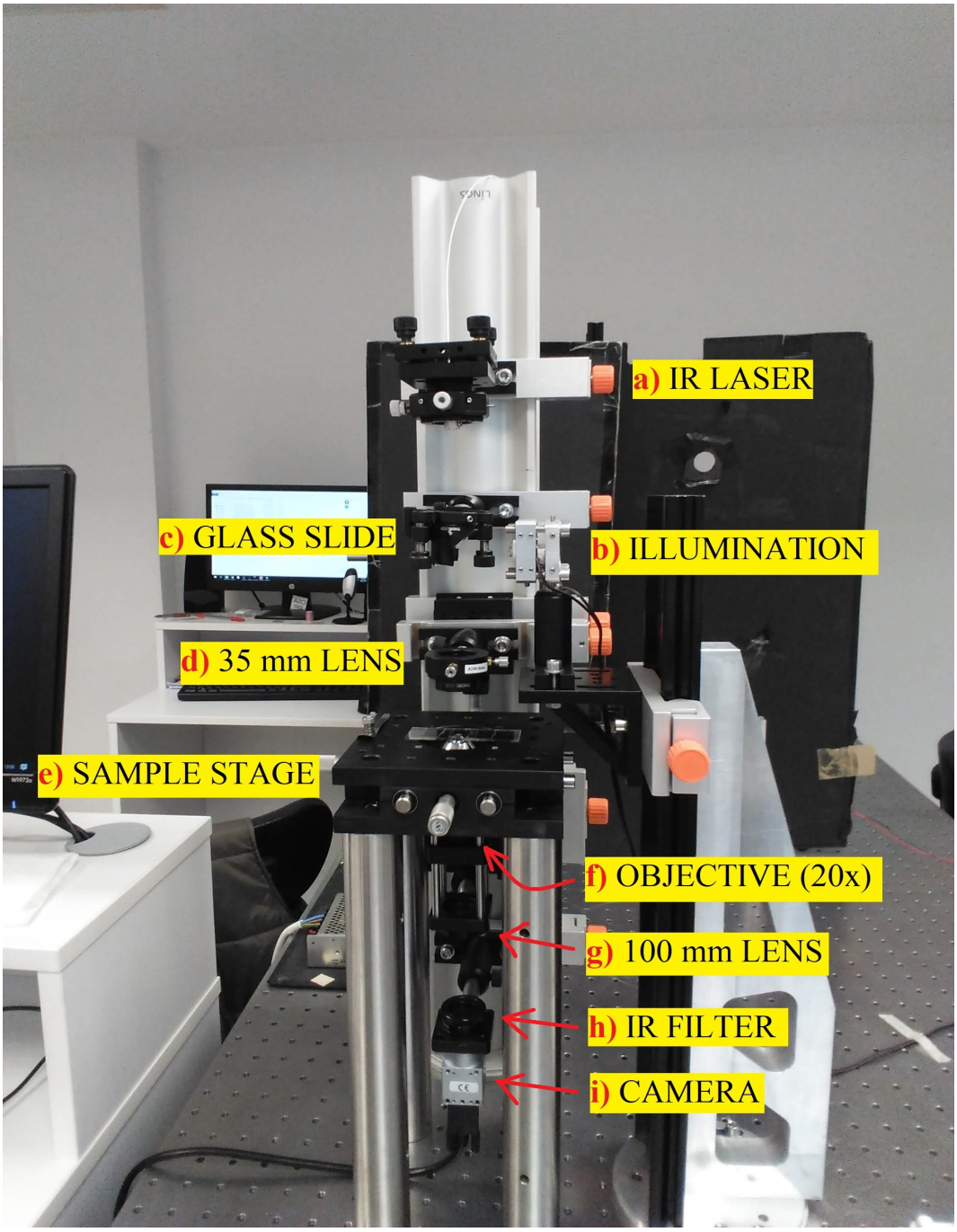


Figure 3.2: Picture of the optical setup.

## 3.2 Sample Properties and Focal Plane

In our experiments, we used two different sample cells. One is manufactured polymer cell designed for biological applications. Other one is hand-made closed volume by sandwiching method with microscope glass slides.

Hence, the experiments are held on 2D plane at the sample bottom surface, the beam is slightly out of focus in one of the cases. In figure 3.3, the places of the focal plane during the experiments for each substrates are shown. Then, below, the properties of the sample cells are separately explained in detail.

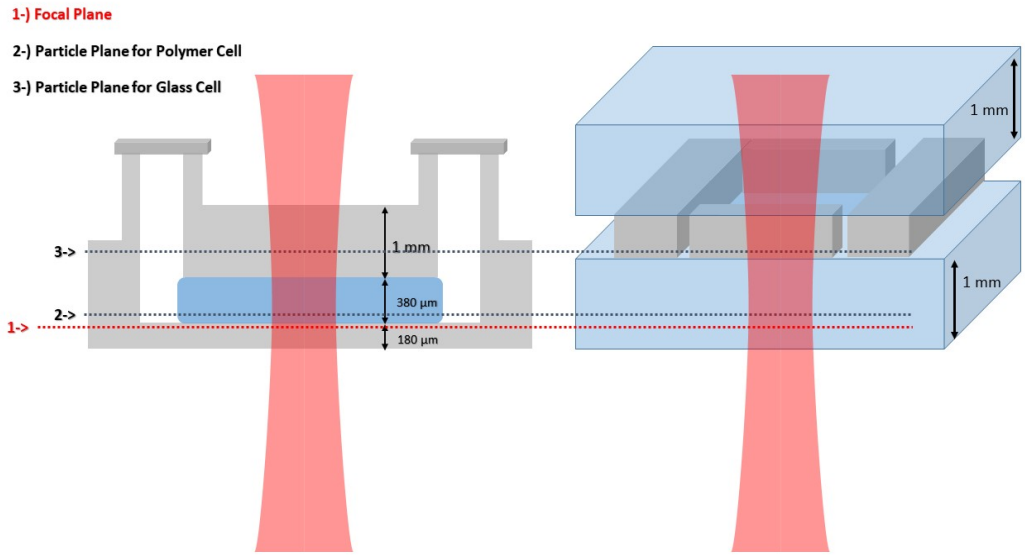


Figure 3.3: Schematic of the place of the focal plane for both the polymer cell (left) and the glass cell (right). The focused Gaussian beam is drawn in an exaggerated way to better present the place of the focal plane and to emphasize the convergence of the beam.

Here, the change of the particle plane doesn't alter the effect of optical beam. This is because the Rayleigh distance is three times bigger than the difference in focal plane. (See Fig 3.4 ) From figure 3.3, the difference in focal plane is approximately 820 $\mu$m. However, the Rayleigh range is around 3.7 mm from the

formula $z_R = \pi\omega_0^2/\lambda$. Indicatively, the change in beam waist doesn't exceed the Rayleigh range, thus it is fair to assume that, *the experimental conditions* can be perceived as *similar enough* to compare the results in two different cells.

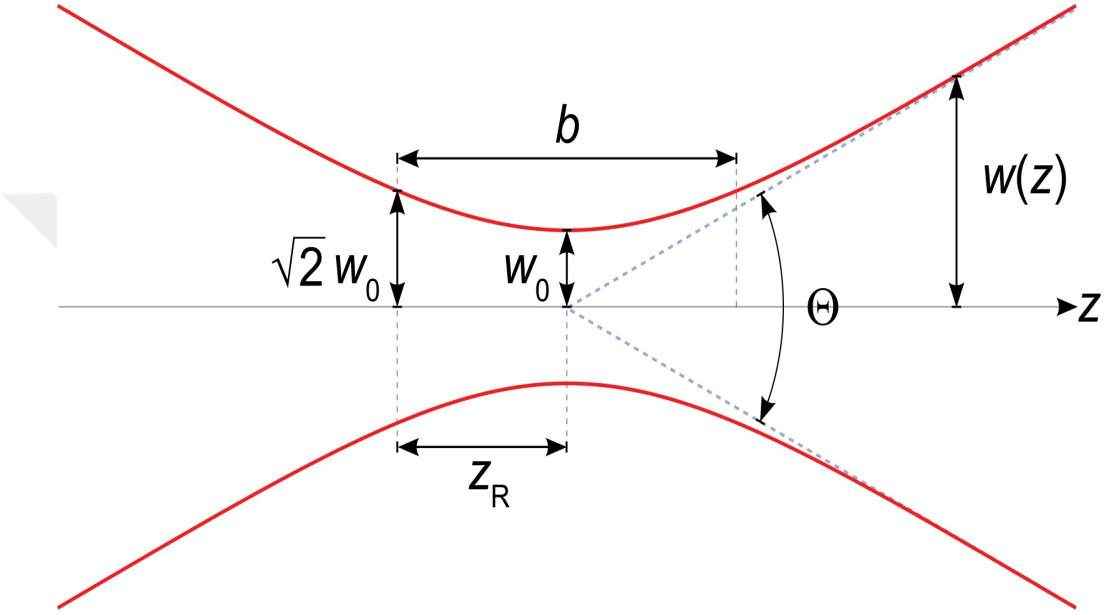


Figure 3.4: The Rayleigh distance or Rayleigh range $z_R$ is defined as the distance between the focal plane and the plane where the beam waist increased $\sqrt{2}$ times. (52)

### 3.2.1 Manufactured Cells

We used a manufactured channel slides which are commonly used for live cell imaging. The reason why we choose to use it as a substrate is that mainly because they are easy to handle, they are more biological friendly and they provide us more controlled environment such as channel size and volume. As these ibidi $\mu$-Slide VI 0.4 Channel Slides (Fig 3.5) has standard size and volume, it is more authentic way to fix the independent variables such as thickness of the sample, flow conditions in the sample, width of the sample and surface property of the sample.

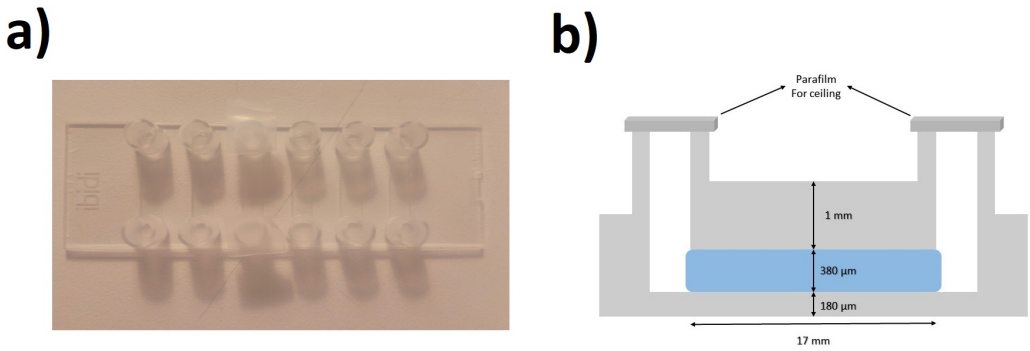


Figure 3.5: The ibidi $\mu$-Slide VI 0.4 Channel Slide a) View from top, b) Sketch from a side. The sample substrate (bottom of the slide) is a derivative of a polyethylene with thickness 180 $\mu$m. The top of the cell is also same material with a thickness 1 mm. One slide consist of 6 cells and one cell has volume 25 $\mu$Liter. The thermal conductivity of this polymer is 0.5 (Watt/(Kelvin.meter)) whereas the water has 0.6 (W/(K.m)) (53). The refractive index of the slide is the same with Glass (n=1.52). After filling the cell with a suspension, each cell is sealed with parafilm.

### 3.2.2 Hand-made Small Chambers

Another method to prepare the sample that I used in my experiments is by using microscope glass slides and parafilm. (Fig 3.6) Simply, sandwiching two glass slides with a parafilm provides an enclosed area which I can fill my sample. Heating the sandwich at 125 °for 1 minute and leaving it to dry make the parafilm tightly stick to the glass surface and water doesn't slip into parafilm. And then, I can fill my sample with a suspension and seal it with parafilm again.

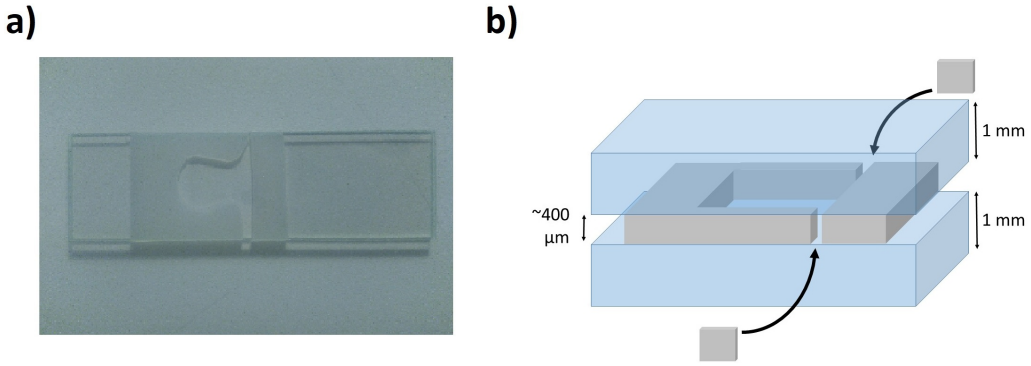


Figure 3.6: The hand-made sample chamber by sandwiching two microscope slides (Marienfeld Germany (54)) with a four folded parafilm (IsoLab Turkey (55)). a) View from top, b) Sketch from a side. In this case, both the sample cell substrate (bottom of the slide) and the top of the cell is glass with thickness 1 mm. is also same material with a thickness 1 mm. One slide consist of 1 cell and one cell has volume approximately 50 $\mu$Liter. The thermal conductivity of glass is 1.05 (Watt/(Kelvin.meter)) while the polymer cell has 0.6 (W/(K.m)) (53). The refractive index of the glass slide is (n=1.52). After filling the cell with a suspension, it is sealed with parafilm from both sides.

Here, I used same cleaning protocol to prepare sample cells (Ethanol, Iso-propanol and Water treatment and air blowing). The microscope slides (Marienfeld, Germany (54)) are cleaned (1-2-3) and treated with NaOH (4-5-6) in a following way;

1) first sonicated in ethanol for 1 minutes,
2) Sonicated in iso-propanol for 1 minutes,
3) Sonicated in distilled water for 1 minutes,
4) Sonicated in 2/3 Molar NaOH for 1 minutes,
5) Sonicated in distilled water for 1 minutes,
6) Dried with air pump.

Additional to cleaning, I treat the glass slides with NaOH to make them more hydrophilic. The reason for this is to prevent the sticking of particles to the surface by the help of hydroxyl groups or ($ONa$ has the same charge '-1' with

$OH$) on the glass substrate. (56) As the colloids are negatively charged and the hydroxyl groups are negatively charged, the particles are not sticking to the glass substrate when they settled down. (Fig 3.7)

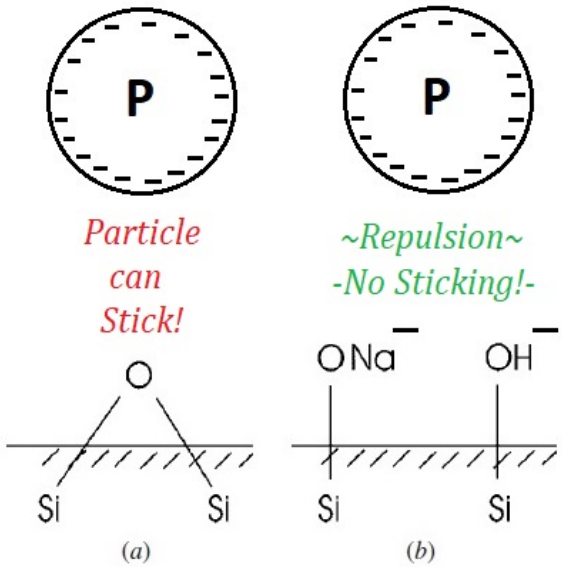


Figure 3.7: a) Before the glass substrate treated with NaOH, the colloids can stick to the glass b) but when the glass substrate is sonicated in NaOH (2/3 Molar) for 1 minute, the surface chemistry changes and it is negatively charged due to hydroxyl groups. As the colloids has negatively charged (Zeta Potential $\zeta \approx -50mV$), there is a repulsive force between surface and the particles and the particles don't stick to the glass substrate. Substrate sketches are taken from (56).

After this protocol, the sample cell can be prepared by sandwiching method that I explained above.

## 3.3 Fabrication of Janus Particles

Our main purpose is to investigate a different system, composed by Janus particles, that, in presence of a proper amount of illumination, may turn to be active

particles. We want to see whether the particles will be assembled, formed regular patterns or will show completely chaotic behaviour.

We fabricated artificial Janus particles in our laboratory not only because they are the simplest version of active particles but also it is easy to achieve them by simple sputtering techniques. It also allows us to tune properly the feature of the particles, such as the thickness. As the name "Janus" implies, Janus particles have two different faces made up of two different elements. There exist a variety of ways to produce Janus particles. ((57; 58; 59; 60))

In our case, we start from a spherical dielectric particle (silica and polystyrene) and coat it with a thin layer of metal (Gold). In short story, the particles are deposited on a substrate in a way that they form monolayer crystalline structure. After that, they are exposed to metallic rain in sputtering systems or thermal/e-beam evaporators. In this way, while the half of the sphere is coated with metallic layer, the other half is clean as before, shaping the Janus faces. Unlinking the particles from the substrate, finally, gives the Janus particle suspensions. Now, I will explain each step in detail.

### 3.3.1 Monolayer Deposition on A Substrate

To make Janus particles, first, it must be obtained a perfectly monolayer crystalline structure with silica or polystyrene spheres on the glass surface so that we can coat them uniformly by sputtering the gold atoms vertically to the plane of the glass.
When the droplet of the particle suspension is gently put on the glass, the liquid solvent starts to evaporate. (Fig 3.8) Meanwhile, the particles arrange themselves in a hexagonal crystalline lattice on the glass surface starting from the edge of the droplet.

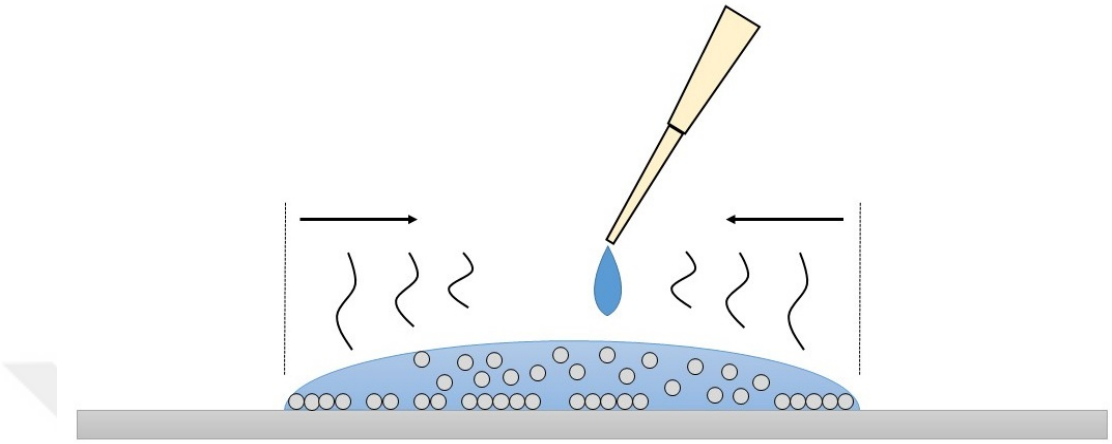

Figure 3.8: To obtain monolayer silica particles on the glass surface, I put the silica particles suspension (diameter: 4.23 $\mu m$ ) on the glass slide. Glass slides are treated in 1 molar NaOH solution for 4 minutes and they become more hydrophilic. To have an optimal crystal monolayer structure it is preferred to have a slow evaporation process. To reduce the evaporation speed, I put the glass slide into a Petri-dish. In 21 degree room temperature, with 40 $\mu L$ particle suspension droplet where the suspension concentration is 2.7 $weight/volume$, I obtained a perfect monolayer crystal shape on the glass slide.

If the droplet is too dense, then the particles are settling on top of each other. For that reason, one must try many the densities to find the optimal density to obtain monolayer crystal. When I tried many spectrum in between 5 w/v and 1 w/v dense suspensions, I concluded that there are more than one optimal density to obtain a well monolayer on the slide surface because there are several factors that affects the formation of crystal on the slide.

For example, depending on the hydrophilicity of the surface, the surface area of the droplet on the slide changes, thus the optimal value of the density of the particles in the suspensions also changes. Moreover, the drying process is very sensitive process. The temperature of the room, the air flow in the environment or the vibration of the slide may affect the crystal shape. In case of fast evaporation, the ring shaped multilayers can be seen after the evaporation. In fact, this is another research of interest for scientists and this effect is known as "Coffee-Ring

effect". (61)

To optimize the conditions, i came up with a usual method after many trials.

Firstly, each slides must have same properties. The same cleaning protocol has to be applied to the clean glass slides, because any difference in the treatment of the slides may affect the hydrophilicity of the slides thus the size of the droplet on the slide. For cleaning protocol of mine, one can see the "Hand-made Small Chambers" subsection.

Secondly, the glasses should be protected from the dust and the air flow as much as possible. For this purpose, I used Petri-dish. First, I put 30 $\mu L$ droplet on the glass surface gently and then put the glass slides into the Petri-dishes. As the air flow in Petri-dishes is slow enough, the water is homogeneously evaporated from the glass within an hour and the rest is just the crystallised particles on the surface without almost any multilayer. The room temperature is also fixed to 21 degree.

### 3.3.2 Coating

After finding an optimal conditions to obtain a monolayer on the surface, the second step is coating particles with a sputtering system or thermal/e-beam evaporators. Usually, sputtering systems are commonly used for contact applications and the resulting coated surface is less homogeneous than other methods. But, for our experiments, each technique is applicable.

The usual protocol for both of the techniques is briefly like following. First the system has to be vacuumed. Then, the argon gas is let to flow into the chambers so that the plasma phase of the metal (e.g. Gold) can be created by applying high current/thermal heating/ion gun bombarding. Finally, the heated metal atoms are raining/bombarding the sample and they attach to the surface.

In sputtering technique, we let the sputtering machine to rain the gold atoms

on the glass for 100 seconds under the 25 mA current. When the particles are coated, we get 50 nanometer thickness gold cap at the top of the silica spheres and this thickness is optimal to observe the effect of Gold cap. (Fig 3.9)

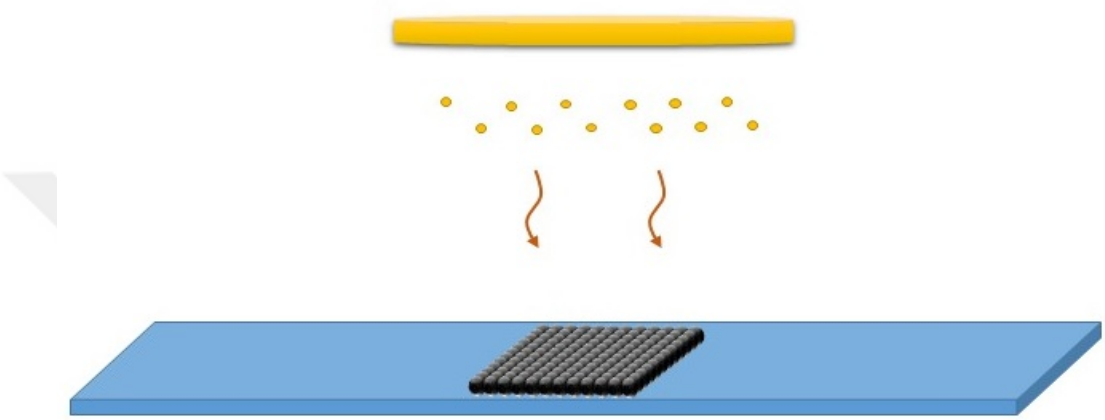

Figure 3.9: Gold atoms are sputtered onto the monolayer crystal of silica/polystyrene particles on the glass slide. (The sputtering machine serial number is C5986-220, model number is 6006-8. V = 220 volt. Frequency is 50 Hz.) The thermal evaporation is from bottom to up. (For the details of thermal evaporation technique, see the appendix.)

After a while, we started to use the thermal evaporation technique because it allows us to have more precise tuning on the thickness. This technique is commonly used for putting contact to sensitive crystals. This is because it allows to fine tune in thickness and it gives smoother coated surface thanks to the rotation and radial radiance of the thermally evaporated atoms. The coating logic is similar that of sputtering which is explained above. Additional to that, we used very thin layer of titanium coating (10 nm) between gold layer (50 nm) and the particle (few microns). This is commonly used technique to increase the bonding of gold layer to the substrate. Each thermal evaporator machine has unique regular values for coating. For our system, see the appendix.

Eventually, we get the growth of gold layer in each colloids, which then can be detached and used as Janus particles. (Fig 3.10)

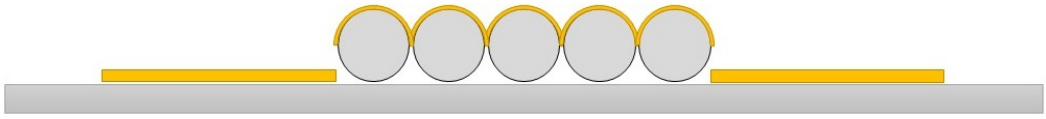

Figure 3.10: Gold layer growth.

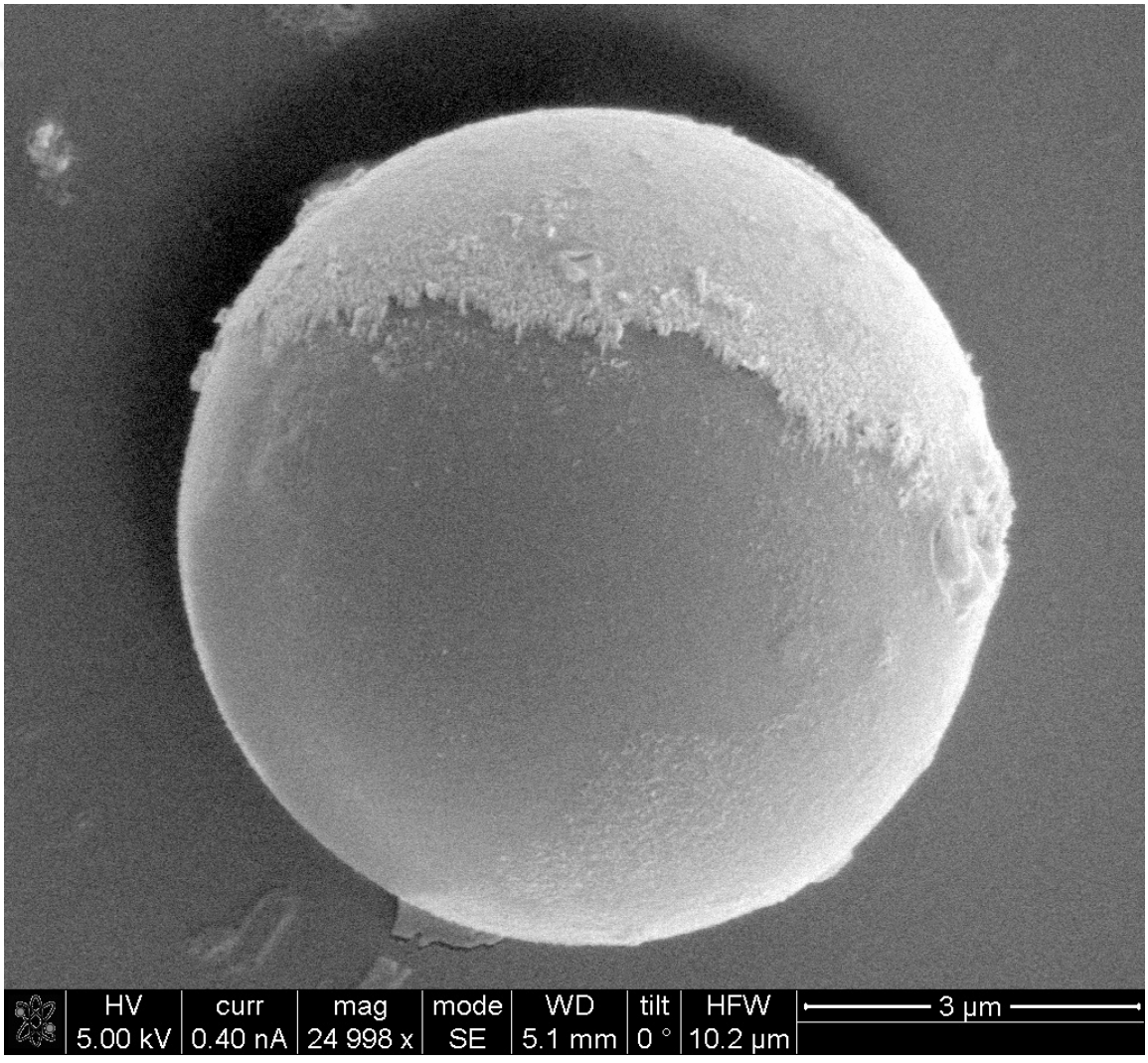


Figure 3.11: SEM image of a janus particle.

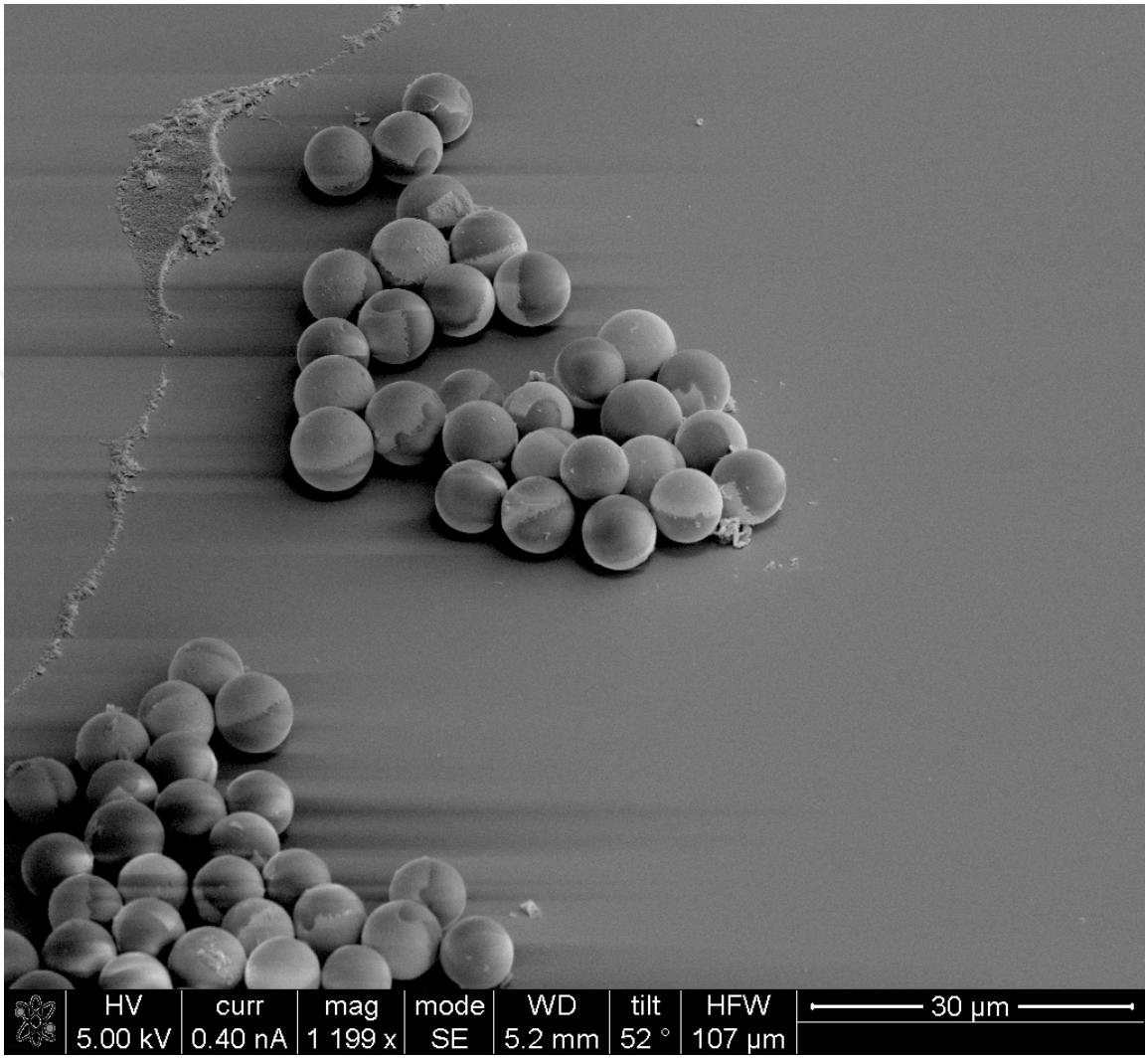


Figure 3.12: SEM image of a collection of Janus particles.

### 3.3.3 Detachement

Finally, we need to separate the half-gold coated silica/polystyrene particles from the glass surface. For this process, we just put the glass in a centrifuge tube and when we sonicate it, the particles are separated from the glass and after the tube is centrifuged, the Janus particles are settled down in the water. When we remove the glass from the centrifuge tube, we get the Janus particle solution as ready to perform experiments. (Figure 3.13)

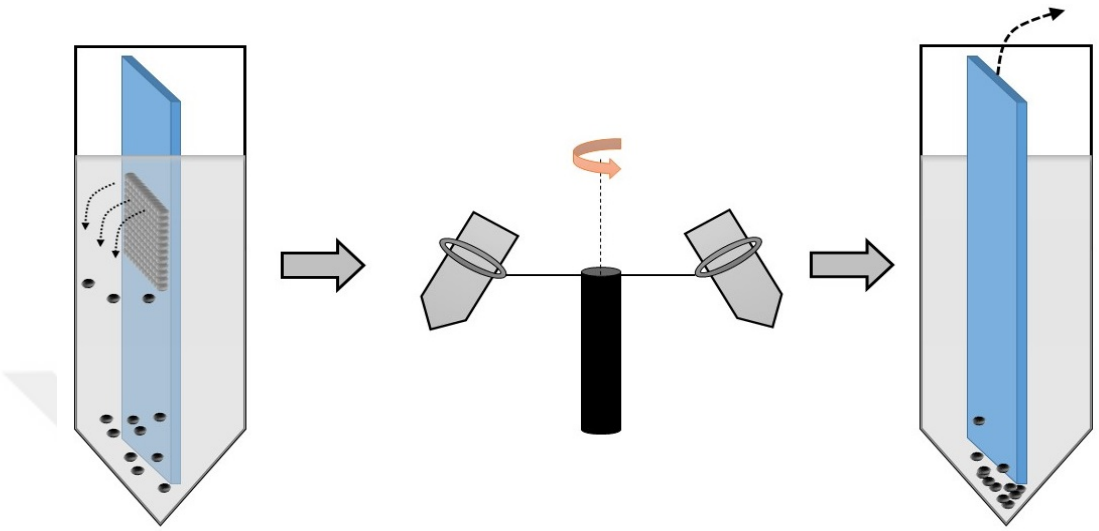

Figure 3.13: To detach the particles from the glass slide, I put them into the falcon tube and sonicate 4-5 minutes. After sonication, the tube is centrifuged and the Janus particles are settled down at the bottom. Finally, I removed the glass from the solution and get the Janus suspension.

# Chapter 4

# Results on Experimental Investigations

## 4.1 Previous Studies: Attractive Hydrodynamic Flow Exerted in the Vicinity of the Janus Particles

It has been experimentally shown that the Janus particles triggers the formation of clusters in a Gaussian optical potential. (1) Mousavi at al showed that the gold-coated silica spheres form *clusters* under smooth Gaussian beam in glass substrates (Fig 4.1). They prepared a sample which contains both silica spheres and gold-coated silica spheres with same dimensions in water medium which is sealed between two sandwiched glass slides. They put the sample under a smooth wide Gaussian optical potential. They recorded the behaviour of the particles by using inverted microscope and CCD camera. They observed that the Janus particles goes out from the center of the Gaussian beam and form a cluster at the periphery of the Gaussian beam waist. Also, in the case of mixture, the passive particles are attracted by the JPs and they form close-packed clusters (Fig 4.1).

Here, the key factor for the clustering is the presence of an *attractive* hydrodynamic flow around the JP vicinity triggered by the local thermal gradient created by light absorption of the Gold coated part.

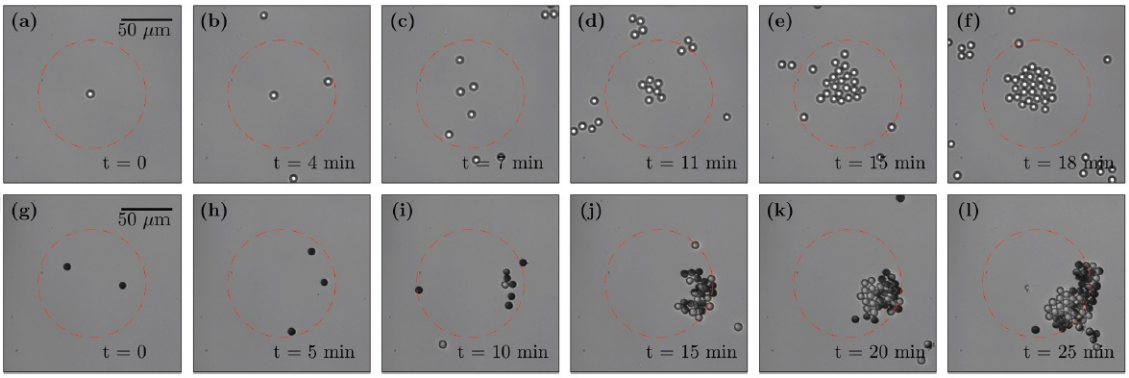


Figure 4.1: Representative pictures from Mousavi at al (1). Experimental time sequence of the dynamics (a–f) of silica particles and (g–l) of a mixture of Janus particles and silica particles (all particles have diameter 6.73 mm) in a Gaussian optical potential (beam waist 90 mm, power 100 mW). (a–f) The silica particles are pulled towards the centre of the optical potential, but do not form a close-packeded colloidal crystal because of the absence of short-range attractive forces. (g–l) When also Janus particles are present, clusters form away from the centre of the optical potential.

Before getting into our work, it is worth to mention another example study on clustering behaviour of JPs which belongs to Singh at al. An attractive forces near Janus particles exerted due to the Janus particles themselves are reported as a result of the observation of formation of flower like structures around JP by passive particles in the case of mixture suspensions where the constituents are the JPs and the passive particles. The driving mechanism for attraction of Janus particles is slightly different in this study. Here, the attractive behaviour of Janus particles is based on diffusiophoresis. Although the activity mechanism for JPs is different, still, the resulting behaviour is the same: close-packed *clustering* (62).

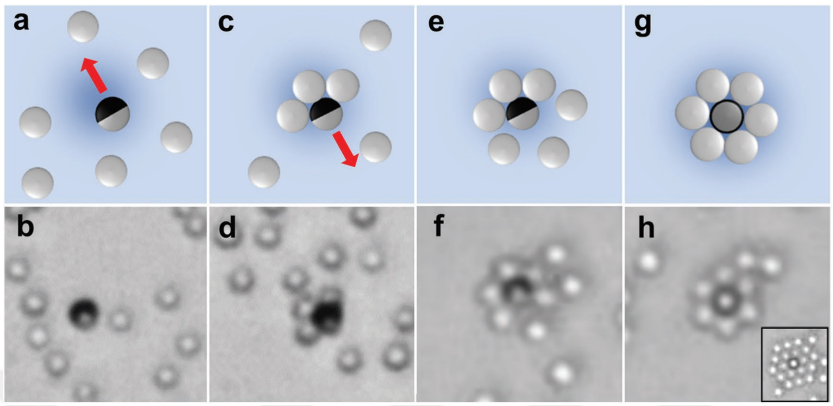


Figure 4.2: Representative picture from Singht at al (62). Growth of a flower-like cluster comprised of a JP (center) and surrounded by the passive particles.

A theoretical suggestion made by Golestanian predicts that depending on the thermal diffusion properties of the material, this clustering can be reversed into short-range repulsive behaviour. (63) Here, in our study, we also investigate the behaviour of a system composed of Janus particles (polystyrene/silica microspheres half-coated with gold) close to the bottom surface of the substrate in the presence of a wide Gaussian optical potential. Normally, Janus particles tend to create close-packed clusters when they are triggered by such an optical potential. However, in our study, we experimentally demonstrate *non-clustering* behaviour of JPs, also reversible, with short range repulsive gathering triggered by the presence of an optical potential in polymer substrate. (Fig 4.6)

Unlike the previous examples given above, we observed that the JPs doesn't form close-packed crystalline clusters in polymer substrate. Our investigations shows that the substrate property plays a critical role for the nature of the interaction among the Janus particles; it can reverse the attraction into repulsion, thus the close-packed clustering into gathering of hard spheres with short-range repulsion.

## 4.2 The Forces Acting on Janus Particles

Starting with a simpler example of spherical particles; if we consider spherically symmetric transparent colloidal particles (e.g. silica or polystyrene), their interaction with light can be modeled by geometrical optics tools and the characteristics of the forces can be described very well with the theory when the dimensions of the particles are bigger than the wavelength of the radiation (in our case, the wavelength ($\lambda$) is 976 $nm$ and the particle size is $r = 3\ \mu m$) (see section 2.4).

When such simpler spherically symmetric particles are exposed to a wide Gaussian beam, like in our case, they are attracted to the center of the beam and form a growing aggregate starting from the center. Although there is no self-induced attraction among particles, these colloids can form tightly packed aggregate depending on particles' concentration; if many particles are attracted, they form a crystal at the center of the Gaussian beam because of the "pressure" due to the outer particles. (For the aggregate caption from an experiment see Fig 4.4b) Mainly, the physical force playing a critical role in aggregate of colloidal particles in this observation is based on the optical force through the direction from outside to the center of the beam. (Fig 4.3 )

In the case of JPs however, the optical potential is not attractive due to the light reflection from the gold-coated part when the orientation is cap down. (Fig 4.3 ) Yet, numerous number of particles keep coming to the beam spot from far distances as long as laser is on. An intriguing question in here is that why the Janus particles are drifted to the Gaussian beam although the optical force is pushing them away.

Furthermore, there seems to be a quasi-equilibrium radial position for Janus particle during the experiments.[1] As if the drifted Janus particles from far distances to the beam are repelled from the center of the Gaussian beam to the periphery of the Gaussian beam waist and stays there as an equilibrium for a while until they become rotated. (Fig 4.4)

[1] What I refer by saying "quasi-equilibrium" is that until the particle change the orientation, the particle seems to be in equilibrium.

To resolve the drifting mechanism of JPs and the non-close pack behaviour of the JPs, we started with the investigations on the effect of the laser power to the JP behaviour. Then, we continued with the two sets of main comparative experiments with two different kind of particles (silica and polystyrene, with diameter $D = 6.73,\ 6.23\ \mu m$ respectively.)

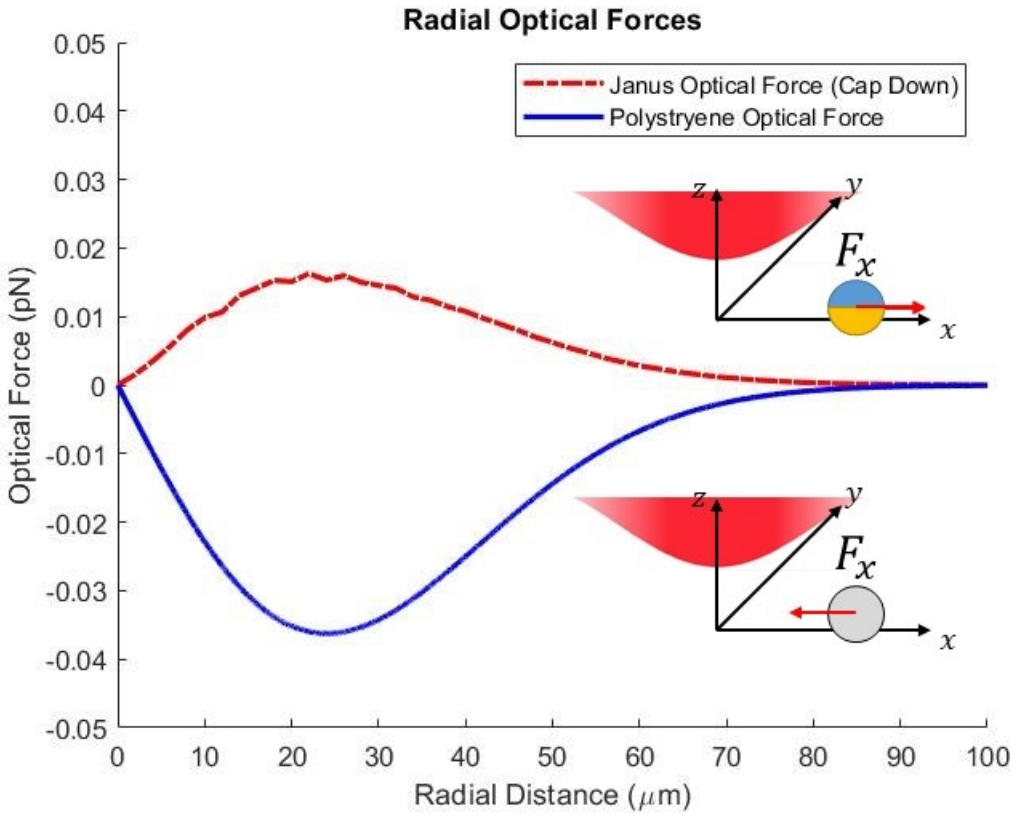


Figure 4.3: The radial optical forces through the direction from the center of the beam to the outside of the beam. The blue line shows attracting force for polystyrene particles. The red-dashed line shows repulsive force for Janus particles with cap-down orientation.

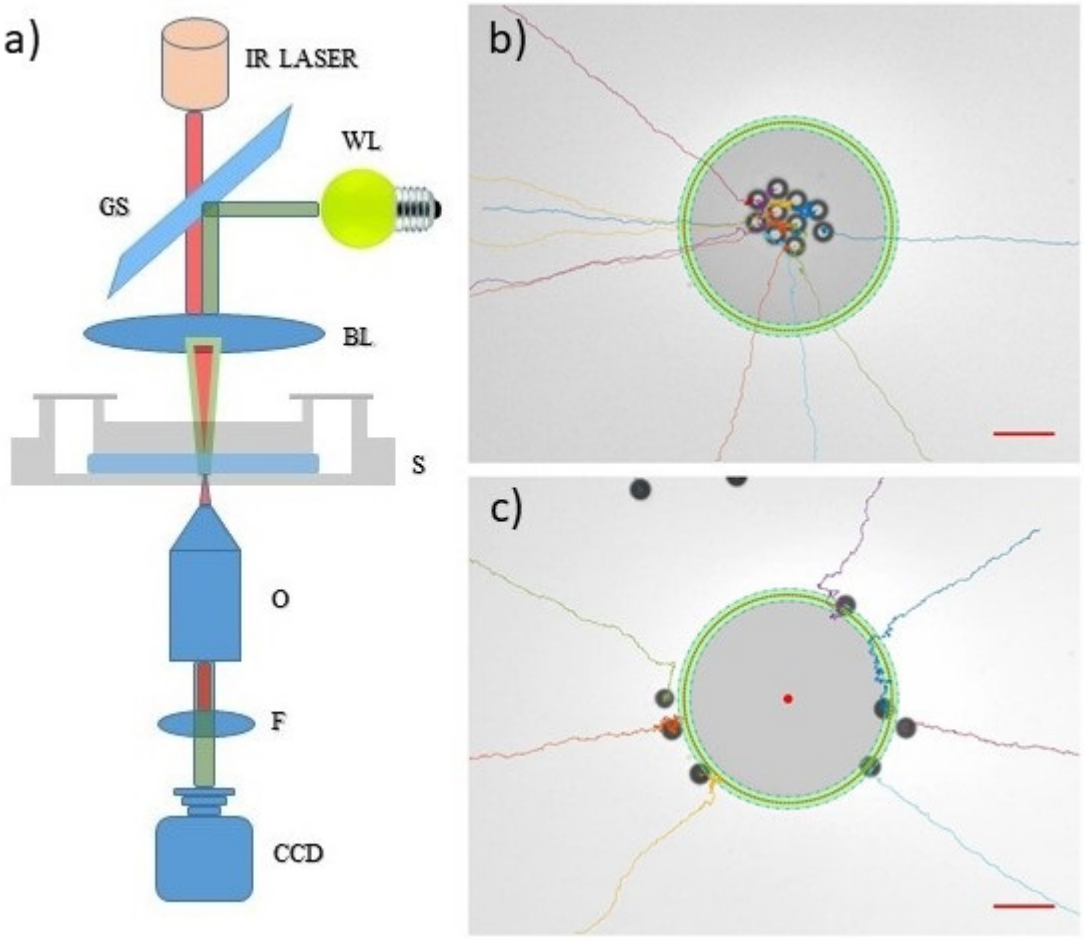


Figure 4.4: a) The schematic of the experimental setup. Infra-Red Laser, (GS) glass slide, (WL) white light, (BL) biconvex lens (f=25,4 mm), (S) sample, (O) objective, (F) infrared filter, (CCD) camera. b) An experiment with only polystyrene particles (D=6.24 micrometer) snaphost with particle trajectories. c) An experiment with only Janus particles (PS D=6.24 micrometer + Gold 50 nm) snaphost with particle trajectories. JPs stay at the periphery of the Gaussian beam while the PS particles goes to the center of the beam. Red arrow indicates a scale which is 20 micrometer.

On preliminary set of experiments, we investigated the effect of the different laser powers [20, 40, 60, 80, 100, 120, 140 mW] to the behaviour of the particles (with only polystyrene particles, with only Janus particles, with mixture of both types of particles) in polymer cell. (Fig 4.5)

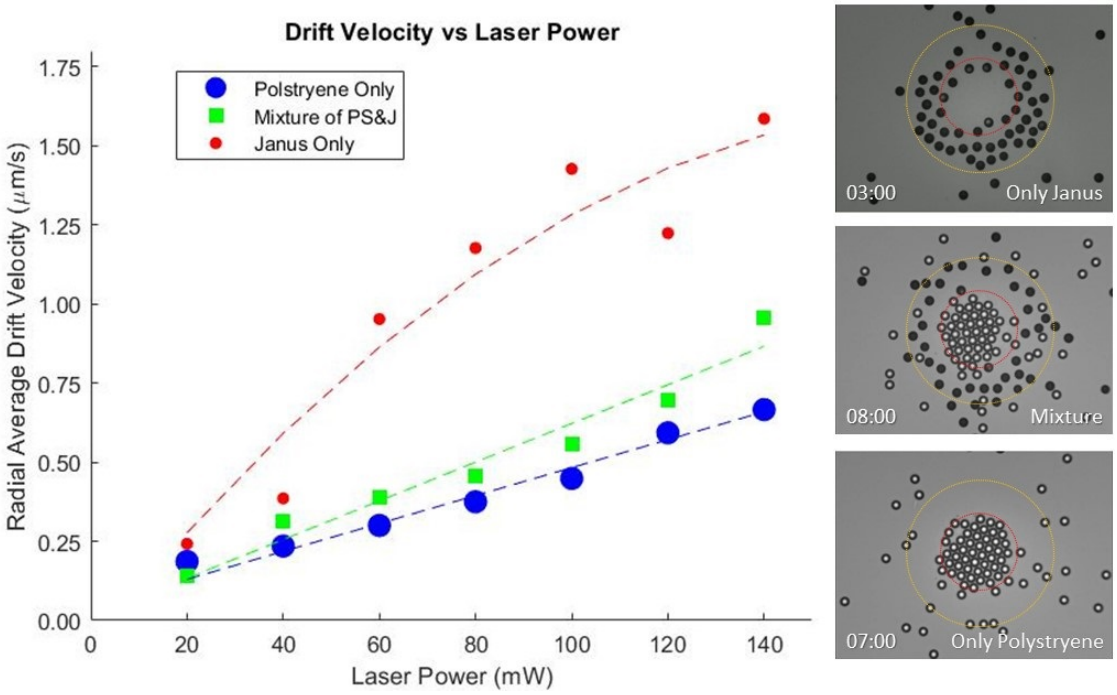


Figure 4.5: Average drift velocity of the particles at the radius in between 60-90 $mu$m. The circular red dots are for the experiments where the sample includes only Janus particles. The circular blue dots are for the experiments where the sample includes only polystyrene particles. The green squares are for the experiments where the sample includes mixture of both Janus and PS particles. The mixture drift velocity value of any green square is the average of drift velocity of two kind (Janus&PS). The drift velocities for Janus particles above are calculated before any of the Janus particles gets into the beam spot.

These experiments indicates that the drift velocities of the particles increases with the laser power increase. (Fig 4.5)

The increase in the drift velocity of the polystyrene particles seems to be linearly fitting with the laser power increase (see Fig 4.5 - blue dots) Even in the

case of the mixture, the increase of the average particle drift velocity of the two kinds (JPs and polystyrene particles) is linear.

However, the increase of the drift velocity of Janus particles does not have a linear tendency when the suspension contains only Janus particles. (see Fig 4.5 - red dots)

This difference in polystyrene and janus behaviour leads us to seek the drift velocity of the Janus particles in temporal evolution in a constant laser power more carefully. In the incoming sections, it is also going to be discussed in detail the importance of these investigations.

Consequently, it turns out that the variance of the laser power (around 40-120 mW) affects only the time-scale of the experiment but not alter the behaviour significantly. After this realization, we continued with the comparative experiments with a fixed laser power 100 mW which is optimal us to analyse various behaviours together.

In this study, the main focus is more of on the effect of the material of the substrate to the *attractive* nature of the Janus particles. To check the effect of the substrate to the JP behaviour, two sets of comparative experiments are conducted with two different substrates: polymer and glass. (Fig 4.6)

When the Janus particles are in glass substrates, they are forming a tightly close-packeded crystalline structure as in Fig 4.6 (c and d). Nonetheless, when the Janus particles are in polymer substrates, they are pushed from the center to the periphery by the optical forces first, when the JPs are in cap down orientation (Fig 4.3). After a while, the JPs are rotated and they are pulled back to the center by the optical forces but they never attract each other and no formation of crystalline cluster is observed (Fig 4.6 a and b).

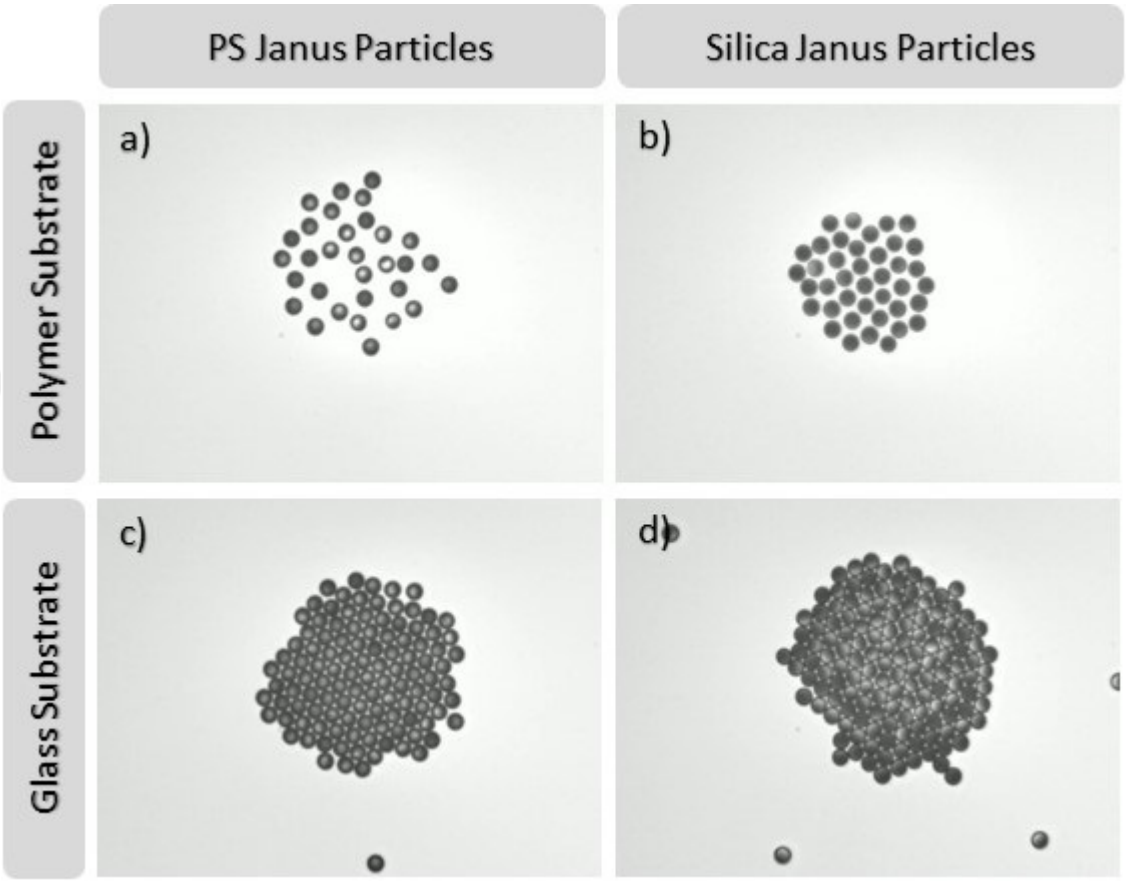


Figure 4.6: The captions showing eventual behaviour in different substrates are from separate experiments. In all 4 experiments, the particles are exposed to a wide Gaussian beam with $w_0 = 34\ \mu m$ beam waist. (a) The PS Janus particles (50 nm Gold half-coated polystyrene colloids with radius $r = 3.12\ \mu m$) are in polymer substrate. (b) The Silica Janus particles (50 nm Gold half-coated silica colloids with radius $r = 3.32\ \mu m$) are in polymer substrate. (c) The PS Janus particles are in glass substrate. (d) The Silica Janus particles are in glass substrate.

Before getting into the detailed explanations of the results of the comparative experiments given in Fig 4.6, it is important to refer some of the physical mechanisms such as the thermal diffusion coefficient and the hydrodynamic flow direction which are playing a key role for the eventual difference in behaviour in two different substrates.

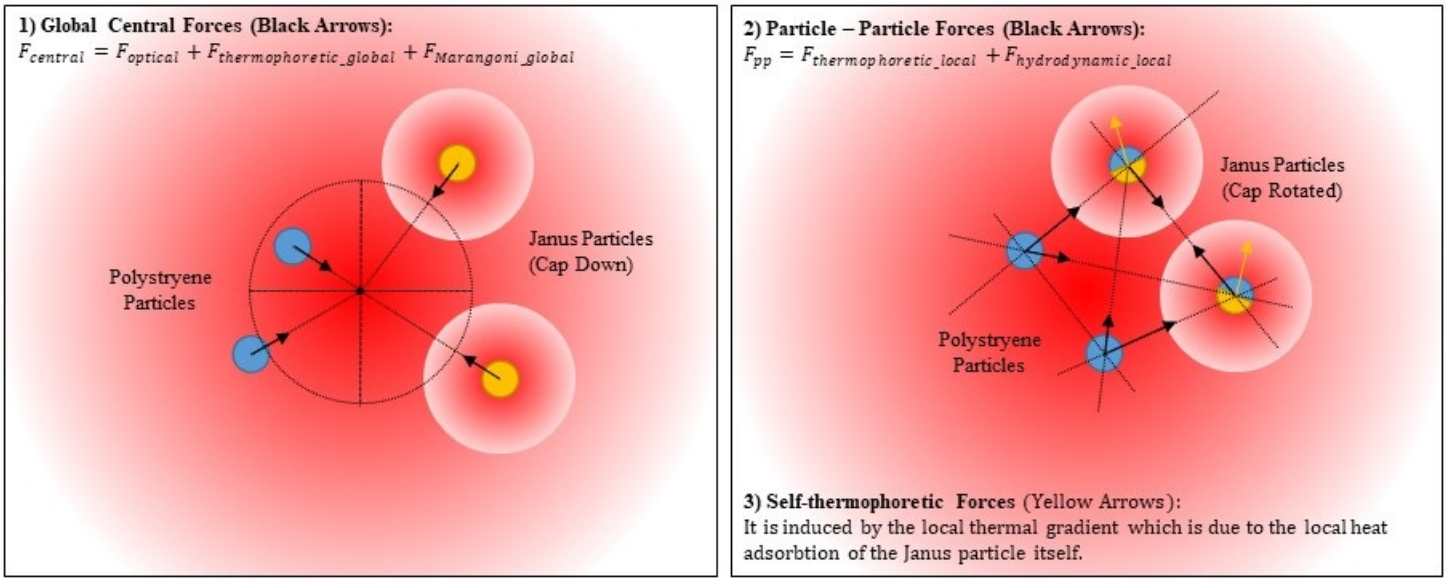


Figure 4.7: Schematic explaining the forces acting on the particles. There are three types of effective external global forces that acts on all kinds of particles. (1) These are the optical forces, the thermophoretic forces and the global hydrodynamic flow inside the sample cell. These are in radial direction for polystryene, silica, and Janus particles with cap down orientation. (2) Apart from the global forces, there are also interparticle forces which is due to the nearby Janus particle. Due to the Janus particle the local thermal gradient results in local thermophoretic forces and local hydrodynamic forces acting on other particles. (3) Finally, the self-thermophoretic force is a type of force on a Janus partice that is caused by the Janus particle itself. It's direction depends on the Janus particle orientation.

Starting with the physical forces that are acting on the particle during the experiments, the effective physical forces that are drifting the particles into the center of the beam by overcoming the Brownian noise are two types (at first glance); the optical forces and the thermophoretic forces. ( For the types of forces see Fig 4.7) As the optical forces are explained in detail in geometrical optics section, I skipped this part as it is already familiar to the reader.

The thermophoretic forces are the forces triggered by the thermal gradient itself without any effect of the hydrodynamic flow in medium. When a colloidal

particle is in a medium which has thermal gradient throughout the medium, the colloidal particles start to move in the direction of the gradient. So, the thermal diffusion coefficient is determining the amount and the direction that the drift velocity of the particles;

$$v_{drift} = -D_T \nabla T \tag{4.1}$$

This coefficient is highly dependent on the particle-medium molecular interaction and it can even reverse its sign.

However, if we consider just these two forces (the optical forces and the thermophoretic forces), we see that the amplitude of the net force at the distances which are far away from the center of the Gaussian beam goes to zero. Thus, none of the far distant particles has to be affected by the presence of the optical potential. Yet, numerous number of particles still keep coming to the central region in time.

Besides, if we analyse the drift velocity of the polystyrene particles from the experiment, we see that the particles that is outside of the beam waist has a constant speed until they come close to the periphery of the Gaussian beam (Fig 4.11). However, the sum of the calculated optical forces and calculated thermophoretic forces are not adding up to the analysed constant value from the experiment. (Fig 4.10 c and d) One would expect that there must be another force to call the particles at far distances.

Rather than a force acting on a particle, a flow of water inside the whole chamber due to the temperature gradient is a worthy option to check in a liquid system. The steady-state temperature gradient profile is triggering the fluid to have continually convective flow inside the chamber, which is called a Marangoni flow in literature. (see section 4.3 ) To gain a better understanding on this observation, it is important to see the results on our investigations of the nature of the Marangoni fluid flow first.

## 4.3 Marangoni Fluid Flow in Sample Cell

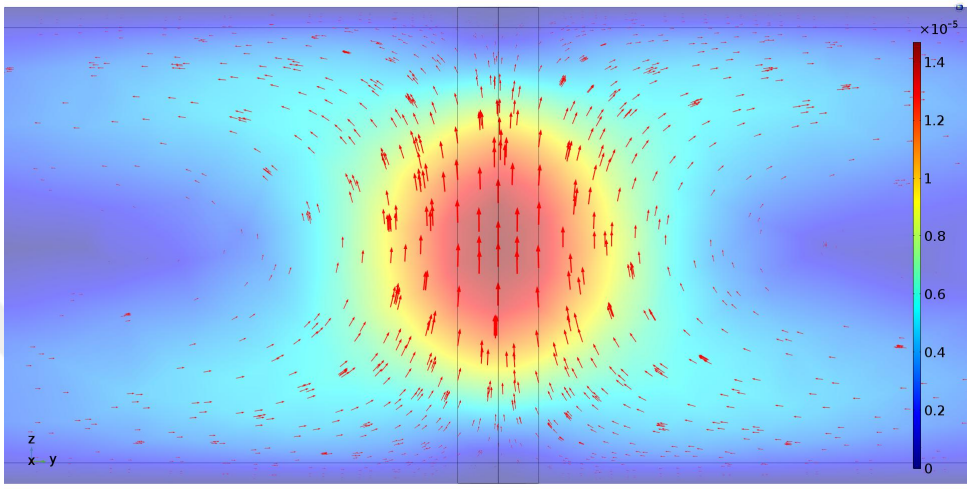


Figure 4.8: The resulting velocity profile of the fluid from the lateral cross section of the sample cell in COMSOL is shown in figure, when the water is exposed to the Gaussian beam in closed sample cells. The arrows shows the direction of the fluid flow. Figure is colour coded.

When an infra-red light is focused onto the particle plane in sample, it is partially absorbed by the water and heats the sample until the temperature profile in water reaches a steady state thermal gradient with the environment. This thermal gradient is resulting in fluid flow due to the stokes boundary conditions. [2] To see the effect of the Marangoni fluid flow, the stokes equation coupled with heat transfer is solved by COMSOL for our experimental conditions (see Sample Properties chapter.). At first glance, the resulting velocity profile (Fig 4.8) is not far away from the order of magnitude of the drift velocity of the particles in our experiment. The cross section from the lateral view of the sample is in Fig 4.8

The fluid flow velocity profile that we are interested in is not the whole sample but is at the particle plane (The longitudinal cross section of the sample cell and the velocity profile is given in Fig 4.9). Considering the fact that the particle

[2]The COMSOL has built in Stoke's equation solver. The stokes boundary conditions indicates that there is no slip and no through flow at the boundary. (64)

radius is around 3.5 micrometer, the center of the particles must be at most 4-5 micrometer up from the bottom sample surface. The particle plane can also be observed and determined experimentally by looking at the particle resolution at the optical focal point on the optical setup.

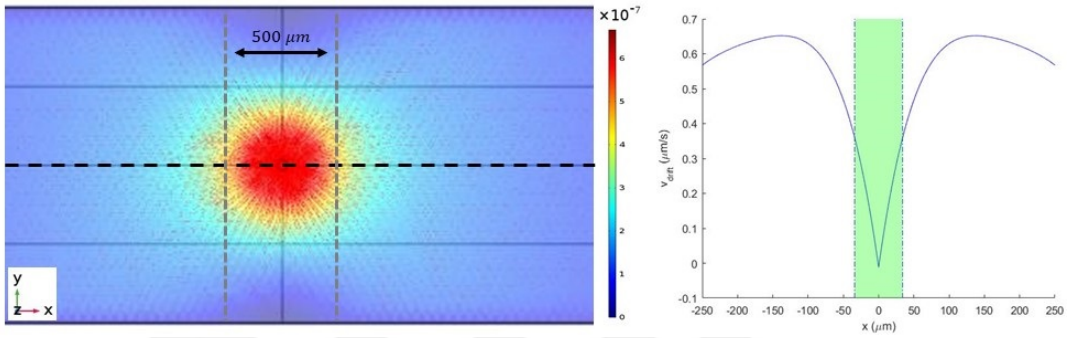


Figure 4.9: The resulting velocity profile of the fluid from the horizontal cross section of at the bottom of the sample cell (4 micron above from the bottom which is approximately ($\pm 1 \mu m$) the particle plane) is shown in figure. Figure is colour coded. The green shaded area is showing the Gaussian optical potential. The velocity of the fluid just outside of the periphery is close to the 0.6 at the bottom plane which is almost the drift velocity of the particles that is measured from the experiments.

At the bottom of the sample cell -at the particle plane-, the COMSOL simulation result of the fluid velocity profile at the outside of the beam agrees with the drift velocity of the particles that is measured far away from the Gaussian beam waist from the experiments (Fig 4.10).

If the optical forces and the thermophoretic forces acting on the PS particles are used in simulation without adding the hydrodynamic pattern drifting, the resulting drift velocity profile wouldn't match with the experimental drift velocity measurements. (Fig 4.10 c and d) However, if the resulting velocity profile from the COMSOL (Fig 4.8) is embedded into the Matlab simulations as an additional drifting velocity, the resulting velocity profile is perfectly matching with the experimental analysis made by digital video microscopy techniques (DVM). (Fig 4.10 e and f)

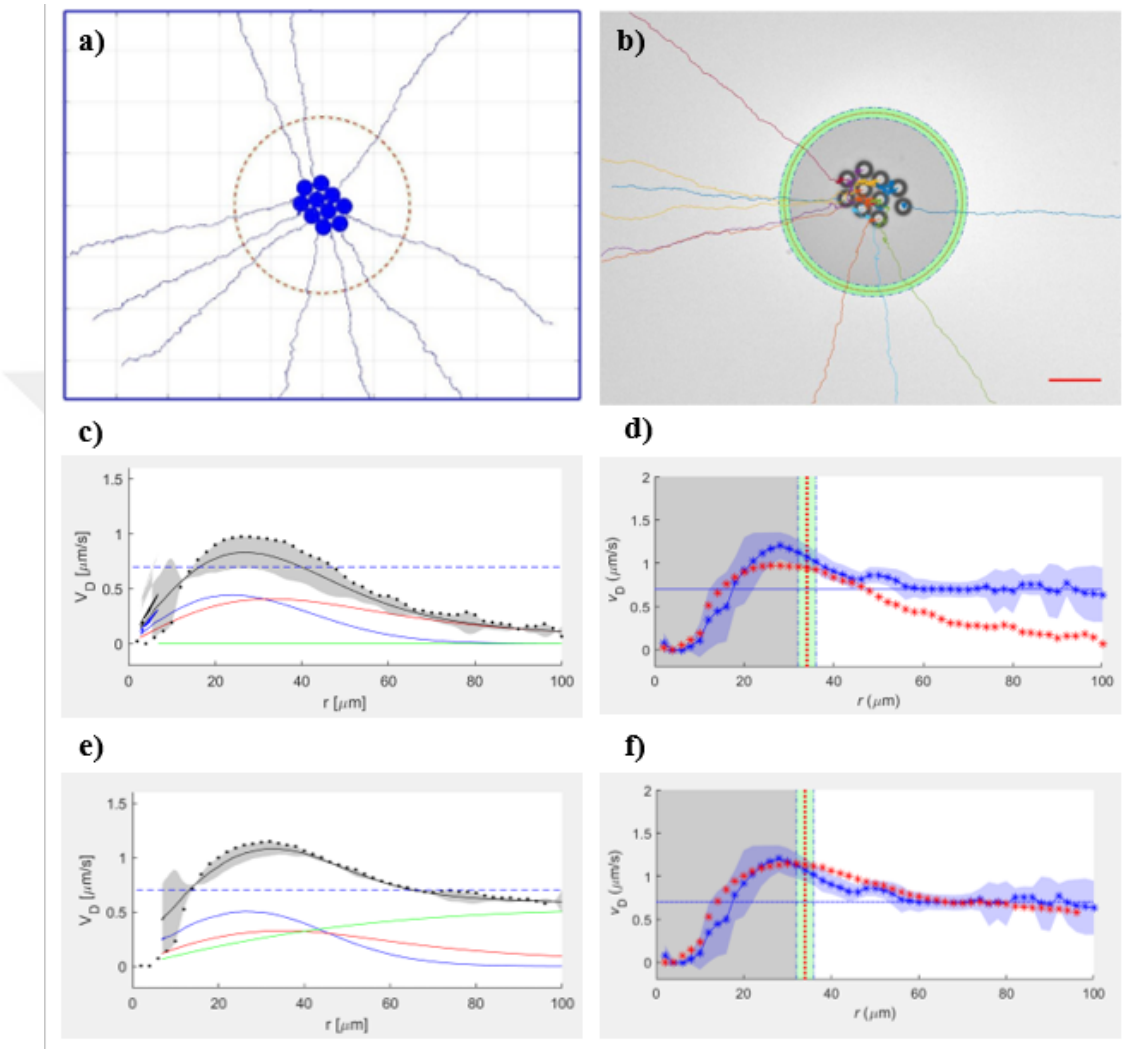


Figure 4.10: The analysed velocity profile of the polystyrene particles (b) are consistent with our simulations (a). In (c) and (e), the simulation outcome of the drift velocity profiles are shown. The optical forces (blue line) and the thermophoretic forces (red line) are the two constituent forces for drifting the particle to the center. The green line in part (e) showing the hydrodynamic pattern profile obtained from COMSOL. If the hydrodyanmic fluid flow is not considered, then the outcome of the drift velocity from the simulation (d-red part) doesn't match with the experiment (d-blue part). But if it is taken into account, then the drift velocity from the simulation (f-red part) perfectly matches with the experiment (f-blue part). The shaded areas are representing the Brownian noise.

Consequently, the hydrodynamic pattern in sample cell is the effective drifting trigger to the particles from the far distances to the center of the beam (Fig 4.9) In another words, the only considerable drifting effect at the outside of the beam waist is coming from the fluid flow inside the overall sample through radial direction. This fluid flow is named Marangoni convective flow. This hydrodynamic effect is directly observable and approved and consistent by the COMSOL simulations outcome. (Fig 4.9 and Fig 4.10)

As this hydrodynamic pattern is triggered by the overall temperature gradient in the sample cell, the JPs heat absorption might have an effect on the overall flow profile. Thus, it is important to analyse the JP drift velocity in temporal evolution.

## 4.4 Drift Velocity Increase Due to the Janus Particles Heat Absorption

If we look at the change of the drift velocities of the Janus particles in time, interestingly, the drift velocity of the Janus particles at the outside of the periphery of the Gaussian beam waist is not constant (Fig 4.11). This is due to the fact that; when the JPs are inside or close to the periphery of the Gaussian beam, the heat absorption of the JPs is dynamically accelerating the Marangoni convection . While the Janus particle drift velocity is increasing in time, the polystyrene particle drift velocity is constant. This is due to the fact that the polystyrene particles don't absorb the IR light. For this reason, the temperature profile inside the chamber, thus the fluid flow as well, is in steady-state and don't vary in time. If we look at the drift velocity of the polystyrene particles in time, we see that it is more or less converging a constant value.[3] (Fig 4.11)

However, the Janus particle drift velocity at the same radius is increasing in

[3]For representative analysis captions; see Appendix **??**, Fig B.4 and Fig B.3

time. (Fig 4.11) This is because the temperature profile changes due to the significant light absorption of the Gold coated part when more particle comes closer to the center of the beam. More Janus particles leads to more heat absorption, thus broader temperature difference occurs in sample, thus significant increase in Janus particles drift velocity from outside to the center.

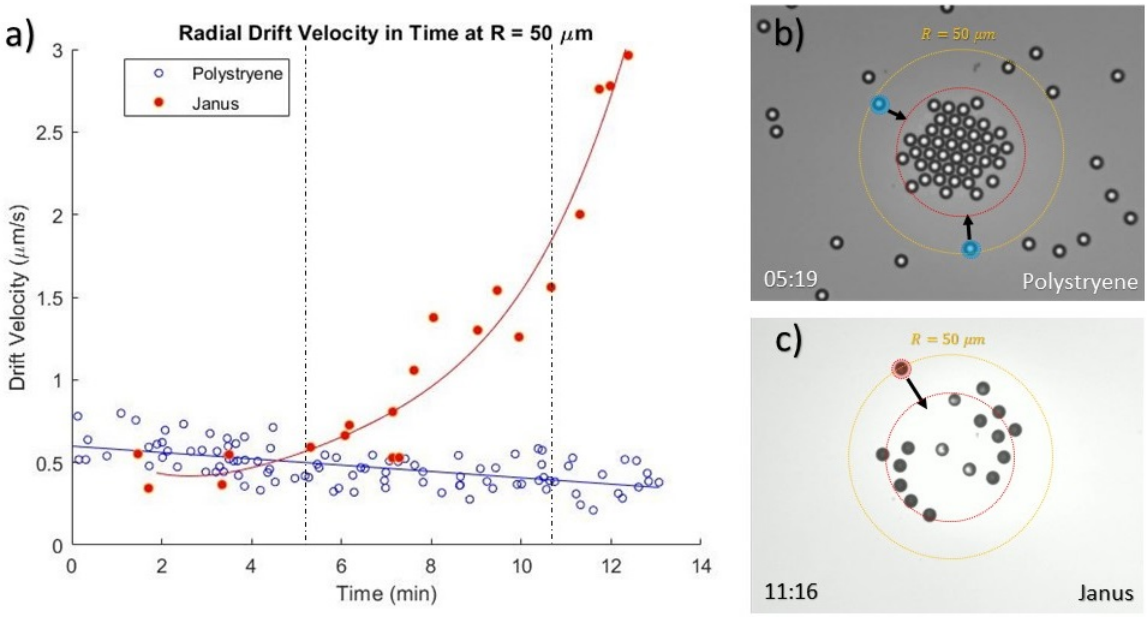


Figure 4.11: The resulting drift velocities of the polystyrene (PS) particles (blue empty circles) and the JPs (red filled dots) in temporal evolution of their experiments. The particles are under 100 mW smooth Gaussian potential with $34\mu m$ beam waist shown in red dashed circle in (b) and (c). The times of the captions (b) and (c) are indicated by dashed straight horizontal lines in graph (a). While the PS particles have constant drift velocity, the JPs drift velocity increase in time. (The little tilt in PS drift velocity linear fit is because the particles fill inside and there is no place to drift anymore after a while.)

Additionally, when the JPs that are drifted to the center of the beam come closer to the beam periphery ($34\mu m$), they don't directly enter inside of the beam waist. They stays at the periphery as long as their orientation is cap-down. As more Janus particles continue to come to the periphery, at some point, they starts to be rotated and get inside the beam waist. This observation indicates that there

seems to be an equilibrium radial position when the JP orientation is cap-down until the JPs are rotated. For this reason, it is also intriguing to understand why the JPs are not entering into the Gaussian beam until a critical point. (Fig 4.14)

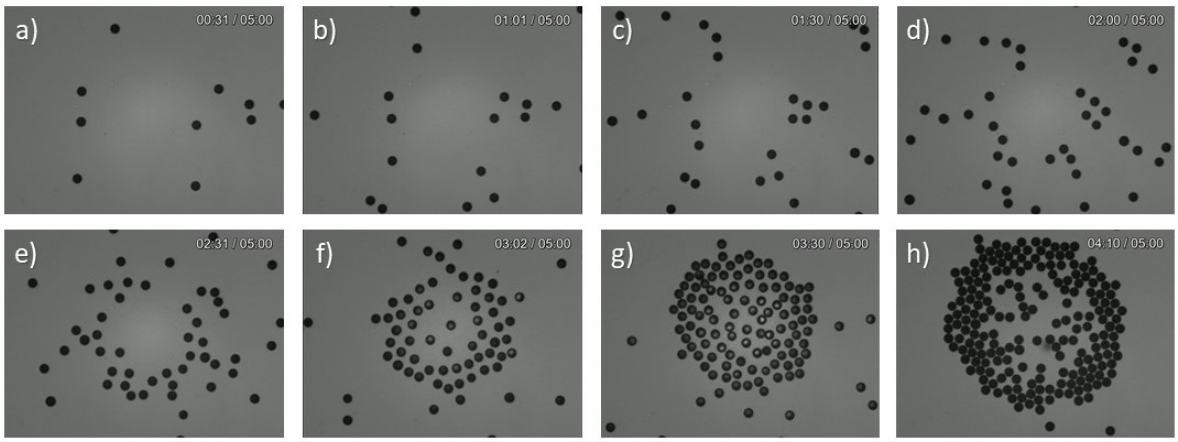


Figure 4.12: The Janus particles are under 100 mW smooth Gaussian potential with $34\mu m$ beam waist. The particles are dragged by the hydrodynamic pattern from far distances to the periphery. Yet, none of the particles enter inside to the Gaussian beam waist (a-b-c-d-e) because the optical force is pushing them away due to the Gold coated part. Whenever they are rotated, the optical force is reversed and starts to pull the rotated JPs back into the center (f-g). After the laser is closed, all the JPs goes to the orientation cap-down due to the gravity (h).

## 4.5 The Janus Particles Entrance into the Gaussian Circle

When the Janus particles are exposed to a wide Gaussian infra-red beam, their motion start to be elongated along the radial direction. The drifting mechanism from far distances to the periphery is mostly the hydrodynamic pattern. The hydrodynamic pattern due to the infra-red heat absorption of water causes drifting more Janus particles from far distances to the center of the Gaussian beam, while

the optical force direction is from inside to the the outside of the beam waist when the particles' orientation is cap-down (Fig 4.3). For this reason, during the Janus particles drifting to the center of the beam, the Janus particles do not directly enter into the center of the Gaussian beam, instead they wait at the periphery.

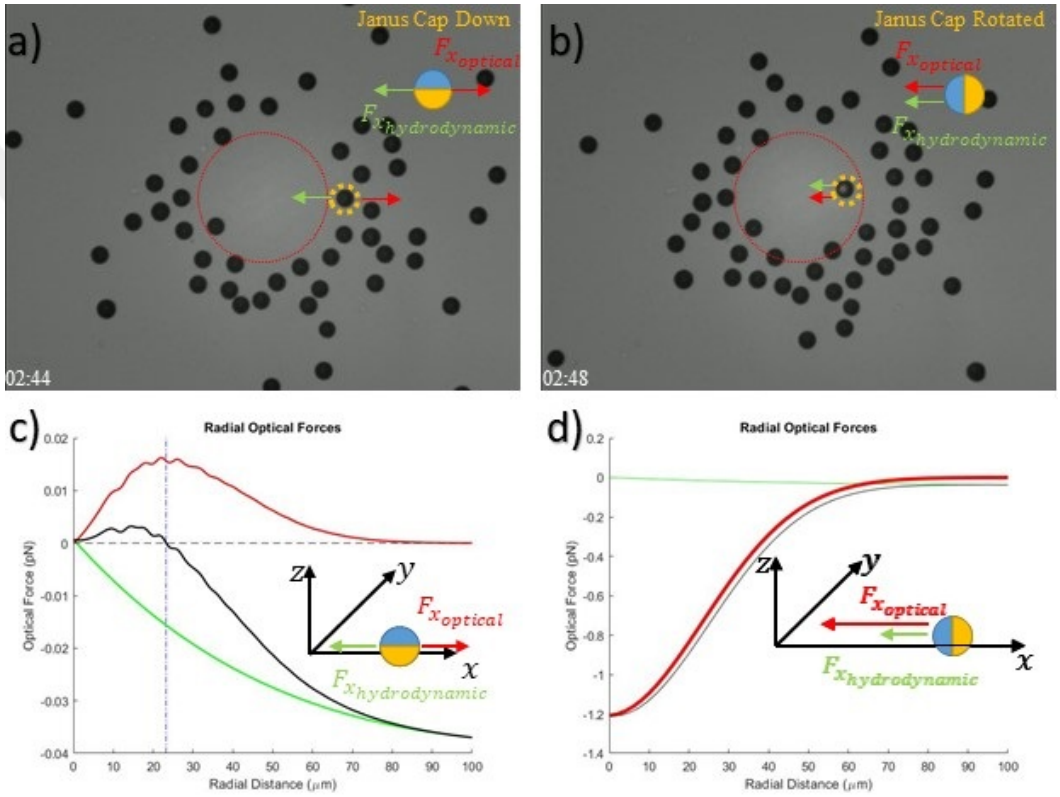


Figure 4.13: The Janus particles are under 100 mW smooth Gaussian potential with $34\mu m$ beam waist. The particles are dragged by the hydrodynamic pattern from far distances to the periphery. Yet, none of the particles enter inside to the Gaussian beam waist for a while as if there is an equilibrium radius at the beamwaist (a) because the sum of the forces is zero near beam waist (c). Whenever a Janus particle is rotated, the optical force is reversed and JP is pulled back into the center (b-d).

Due to the heat absorption by the particles that are near the beam waist, the temperature gradient increases. The increase in the temperature gradient increases the hydrodynamic pattern magnitude, thus the particles at the periphery

started to be pushed inside of the beam waist a little bit more by the hydrodynamic pattern.

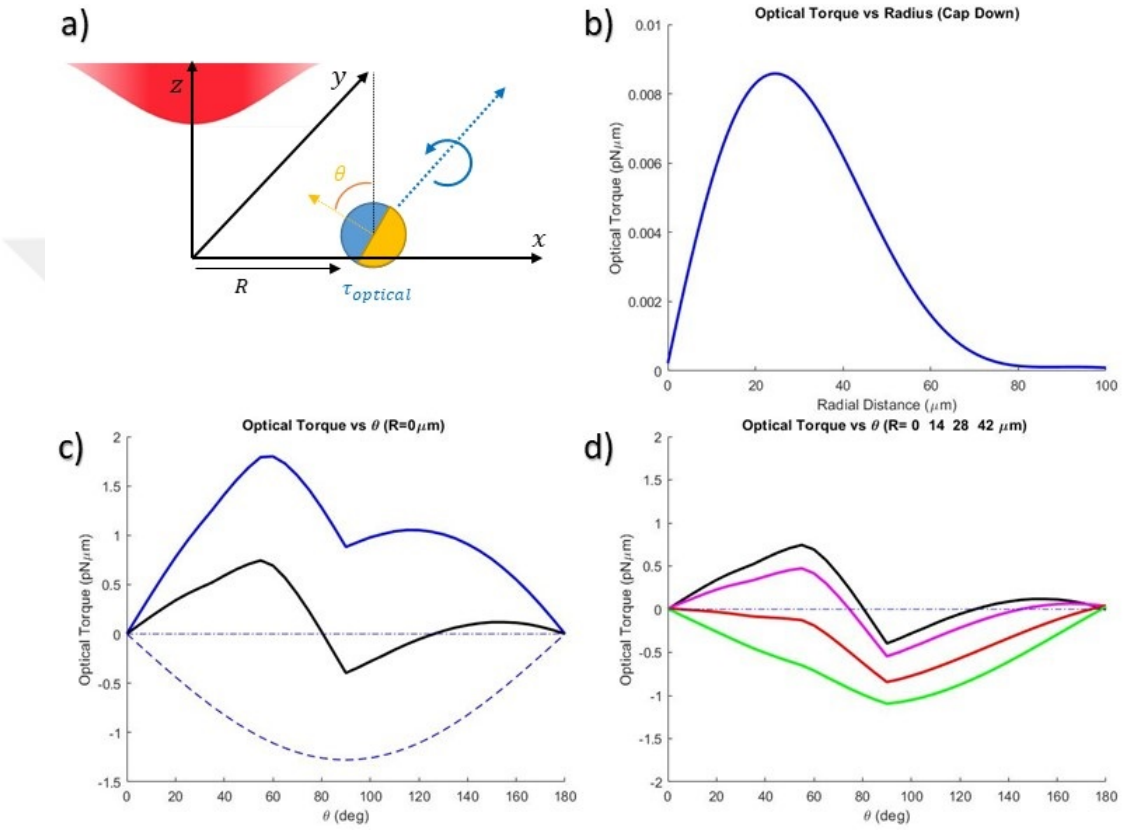


Figure 4.14: The torque exerted by the optical forces and gravity on Janus particle. (a) The schematic of the Janus particle coordinates. (b) Radial variance in optical torque when the JP orientation is cap-down. (c) The optical torque for different orientations of JP when R=0. Blue line solid is the optical torque, the blue dashed line is the buoyancy torque and the black line is the sum of all torques. (d) The optical torque for different orientations of JP when R=0 (black), R=14 (magenta), R=28 (red), R=42 (green) lines.

When the particles get further close to the beam center, the optical torque inside the beam waist overcomes the buoyancy (Fig 4.14), thus with very small a Brownian effect on rotational diffusion, the particle orientation changes from cap-down to some angle immediately. When the particle orientation changes, the optical forces on the particle turns out to be strongly attractive, thus the Janus

particles start to move very fast through the center of the beam.

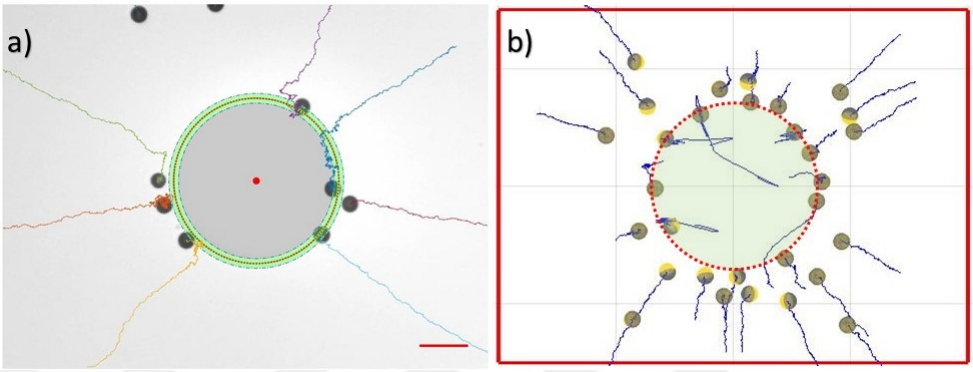


Figure 4.15: (a) The experiment of Janus particles (50 nm Gold coated polystyrene particles) and their analyzed trajectories. The JPs are drifted to the periphery of the Gaussian beam and stays there as an equilibrium radius until they are rotated. (b) The simulation of Janus particles (50 nm Gold coated polystyrene particles) and their trajectories. Similarly with experiment, the JPs stays at the periphery. Also, the JPs inside the beam waist are expelled out to the perphery.

Similarly with what happened in only janus experiments experiments (Fig 4.14), the simulations also shows clearly that the Janus particles are waiting at the periphery until they are rotated. When the hydrodynamic pattern is embedded as an additional drag to the JPs in simulation, naturally, there occurs an equilibrium radial position for JPs. In Fig 4.15, the captions from the experiment and the simulation are given. In simulation, one of the JPs is starting from the central region and it is also going to the periphery rapidly due to the strong optical attractive force.

Together with the heat absorption of the insider Janus particles, the hydrodynamic pattern magnitude from outside to the inside of the beam increases. Moreover to that, the attractive optical force is accelerating the Janus particles velocity in radial direction, through the center of the beam, resulting in very high speed of JPs inside the beam waist.

With very high speed, a particle go across the other side of the beam circle rapidly. When a particle come across to the periphery back, it looses it's attractive forces and slow down and rotate back to the cap-down. Again, the torque rotates particle from cap-down to a some angle looking back to the center. This kind of strong call-back to the center of the beam leads to a chaotic mixing at the center of the beam.

This strange chaotic mixing is only possible when the particle-particle interaction is repulsive. If the particles are attracting each other, then they tend to form a cluster as it is shown in Mousavi's work. We also replicate their experiments to approve the self-induced hydrodynamic attraction. Our comparative experiments also show the drastic difference in behaviour of Janus particles in between the two substrates.

## 4.6 Janus Particle Behaviour in Different Substrates: Attraction & Repulsion

There are two kinds of hydrodynamic flow that is mentioned in this thesis. One type is the Marangoni fluid flow inside the whole sample (hydrodynamic pattern) (Fig 4.16 red arrows). This is discussed in detail before. Another type of fluid flow is occurring among individual particles (Fig 4.16 blue arrows). The local temperature gradient around Janus particles causes a fluid flow in their vicinity. Because of the boundary of the bottom substrate, the fluid flow is curved from horizontal direction to the vertical direction. So, if two particles come close to each other, their reciprocal individual fluid flows causes an interactive force to each other. The nature of individual interaction (attraction or repulsion) is determined by the direction of flow, and the direction of flow is correlated with the thermal diffusion coefficient.

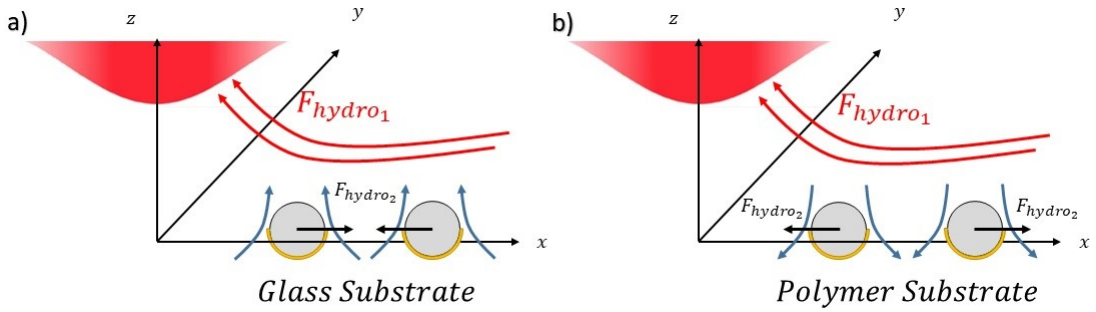


Figure 4.16: The representative drawing that is showing the two types of hydrodynamic flow in experiments. The red arrows shows the Marangoni convection (hydrodynamic pattern) in the overall sample. The blue lines are local hydrodynamic flow due to the local thermal gradient due to the light absorption of JPs. The black arrows shows the individual interaction among Janus particles due to the local hydrodynamic flow. (a) In glass substrate, the force is attractive. (b) In polymer substrate, the force is repulsive.

While the optical forces and Marangoni fluid flow are pulling the particles towards the center of the Gaussian beam, the thermophoretic forces can be either pulling (for silica) or pushing (for polystyrene) the particles depending on the thermal diffusion coefficient of the particle (remember eq. 4.1 )(12). However, the thermal diffusion coefficient is determined by various micro molecular factors (e.g. solvent-particle interaction, charge of the particle, charge of the surface) (65). Thus, it should be determined by the careful analysis of the trajectory of the particles from the experimental observations. Our main concern is that, the thermal diffusion coefficient is highly dependent on particle-environment interaction, and it can reverse it's sign accordingly.

There is a well developed theory that connects the hydrodynamic flow velocity and the thermal diffusion coefficient by Wurger et al. The radial component of the flow velocity at a horizontal distance $\rho$ from the centre of one of the Janus particle, $u_\rho$, is given by [4] (66):

[4]In the equation, $\Delta T = P/((2\pi + 4)\kappa a)$, P is the absorbed power by the gold cap from the infra-red light, $\kappa = 3\kappa_s/(2\kappa_s + \kappa_p)$ ($\kappa_s$ and $\kappa_p$ are the thermal conductivity of the medium and particle, respectively), $p_1 = 1 + \frac{9}{8}\epsilon_h$, $q_3 = -1 - \frac{3}{8}\epsilon_h$, $\epsilon_h = a/h$, h is the distance of the centre of the particle from the wall, a is radius of the particle, and $r = \sqrt{\rho^2 + 4h^2}$.

$$u_\rho = \frac{D_T \Delta T}{\pi a}\left[6\frac{\rho a h^3(\epsilon_h^2 q_3 - p_1)}{r_h^5} - 60 q_3 \frac{\rho a^3 h^3}{r_h^7}\right] \tag{4.2}$$

By using the flow velocity $u_\rho$, the effective hydrodynamic force [5] on a nearby particle is;

$$F = 6\pi\eta a \delta_w u_\rho \tag{4.3}$$

The equation 4.2 shows that the flow direction of the fluid is linearly dependent on the thermal diffusion coefficient, thus it can be repulsive if the flow direction is reversed (from vertical to the horizontal).

Because of the dependence on the thermal diffusion coefficient, the fluid flux effect can be either attractive or repulsive among individual particles. For this reason, when the substrate changes, it affects the thermal diffusion coefficient thus yielding with different behaviour in different substrates.

To see the difference, two different samples are prepared with same concentration of JPs. A comparative pictures are given in Fig 4.17. The laser power is 100 mW in both cases. And the sample position on optical setup are very close to each other so that the beam waist is the same (see the Rayleigh regime discussion in part 3.2)

[5] In the equation, $\delta_w$ is unitless friction coefficient depending on the particle height from the wall. (1)

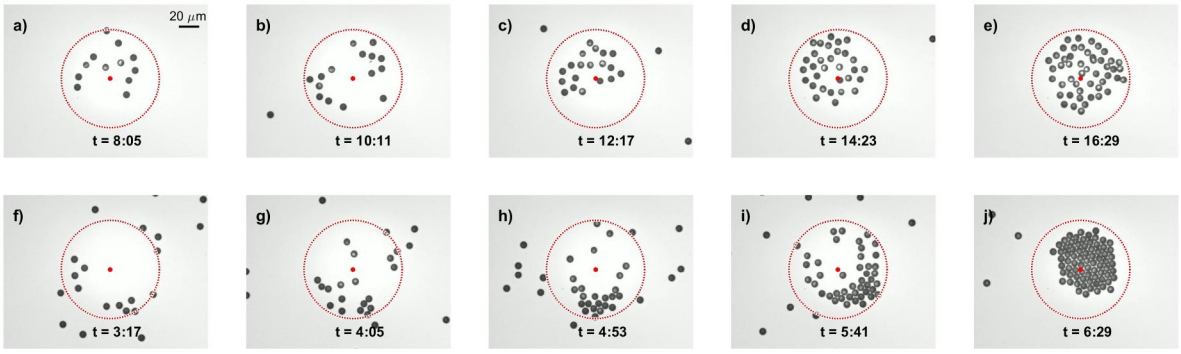


Figure 4.17: The figure is showing the difference of glass and polymer substrates to the JPs aggregate behaviour. When the particles are exposed to Gaussian defocused beam, while the particles in a cell with glass substrate (a-e) shows an aggregation due to self-driven mechanism e.g. thermophoresis (1), the particles in a cell with polymer substrate (f-j) doesn't show any aggregate, instead the JPs undergo ballistic motion inside of the Gaussian beam waist.

The glaring outcome of the second set of experiments is the drastic difference in behaviour of the Janus particles in two different substrates (glass and polymer substrates). In polymer, particle-particle interaction is repulsive, thus yielding with short-range repulsive gathering at the center of Gaussian (Fig 4.17 a-e). While in glass, particle-particle interaction is attractive, thus yielding with close-packeded crystalline cluster in which it's center is a bit shifted from the center of the Gaussian beam (Fig 4.17 f-j).

The change in behaviour of the Janus particle in polymer cell has an interesting outcome in mixture suspensions (Janus particle & Colloidal particle). In the case of mixture suspensions, Mousavi et al reported a mixed cluster of Janus particle and silica particle because the attractive forces exerted due to the Janus particles. However, in our case, as the Janus particles are not attracting the agents in their vicinity, there is no mixed cluster formation in the case of mixed suspensions. Instead, an interesting outcome of this repulsive force is emerged, possibly useful for applications.

## 4.7 Separation of Mixture (JP & PS)

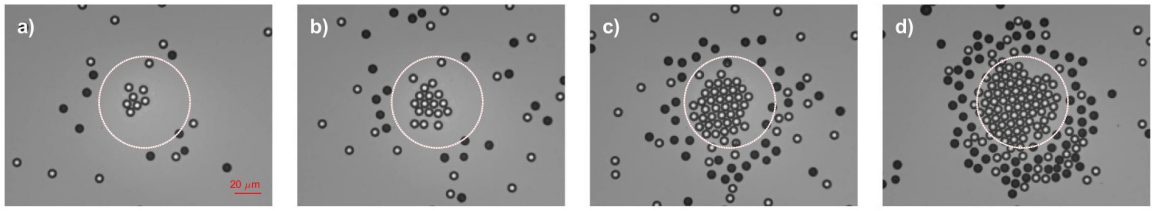


Figure 4.18: Gathering and separation of colloids in a Gaussian optical potential. Bright particles are PS particles (6.24 m size) and dark particles are Janus particles (6.24 m PS size, 50 nm Gold cap). The white circle indicates the beam waist of the Gaussian potential ($34\mu m$).

A useful outcome of the repulsive behaviour of the JPs is that; in the case of mixture, the JPs preferred to stay at the outside of the periphery while the normal polystyrene particles gather at the center of the beam, results in delicate separation eventually. (Fig 4.18) While the Janus particles from far distances also keep coming to the beam spot , they are not allowed to enter the central area of the Gaussian beam. The reason for this is simply because the colloidal particles are filling the central area before the JPs rotated. For this reason, while the JPs are expelled out from the beam waist, the colloidal particles are gathered inside the beam waist, thus sorting of particles is observed.

This sorting of the two different kinds of particles (JPs & PS particles) is achievable also by simulations. In Fig 4.19, the captions from the end of both experiment and simulation are given. In simulation, 13 polystyrene particles and 17 Janus particles are randomly located on the screen. The JPs at the inside of the beam waist are collapsed to the periphery and the polystyrene particles filled the central area, while the far distant JPs also gathered at the periphery.

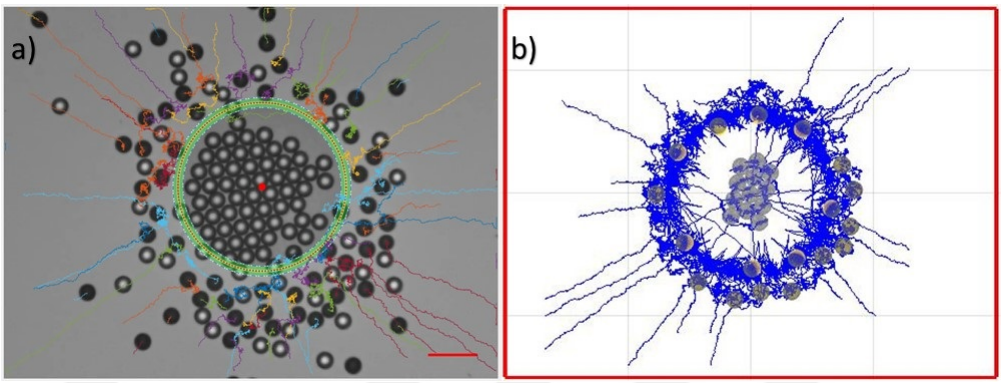


Figure 4.19: (a) The experiment of mixture and their analyzed trajectories. (b) The simulation of mixture of JPs and PS particles and their trajectories.

## 4.8 Summary

Optical tweezers are providing a very useful tool to control individual micro and nano particles via only light. Recently in 2018, Prof Arthur Ashkin is awarded with a Nobel prize for the discovery of optical tweezers (18).

Differently from the tightly focused optical tweezers, we designed an optical system where the optical potential is widely spread on the sample with a Gaussian profile. In this way, we aim to control the collective behaviour of microparticles. (1; 62)

Similarly in Mousavi's work, we focused on the behaviour of the Janus particles (half coated spherical colloids) under smooth wide Gaussian optical potential. Janus particles have been of interest mostly for their capability of self-assembly in various studies. Unlike their passive encounters, they tend to form clusters which is called self-aggregate or self-assembled clusters when they are triggered by light.

To see the differences in behaviour of the Janus particles and their spherically

symmetric counterparts, we started with the spherically symmetric colloidal behaviour under smooth Gaussian potential. The experiments on symmetric colloids shows that the driving mechanism to attract the far distant particles to the beam spot is mainly the overall hydrodynamic flow pattern inside the sample cell due to the overall temperature gradient exerted by the infra-red light absorption of the water. Thus, when we calculate the radial drift velocity profile of simple colloids by considering the additional hydrodynamic fluid flow pattern obtained from COMSOL calculations, the drift velocity profile of the particles in simulations and the experiments are perfectly matching with each other.

We continued our investigations with the comparative experiments on Janus particles in different substrates. In Mousavi's study and several other studies shows the clustering behaviour of Janus particles. However, in our observations, the Janus particles do not form close pack cluster in polymer based substrate. Our results yields in non-clustering behaviour of Janus particles. This is mainly due to the repulsive forces among individual Janus particles unlike the attractive forces observed in Mousavi's study. The main factor for this difference in forces being repulsive instead of attractive comes from the opposite local hydrodynamic flow direction which is mainly determined by the thermal diffusion coefficient. We also approved our hypothesis about the opposite (repulsive) short-range forces by simulating the Janus particle behaviour in Matlab via using force profile that we employed to the particles obtained by optical tweezer software (OTS) by Callegari et al (49). The resulting behaviour is the same as in experiments.

One of the useful outcome of the short-range repulsive behaviour of Janus particles is the separation of Janus particles from their spherically symmetric counterparts under smooth Gaussian optical potential in the case of mixture suspensions. We also simulate to see if this peculiar behaviour is attainable when we inverse the attractive forces into repulsive forces in simulations. Eventually, the simulations also shows the separation is natural outcome when we employ all the force profiles and Brownian noise to the system.

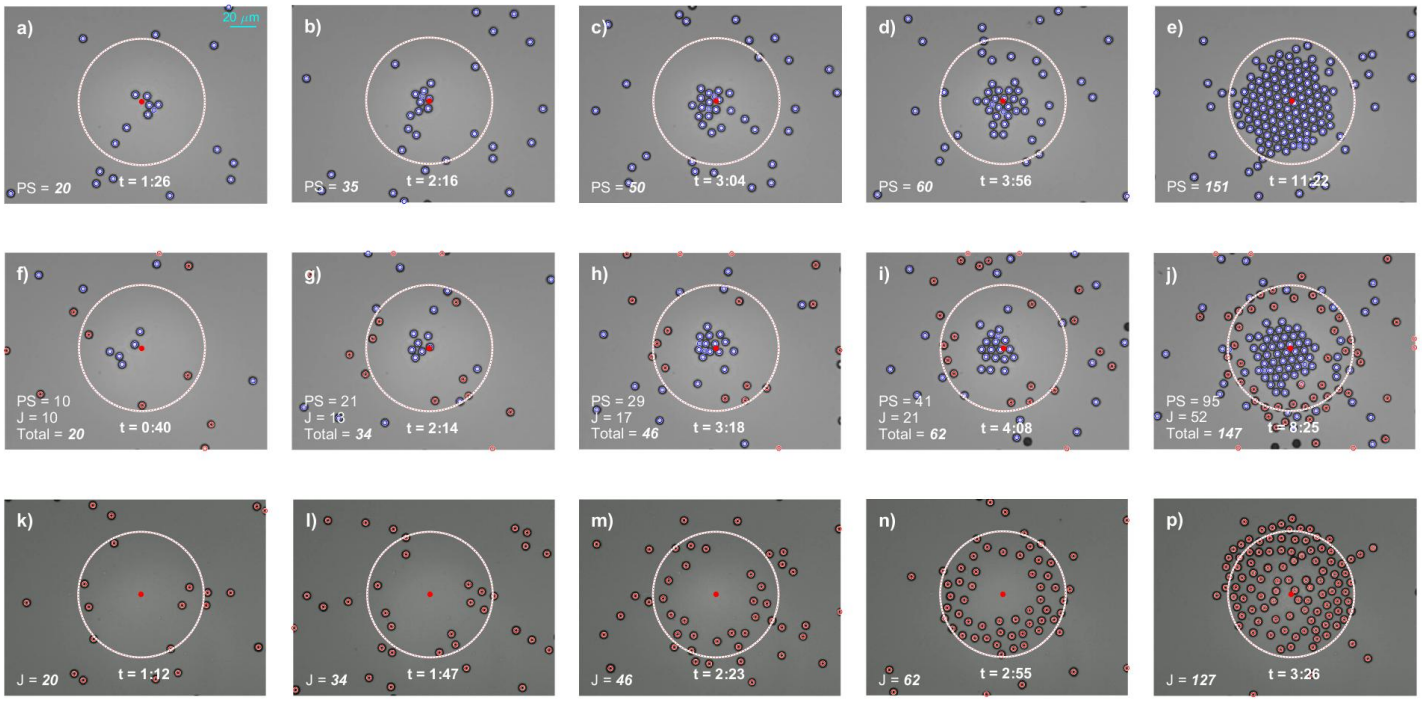


Figure 4.20: The figure shows three separate rows which are for three separate experiments with different suspensions. (a-b-c-d-e) are showing sequence of frames for polystyrene only experiment. The polystyrene (PS) beads $(6, 24\mu m)$ comes to the beam center and form a compact crystal cluster due to the squeezing forces which are the sum of the attractive forces e.g. optical and hydrodynamic forces. (k-l-m-n-p) are showing sequence of frames for Janus particles (JPs) "$(6, 24\mu m)$ PS + $(10nm)$ Ti + $(50nm)$ Gold" only experiment. The JPs are also dragged to the center of the beam. However, when they come inside to the beam waist ($r = 48\mu m$, 'red' dashed line) they are being "active" and they undergo ballistic motion. Outside of beam waist, there are fighting forces e.g. hydrodynamic flow pattern which appears to be attractive force to the center and the optical repulsive force. Thus, the particles can't get inside of the beam instantly, inversely they wait at around the beam waist for a while (see frames k-l-m-n). In the case of mixture (f-g-h-i-j), the Janus particles stays outside of the beam waist while the polystyrene particles fill the central area, thus resulting with particle separation at the end.

# Chapter 5

# Conclusion

The fabrication of self-propelled microparticles and nanoparticles is of interest in physical and chemical sciences not only because of their distinctive fundamental property related with out-of equilibrium phenomena, but also because they are promising agents in various practical purposes such as in the design of smart materials, cargo transport or chemical sensing (67).

One of the promising self-propelled particles is called Janus particles, usually comprised of two different materials in one body (e.g. gold coated silica microspheres). Janus particles offers a promising scope to the design of smart materials such as in generation of array structures. Up-to-date lithography techniques are the main approach in generating array structures by now. In lithography techniques, to create array structures in optical mask, one has to process photoresist accurately with laser exposure for a long time for large areas. This technique is fairly expensive, complicated, and time consuming. An alternative production route to this top-down approach is the bottom-up procedure of self-assembly. Mono-disperse spheres of sub-micron size (e.g. Janus particles) can readily self-assemble into highly ordered and close-packed arrays, so-called colloidal crystals (68). Fast aggregates on periodical optical potentials might help to design and create periodic arrays achievable by drying and etching eventually, which is an alternative approach for lithography techniques.

Mousavi et al studied the self-assembly of Janus particles (gold coated silica spheres) to understand the mechanism of self-assembling under the smooth Gaussian beam in a water medium. They have found that there is a local hydrodynamic attractive forces exerted by Janus particles. The effective ingredients for these forces are highly dependent on the diffusion coefficient of JP, which also depends on the intrinsic properties of Janus particles and the interaction of a Janus particle with it's vicinity.

We wondered if we can reverse the attractive force by changing one of these properties. We achieved the separation of JPs from their spherically symmetric counterparts, which might be useful for particle separation in medicine.

Further investigations can be done whether the similar behaviour can be observed under speckle optical potentials because most of the time in nature, a perfect Gaussian beam can be distorted by the richness of the medium. Also the pH of the solution and surface chemistry can be manipulated incrementally during the experiments to see the change in the hydrodynamic forces in real time.

In a different perspective, it might also be interesting to analyse the spatial and temporal evolution of the correlation function of the particles to see the perfection of the crystallized aggregate of the PS/Silica particles at the end.

Effectiveness of this method of separation of mixed particles can be implemented into drug separation, which might play an accelerating role into sorting strategies for medicine from toxins.

# Bibliography


[1] S. M. Mousavi, I. Kasianiuk, D. Kasyanyuk, S. K. Velu, A. Callegari, L. Biancofiore, and G. Volpe, "Clustering of Janus particles in an optical potential driven by hydrodynamic fluxes," Soft matter, vol. 15, no. 28, pp. 5748–5759, 2019.

[2] B. Ivo, Self-propelled particles driven by light. PhD thesis, University of Stuttgart, Keplerstraße 7, 70174 Stuttgart, Germany, 2013.

[3] E. M. Purcell, "Life at low Reynolds number," American journal of physics, vol. 45, no. 1, pp. 3–11, 1977.

[4] M. Kardar., "Lecture 6: Brownian Motion," in IITS: Statistical Physics in Biology, 2013. At Leuven.

[5] A. Einstein, "On the theory of the Brownian movement," Ann. Phys, vol. 19, no. 4, pp. 371–381, 1906.

[6] T. Scientific, "Fact sheet on escherichia coli." https://www.thermofisher.com/blog/food/fact-sheet-on-escherichia-coli/. Accessed: 2019-04-05.

[7] H. C. Berg, E. coli in Motion. Springer Science & Business Media, 2008.

[8] L. Zhang, K. E. Peyer, and B. J. Nelson, "Artificial bacterial flagella for micromanipulation," Lab on a Chip, vol. 10, no. 17, pp. 2203–2215, 2010.

[9] C. Bechinger, R. Di Leonardo, H. Löwen, C. Reichhardt, G. Volpe, and G. Volpe, "Active particles in complex and crowded environments," Reviews of Modern Physics, vol. 88, no. 4, p. 045006, 2016.

[10] M. Silverman and M. Simon, "Flagellar rotation and the mechanism of bacterial motility," Nature, vol. 249, no. 5452, p. 73, 1974.

[11] L. Zhang, J. J. Abbott, L. Dong, B. E. Kratochvil, D. Bell, and B. J. Nelson, "Artificial bacterial flagella: Fabrication and magnetic control," Applied Physics Letters, vol. 94, no. 6, p. 064107, 2009.

[12] H.-R. Jiang, N. Yoshinaga, and M. Sano, "Active motion of a Janus particle by self-thermophoresis in a defocused laser beam," Physical review letters, vol. 105, no. 26, p. 268302, 2010.

[13] J. R. Howse, R. A. Jones, A. J. Ryan, T. Gough, R. Vafabakhsh, and R. Golestanian, "Self-motile colloidal particles: from directed propulsion to random walk," Physical review letters, vol. 99, no. 4, p. 048102, 2007.

[14] I. Buttinoni, G. Volpe, F. Kümmel, G. Volpe, and C. Bechinger, "Active Brownian motion tunable by light," Journal of Physics: Condensed Matter, vol. 24, no. 28, p. 284129, 2012.

[15] W. F. Paxton, K. C. Kistler, C. C. Olmeda, A. Sen, S. K. St. Angelo, Y. Cao, T. E. Mallouk, P. E. Lammert, and V. H. Crespi, "Catalytic nanomotors: autonomous movement of striped nanorods," Journal of the American Chemical Society, vol. 126, no. 41, pp. 13424–13431, 2004.

[16] "Richard feynman photo." http://archives-dc.library.caltech.edu/islandora/object/ct1%3A570. Accessed: 2020-05-19.

[17] R. Feynman, "There is plenty of room at the bottom: An invitation to enter a new field of physics," in Lecture at American Physical Society Meeting, vol. 29, 1959.

[18] "The nobel prize in physics 2018." https://www.nobelprize.org/prizes/physics/2018/ashkin/facts/.

[19] A. Ashkin, J. M. Dziedzic, J. Bjorkholm, and S. Chu, "Observation of a single-beam gradient force optical trap for dielectric particles," Optics letters, vol. 11, no. 5, pp. 288–290, 1986.

[20] T. Mirkovic, N. S. Zacharia, G. D. Scholes, and G. A. Ozin, "Fuel for thought: chemically powered nanomotors out-swim nature's flagellated bacteria," Acs Nano, vol. 4, no. 4, pp. 1782–1789, 2010.

[21] F. Schmidt, A. Magazzù, A. Callegari, L. Biancofiore, F. Cichos, and G. Volpe, "Microscopic engine powered by critical demixing," Physical review letters, vol. 120, no. 6, p. 068004, 2018.

[22] N. Simpson, K. Dholakia, L. Allen, and M. Padgett, "Mechanical equivalence of spin and orbital angular momentum of light: an optical spanner," Optics letters, vol. 22, no. 1, pp. 52–54, 1997.

[23] M. Friese, T. Nieminen, N. Heckenberg, and H. Rubinsztein-Dunlop, "Optical alignment and spinning of laser-trapped microscopic particles," Nature, vol. 394, no. 6691, pp. 348–350, 1998.

[24] S. L. Biswal and A. P. Gast, "Micromixing with linked chains of paramagnetic particles," Analytical chemistry, vol. 76, no. 21, pp. 6448–6455, 2004.

[25] A. Ghosh and P. Fischer, "Controlled propulsion of artificial magnetic nanostructured propellers," Nano letters, vol. 9, no. 6, pp. 2243–2245, 2009.

[26] V. Blickle and C. Bechinger, "Realization of a micrometre-sized stochastic heat engine," Nature Physics, vol. 8, no. 2, pp. 143–146, 2012.

[27] S. Granick, S. Jiang, and Q. Chen, "Janus particles," Phys. Today, vol. 62, no. 7, pp. 68–69, 2009.

[28] B. Öktem, I. Pavlov, S. Ilday, H. Kalaycıoğlu, A. Rybak, S. Yavaş, M. Erdoğan, and F. Ö. Ilday, "Nonlinear laser lithography for indefinitely large-area nanostructuring with femtosecond pulses," Nature photonics, vol. 7, no. 11, p. 897, 2013.

[29] D. Babič, C. Schmitt, and C. Bechinger, "Colloids as model systems for problems in statistical physics," Chaos: An Interdisciplinary Journal of Nonlinear Science, vol. 15, no. 2, p. 026114, 2005.

[30] M. E. Cates, "Diffusive transport without detailed balance in motile bacteria: does microbiology need statistical physics?," Reports on Progress in Physics, vol. 75, no. 4, p. 042601, 2012.

[31] A. Einstein, Investigations on the Theory of the Brownian Movement. Courier Corporation, 1956.

[32] R. Brown, "XXVII. A brief account of microscopical observations made in the months of June, July and August 1827, on the particles contained in the pollen of plants; and on the general existence of active molecules in organic and inorganic bodies," The Philosophical Magazine, vol. 4, no. 21, pp. 161–173, 1828.

[33] D. S. Lemons and A. Gythiel, "Paul langevin's 1908 paper "on the theory of brownian motion"["sur la théorie du mouvement brownien," cr acad. sci.(paris) 146, 530–533 (1908)]," American Journal of Physics, vol. 65, no. 11, pp. 1079–1081, 1997.

[34] P. H. Jones, O. M. Maragò, and G. Volpe, Optical tweezers: Principles and applications. Cambridge University Press, 2015.

[35] B. Lukić, S. Jeney, C. Tischer, A. Kulik, L. Forró, and E.-L. Florin, "Direct observation of nondiffusive motion of a Brownian particle," Physical review letters, vol. 95, no. 16, p. 160601, 2005.

[36] G. E. Uhlenbeck and L. S. Ornstein, "On the theory of the Brownian motion," Physical review, vol. 36, no. 5, p. 823, 1930.

[37] M. O. I. Prirody, Nouveaux mémoires de la Société impériale des naturalistes de Moscou, vol. 10. l'Université impériale, 1855.

[38] C. Ludwig, "Diffusion zwischen ungleich erwärmten orten gleich zusammengesetzter lösung, sitz," Ber. Akad. Wiss. Wien Math-Naturw. KI, p. 539, 1856.

[39] J. Platten and P. Costesèque, "Charles Soret. A short biography a," The European Physical Journal E, vol. 15, no. 3, pp. 235–239, 2004.

[40] M. Polyanskiy, "Refractive index database." https://refractiveindex.info/. Accessed: 2019-04-18.

[41] A. Würger, "Self-diffusiophoresis of Janus particles in near-critical mixtures," Physical review letters, vol. 115, no. 18, p. 188304, 2015.

[42] J. L. Anderson, "Colloid transport by interfacial forces," Annual review of fluid mechanics, vol. 21, no. 1, pp. 61–99, 1989.

[43] A. Tiselius, "A new apparatus for electrophoretic analysis of colloidal mixtures," Transactions of the Faraday Society, vol. 33, pp. 524–531, 1937.

[44] P. H. O'Farrell, "High resolution two-dimensional electrophoresis of proteins.," Journal of biological chemistry, vol. 250, no. 10, pp. 4007–4021, 1975.

[45] E. Vela, M. Hafez, and S. Régnier, "Laser-induced thermocapillary convection for mesoscale manipulation," International Journal of Optomechatronics, vol. 3, no. 4, pp. 289–302, 2009.

[46] L. Onsager, "Reciprocal relations in irreversible processes. I.," Physical review, vol. 37, no. 4, p. 405, 1931.

[47] A. Würger, "Thermophoresis in colloidal suspensions driven by Marangoni forces," Physical review letters, vol. 98, no. 13, p. 138301, 2007.

[48] F. M. Weinert and D. Braun, "Observation of slip flow in thermophoresis," Physical review letters, vol. 101, no. 16, p. 168301, 2008.

[49] A. Callegari, M. Mijalkov, A. B. Gököz, and G. Volpe, "Computational toolbox for optical tweezers in geometrical optics," JOSA B, vol. 32, no. 5, pp. B11–B19, 2015.

[50] K. F. Palmer and D. Williams, "Optical properties of water in the near infrared," JOSA, vol. 64, no. 8, pp. 1107–1110, 1974.

[51] B. Company, "Basler ac a640-750 um." https://www.baslerweb.com/en/products/cameras/area-scan-cameras/ace/aca640-750um/#tab=specs. Accessed: 2019-04-30.

[52] Wikipedia, "The rayleigh length." https://commons.wikimedia.org/wiki/File:GaussianBeamWaist.svg.

[53] E. ToolBox, "Thermal conductivity of common materials and gases." https://www.engineeringtoolbox.com/thermal-conductivity-d_429.html, 2003. Accessed: 2019-03-19.

[54] "Marienfeld company, microscope slides." https://www.marienfeld-superior.com/microscope-slides-thickness-approx-1-mm.html. Accessed: 2019-02-18.

[55] S. Aldrich, "Parafilm product of bemis company information on sigma aldrich webcite." https://www.sigmaaldrich.com/content/dam/sigma-aldrich/docs/Sigma/Product_Information_Sheet/1/p7793pis.pdf. Accessed: 2019-03-20.

[56] W. L. Hau, D. W. Trau, N. J. Sucher, M. Wong, and Y. Zohar, "Surface-chemistry technology for microfluidics," Journal of micromechanics and microengineering, vol. 13, no. 2, p. 272, 2003.

[57] T. Nisisako, "Recent advances in microfluidic production of Janus droplets and particles," Current opinion in colloid & interface science, vol. 25, pp. 1–12, 2016.

[58] T. Nisisako and T. Torii, "Formation of Biphasic Janus Droplets in a Microfabricated Channel for the Synthesis of Shape-Controlled Polymer Microparticles," Advanced materials, vol. 19, no. 11, pp. 1489–1493, 2007.

[59] A. M. Grumezescu, Design and Development of New Nanocarriers. William Andrew, 2017.

[60] A. Perro, F. Meunier, V. Schmitt, and S. Ravaine, "Production of large quantities of "Janus" nanoparticles using wax-in-water emulsions," Colloids and Surfaces A: Physicochemical and Engineering Aspects, vol. 332, no. 1, pp. 57–62, 2009.

[61] T. Andac, P. Weigmann, S. K. Velu, E. Pinçe, G. Volpe, G. Volpe, and A. Callegari, "Active matter alters the growth dynamics of coffee rings," Soft matter, vol. 15, no. 7, pp. 1488–1496, 2019.

[62] D. P. Singh, U. Choudhury, P. Fischer, and A. G. Mark, "Non-Equilibrium Assembly of Light-Activated Colloidal Mixtures," Advanced Materials, vol. 29, no. 32, p. 1701328, 2017.

[63] R. Golestanian, "Collective behavior of thermally active colloids," Physical review letters, vol. 108, no. 3, p. 038303, 2012.

[64] C. Wang, "Exact solutions of the steady-state Navier-Stokes equations," Annual Review of Fluid Mechanics, vol. 23, no. 1, pp. 159–177, 1991.

[65] R. Piazza and A. Parola, "Thermophoresis in colloidal suspensions," Journal of Physics: Condensed Matter, vol. 20, no. 15, p. 153102, 2008.

[66] J. Morthomas and A. Würger, "Hydrodynamic attraction of immobile particles due to interfacial forces," Physical Review E, vol. 81, no. 5, p. 051405, 2010.

[67] P. Illien, R. Golestanian, and A. Sen, "'Fuelled'motion: phoretic motility and collective behaviour of active colloids," Chemical Society Reviews, vol. 46, no. 18, pp. 5508–5518, 2017.

[68] M. S. Fernández, V. Misko, and F. Peeters, "Self-assembly of Janus particles into helices with tunable pitch," Physical Review E, vol. 92, no. 4, p. 042309, 2015.

[69] "Thermofisher company, useful latex bead formulates." https://www.thermofisher.com/tr/en/home/life-science/cell-analysis/qdots-microspheres-nanospheres/idc-surfactant-free-latex-beads/latex-bead-technical-overview/useful-latex-bead-formulae.html. Accessed: 2019-02-18.

# Appendix A

# Sample Cleaning Treatment Protocols

I conduct two set of experiments. First, I scan the different laser powers (20-140 mW) to see the effect of the laser power to the aggregation. Second, I tried the different substrates with a fixed laser power (100 mW). The detailed conditions of sample cell and Janus particles are explained below.

## A.1 First Set of Experiments

The polystryene particles (with 6.24 micrometer diameter) are deposited on glass substrate with the following protocol; The microscope slides (Marienfeld, Germany) are cleaned in a following way;
1) First, sonicated in 2-propanol for 2 minutes,
2) Then sonicated in water for 2 minutes,
3) And then sonicated in 2/3 Molar NaOH for 2 minutes,
4) And then sonicated in water for 2 minutes,
5) And dried with air pump.

After this operation, I made a 30 microLiter droplet of %2(w/v) polstryene particle suspensions(69) onto the glass slides and leave them to dry slowly in pedri-dishes.

Having these dried particles on the substrate, the best monolayered samples are coated by thermal evaporation ('VAKSIS MiDAS PVD 3T' Thermal Evaporator, TURKEY) in (National NAnotechnology Research Center, Bilkent, TURKEY) UNAM facilities.

With the parameters as the following; "$2.10^{-5}$ Torr pressure, heating the Titanium with 140 Ampere current (for Gold, 100 Ampere), material density for (Titanium 4.5 $g/cm^3$ and Gold 19.3 $g/cm^3$ ), material impedance ( for Titanium 14.06 $\Omega$ , and Gold 23.18 $\Omega$ ) and tooling factor (for Titanium 100, and Gold 75)."

The outcome is 10 nm thick Titanium and 50 nm thick Gold coated Janus (Polystryene(6.24$\mu$m)-Ti(10nm)-Gold(50nm)) particles.

After this process, the particles are sonicated in falcon tubes in water and settled down to the bottom of the falcon tube. Then, the additional water is taken out and only 1 microLiter water left in the tube. And then the particles are left in clean small tubes.

And all the data taken for different powers with PS-Janus-Mixture cases are done with this protocol. The tuning of final JP solution concentration is obtained by diluting the main suspension by preserving the dilution rate.

## A.2 Second Set of Experiments

In the experiments, I used common cleaning protocol to prepare sample cells (Ethanol, Iso-propanol and Water treatment and air blowing). However, I add and additional step (NaOH treatment) to make the glass slides more hydrophilic. The reason for this is to prevent the sticking of particles to the surface with the

hydroxil groups on the glass substrate. (56)

The microscope slides (Marienfeld, Germany) (54) are cleaned in a following way;
1) first sonicated in ethanol for 1 minutes,
2) And then sonicated in 2-propanol for 1 minutes,
3) Then sonicated in water for 1 minutes,
4) And then sonicated in 2/3 Molar NaOH for 1 minutes,
5) And then sonicated in water for 1 minutes,
6) And dried with air pump.

And after these steps; droplets of %2 PS particles and %3 Silica particles on the glass substrates are left to dry inside a seperate pedri-dishes to prevent air flow.

Solution concentration properties;

1) PS only experiments; %10 (w/v) PS particles from the main batches (microparticles GmbH, GERMANY) diluted by adding deionized water until %2 (w/v). Then, 30 $\mu L$ of suspension (%2 (w/v)) is diluted by adding 970 $\mu L$ deionized water.

2) Silica only experiments; %5 (w/v) Silica particles from the main batches (microparticles GmbH, GERMANY) diluted by adding deionized water until %2 (w/v). Then, 30 $\mu L$ of suspension (%2 (w/v)) is diluted by adding 970 $\mu L$ deionized water.

3) PS Janus experiments; two droplets of 30 $\mu L$ of PS suspension (%2 (w/v)) are dried on same glass substrate. And they are coated as in explained above. And then, they are sonicated and immersed into deionized water. And I waited until the particles settled down ($\approx$ 5 hours). And then, additional water is extracted out and 1000 $\mu L$ water left in suspension. Then this suspension is divided into 2 and each one of them are diluted twice. (So, again (%2 (w/v)) suspension in 1000 $\mu L$ water. )

4) Silica Janus experiments; one droplets of 30 $\mu L$ of Silica suspension (%3 (w/v)) are dried on same glass substrate. And they are coated as in explained above. And then, they are sonicated and immersed into deionized water. And I waited until the particles settled down ( 5 hours). And then, additional water is extracted out and 1500 $\mu L$ water left in suspension. (So, (%3 (w/v)) suspension in 1500 $\mu L$ water. Resulting same concentration with (%2 (w/v)) suspension in 1000 $\mu L$ water.)

# Appendix B

# Data Analysis and Simulation Methods

## B.1 Data Analysis

The data is taken by Basler ac A640-750 and analyzed by digital video microscopy via matlab. Mainly two methods are used to track the particle positions in every frame. First one is tresholding the image and then taking the center of mass of the brigth parts of each particle [(34)]. The accuracy of this method is approximately 1 pixel which is 0.3 micron. The second method is direct usage of imfindcircle function which is based on circulating the edges and looking for the intersection point to find the center of mass of circular objects. Both analysis methods are used in accordance with their convenience to the brightness of the data.

### B.1.1 Pixel-to-Micron Ratio Determination

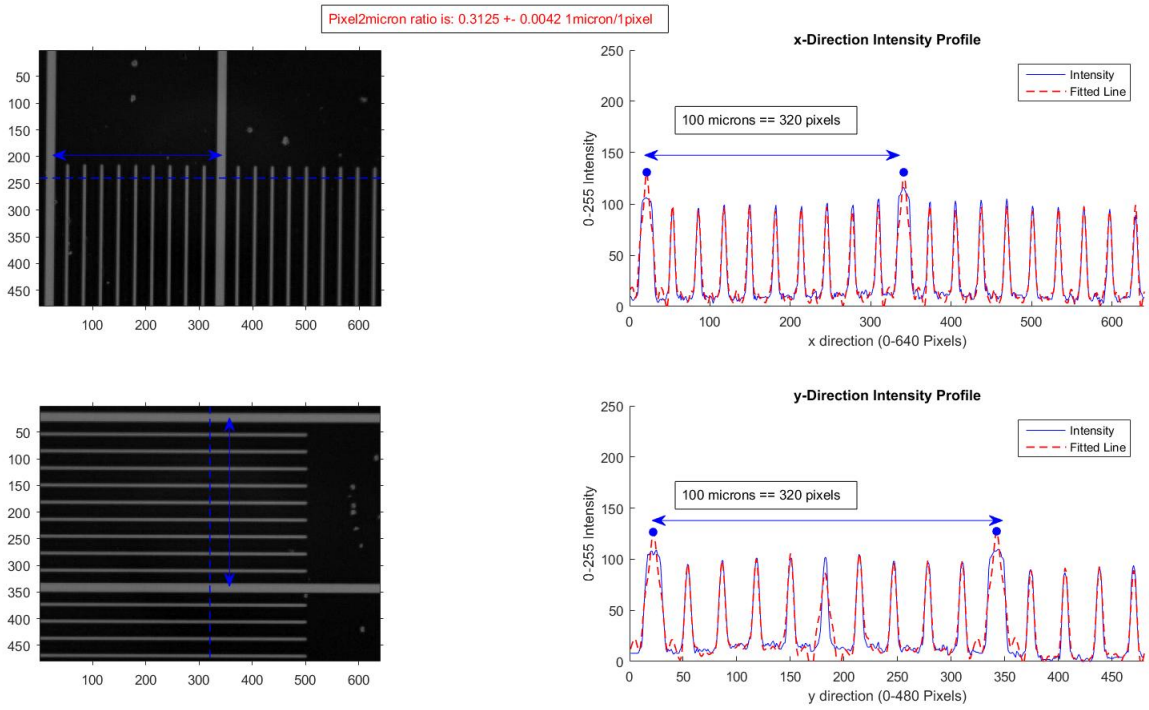


Figure B.1: Pixel to micron ratio determination.

### B.1.2 The Gaussian Beam Center and Beam Waist Determination

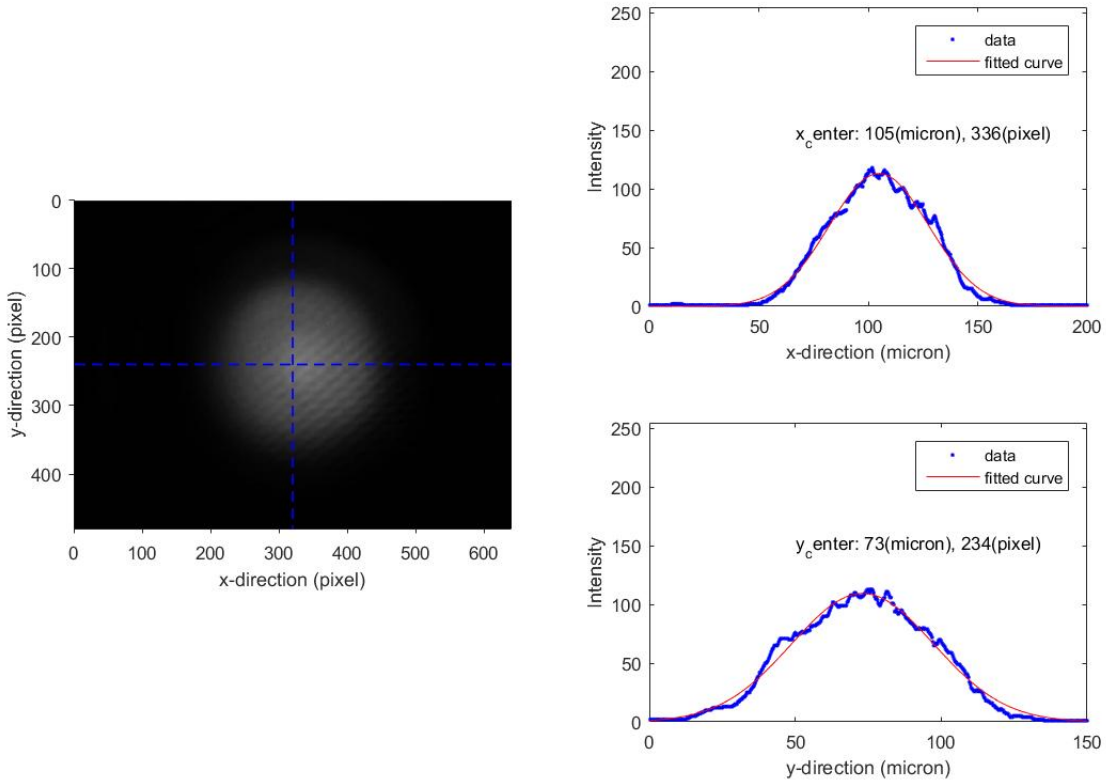


Figure B.2: Center of the Gaussian beam and beam waist determination.

### B.1.3 Example Analysis Captions

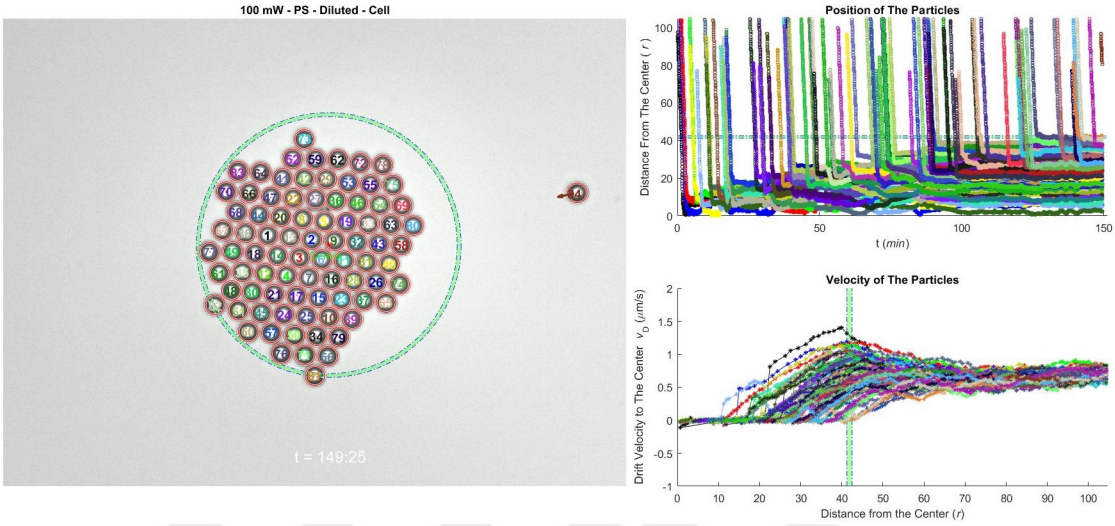


Figure B.3: The Polystryene particles are under 100 mW smooth Gaussian potential with $34\mu m$ beam waist. The resulting trajectories and the drift velocities.

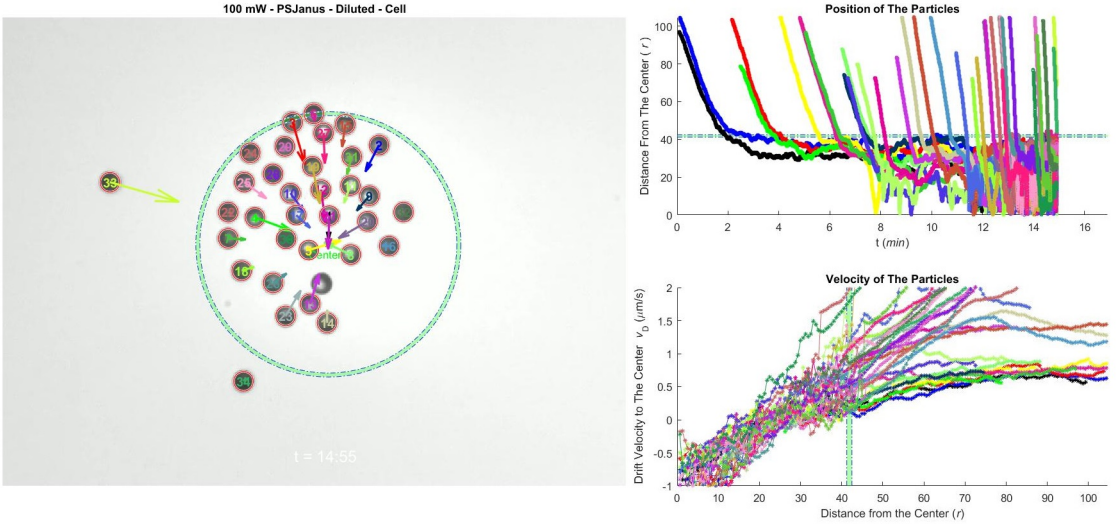


Figure B.4: The Polystryene particles are under 100 mW smooth Gaussian potential with $34\mu m$ beam waist. The resulting trajectories and the drift velocities.

## B.2 Simulation Methods

The simulations are held on by applying the Brownian noise as a random walk term and the optical forces and torques are taken from the OTGO package written by Volpe group. [(49)]. The Janus particle object is taken by Masomeh Mausavi work [(1)]. The thermophoretic forces and the hydrodynamic forces for Janus particles are applied in accordance with the Wurger studies [(47)]. The COMSOL simulations for Marangoni convective flow in sample cell are designed as the heat source to the water as a cylindrical shape with Gaussian beam radius. The fluid flow and the heat flux are solved by COMSOL via coupled stokes equation and heat flux equation for stationary condition. The resulting velocity profile is directly implemented in Matlab as an additional drift velocity.

The algorithm that we used is based on the discrete time evolution of the Langevin equation. In each iteration, the forces are calculated by using geometrical optics tools (OTGO) and the approximated formulation for self-propelling mechanism of Janus particles. (49) These forces are converted into the displacement of a particle by multiplying a factor of gamma $\gamma$. In this way, the trajectories and the orientations of the particles are recorded to a data file for further comparison between the experimental observations.